MULTI-HAZARD DESIGN OF MID- TO HIGH-RISE STRUCTURES

BY

ELISA Y. CHEN

THESIS

Submitted in partial fulfillment of the requirements
for the degree of Master of Science in Civil Engineering
in the Graduate College of the
University of Illinois at Urbana-Champaign, 2012

Urbana, Illinois

Adviser:

Professor Amr S. Elnashai

ABSTRACT

The importance of multi-hazard design of structures has emerged in the last decade, as extensive media coverage of natural disasters have increased public awareness of the catastrophic damage that hurricanes and earthquakes can wreak on buildings and infrastructure. Current design codes treat hurricanes and earthquakes as completely independent, which, while true in the physical sense, does not account for the increased risk to structures in regions where both hazards are present. The application of multi-hazard design to mid- to high-rise structures is advantageous, as they have the potential of being governed by either load and have high costs and large occupancy. This study, which develops multi-hazard design, is essential for improving the safety of structures, reducing building life cycle costs, and increasing efficiency in design.

Presently, experts in the fields of seismic and wind structural engineering conduct research autonomously and possess only basic knowledge in the other area of study. To encourage an interdisciplinary approach to multi-hazard design, this thesis presents a comprehensive review of the characteristics of hurricanes and earthquakes along with an explanation of how physical features of the hazards are represented in design codes. With a knowledge baseline established, an analytical model representing earthquake design and one representing wind design can be created and assessed for structural behavior under various loading. With the use of eigenvalue, static pushover, and dynamic time history analyses, it is possible to evaluate the structural response of each model to wind and earthquake loading and compare the behavior of each at a global, intermediate, and local level.

Results of this thesis research show that structural response differs significantly for buildings designed for different hazards. Wind designed buildings are more flexible than those designed for earthquake due to lower lateral load demands, however earthquake designed structures have much greater strength and ductility due to its capacity for substantial plastic hinge development before structural failure. The findings on the variation in structural behavior from the analyses provide a unique understanding of the effects of wind and earthquake is necessary for the advancement of multi-hazard design.

TABLE OF CONTENTS

LIST OF FIGURES

LIST OF TABLES

CHAPTER 1: INTRODUCTION

1.1 Foreword

While the effects of individual natural disasters on buildings have been extensively researched, the study of the design of structures subjected to multiple hazards has been very limited. The type of damage caused by earthquakes and hurricanes differ, but the social and economic impacts are equally significant. Perhaps the most catastrophic natural disaster in recent history is the 2010 Haiti Earthquake. With a reported 222,570 fatalities and estimated $11.5 billion in cost − almost double its estimated GDP in 2009 − the social and economic impact of this single event is staggering (State, 2011). The damage from the 2011 Tohoku Earthquake and subsequent tsunami in Japan is estimated to be in the range of $122 to $235 billion with a death toll of 15,214, making it the most expensive natural disaster to date (World Bank, 2011). Following the March 11, 2011 earthquake in economic cost is Hurricane Katrina in 2005, with an estimated cost of $125 billion, and death toll of 1,836 (NOAA, 2007).

For mid- and high-rise buildings, both high wind events and earthquakes are paramount concerns for their structural design. Earthquakes and high-wind hurricanes have the capacity to cause significant damage; and therefore, the lack of consideration of multi-hazard design in regions with high probabilities of both events could result in high casualties and economic losses. For the Haiti Earthquake, although poor construction practices were the central factor contributing to the tremendous amount of structural failure, it has been suggested that much of the damage was because most structures were designed to consider the more immediate threat from hurricanes instead of the rare earthquake (Taher, 2010). Through the assessment of the behavior of mid- to high-rise buildings under wind and seismic loads, recommendations can be made on the earthquake resistance of wind-designed buildings and wind resistance of seismic-designed buildings to achieve an efficient and sustainable design.

Because the approaches of wind and seismic design are typically opposite, with wind favoring higher stiffness and earthquake favoring higher ductility, this thesis is based on

the concept that buildings subjected to both hazards must be designed with considerations for both. Finding the design that adequately balances the requirements of both hazards, where the structure can withstand persistent strong winds as well as a major earthquake within its lifetime, is the overall purpose of this research. Presently, the American Society of Civil Engineers (ASCE) standards require structural engineers to design buildings for the controlling load case. While this practice is sufficient for single-hazard design, it neglects to consider the increased load due to higher probability of hazard occurrence and the differences in local structural response due to load application for structures in multiple hazard regions. By obtaining a more complete understanding of the local, intermediate, and global behavior of structures under wind and earthquake loading, a method to create efficient multi-hazard design can be achieved.

There are three main phases of the research: hazard definition, model analysis and assessment of results. Hazard definition includes the establishment of the necessity for multi-hazard design, the specification of the characteristics of the applied loads, and the designation of appropriate limit states. The model analysis phase is comprised of the creation of two 2-D steel frame models: one designed for the specified design wind load and one designed for the defined earthquake load. Following the design of the models, each model is analyzed under the application of both load types, using static and dynamic analysis. The final phase is to assess the results and determine the implications that can be derived from the analysis; the results of the analyses can be interpreted to further the understanding of the structural behavior and redundancies in wind and seismic design.

Results acquired from this thesis research can be used by engineers and academics to predict the inherent earthquake resistance of wind designed buildings and the inherent wind resistance of seismically designed buildings. Furthermore, by assessing the differences in local structural behavior, recommendations can be made on the retrofit of wind designed buildings for earthquake resistance. The stiffening of certain beam or column members based on the differences between seismic and wind design can be used to achieve a certain amount of earthquake resistance in wind designed buildings.

1.2 Objectives

As the impact of individual extreme events on structural systems is increasingly studied and understood, it is important to begin expanding on the effects of multiple hazards on a system. Up to this point, the design of structures for high-wind and earthquake events has been conducted separately, even though the fact that both events induce horizontal loads indicates to an interaction between the components of each design. It is therefore reasonable to believe that there exist some components of the design that are redundant and others which may be incongruous. Currently, design codes specify that buildings be designed for either wind or seismic depending on which is the controlling load case, but there are no further design guidelines to consider the different requirements for the non-controlling load. Combining the design process for multiple hazards will allow for more efficient structures which resist both earthquakes and high-wind. The foremost objective of this research is to create a model of a mid- to high-rise building and to study its behavior under wind and seismic loads.

More specifically, the intent of this study is to:

1. Assess the response and damage to mid- and high-rise buildings in previous hurricane and earthquake events.
2. Define the characteristics of each hazard.
3. Develop a frame model that can be used to analyze building behavior.
4. Ascertain local, intermediate, and global demands for wind designed buildings and earthquake designed buildings which are complementary and contradictory.
5. Find the unintentional seismic resistance of the structure to the non-controlling load.

A greater comprehension of the response of mid- to high-rise structures to multiple hazards can be used to improve the design of structures subjected to strong earthquake and wind loads.

1.3 Thesis Organization

This thesis is primarily concentrated on the development of multi-hazard design for mid- to high-rise buildings. The goals of this study, provided in Section 1.2, will be covered within seven chapters. CHAPTER 2 is a literature review that discusses previously conducted studies on multi-hazard design. Research in the area of multi-hazard design is relatively limited; a majority of papers on the subject focus more on seismic retrofit than actual multi-hazard design, or are studying the increased risk for regions with multiple hazards with little structural design consideration. CHAPTER 3 describes the two types of natural disasters this study is concerned with, by investigating damage caused in previous hurricane and earthquake events. The chapter also explores the principal concerns in the design of tall structures in wind design and seismic design separately, paying special attention to limit state conditions. Detailing of the characteristics of each hazard and the factors that influence the distribution and scale of the loads are outlined. Simultaneously, the relationship between physical load characteristics and code based design load calculations are explained. CHAPTER 4 provides an in-depth description of the procedure and model development for this study. The modeling of a sample 47 story steel frame building, one designed for wind load and another for the design earthquake load, was done using the analysis program Zeus-NL. CHAPTER 5 is a definition of the earthquake demand used in this study, and contains explanations on how records used in analysis were selected and scaled. CHAPTER 6 includes the analyses performed using the Zeus-NL program to study the behavior of the models under the loads from the two hazards of interest. Through the performance of static constant load analysis, eigenvalue analysis, static pushover analysis, and dynamic time-history analysis, as well as a thorough examination of the resulting data, the differences between the models can be determined. CHAPTER 7 provides a summary of the conclusions made in this research and makes recommendations for future studies.

CHAPTER 2: LITERATURE REVIEW

This chapter presents the research and conclusions of previous studies in multi-hazard design. Among peer reviewed journal papers, there are very few previous studies in this field. Extensive research in this field mostly began within the last decade. The majority of the research that investigates multiple load loading conditions is concerned with coincident loads from a single hazardous event, such as strong wind and flooding from a hurricane, or seismic and tsunami impact loads from an earthquake. Even among multi-hazard design research, the specific areas of interest vary vastly from increases in probabilistic risk for structures in multi-hazard regions to recommendation on practices that assist in multi-hazard construction. The details of these studies are examined in this literature review.

2.1 Necessity of Multi-Hazard Design

Considerations for multi-hazard engineering emerged at the beginning of the twenty-first century when terrorism concerns raised the importance of designing buildings against blast loads as well as other natural hazards. Though the risk of blast loads for a typical structure is still relatively minor, the events of September 11, 2011 spurred interest in the field. Since loading from multiple hazards can result in conflicts in load demands on the structure, considerations for each of the differing loads must be considered. With regards to the architectural elements in a building, an example of conflicting demands would be the drop ceilings that are common in office buildings. The suspension of the ceiling tiles may be beneficial in terms of reducing seismic loads, but they become safety risks when blast pressures lift the tiles which then fall on the building's occupants (Ettouney and Glover, 2002). While not directly related to the multi-hazard design of structural systems, Ettouney and Glover in 2002 did present an argument for increasing research in the area of multi-hazard design of buildings.

In subsequent years, further studies continued to make the argument that multi-hazard design of tall buildings and bridges would be very beneficial for both costs and safety (Ettouney et al., 2005), but did not delve into studying the structural behavior of buildings. Ettouney and Sreenivas Alampalli, briefly expanded on the subject in 2006, to propose that

when considering the life-cycle costs of a building, multi-hazard design can be economical while meeting safety standards. They state that the complex nature of analyzing structures under multiple loads along with the unclear relationships between code standards and physical application make it a difficult field to investigate, but demonstrate that when the demands of the different loads are consistent, the costs of the building decrease. The consideration of multiple hazards in the initial design of a structure as opposed to retrofitting later on was also found to reduce the life-cycle cost of the structure (Ettouney and Alampalli, 2006). Although Ettouney and his co-authors did not develop methods in the structural design of buildings, they presented strong and valid arguments for the necessity of multi-hazard design.

2.2 Case Studies for Multi-Hazard Design

While the research conducted by Ettouney et al. from 2002 to 2006 centered on the motivations for structural design for multiple hazards, other studies attempted to demonstrate the applicability of multi-hazard design through specific case studies. Charleston, South Carolina is a region in the United States that is particularly susceptible to both hurricanes and earthquakes. Traditionally, the state used ASCE standards, and therefore the 130mph winds from hurricanes controlled most building designs. With the adoption of the International Building Code in 2004, the design seismic load was more than doubled, leading to a switch in controlling load case. Due to this increased seismic demand, existing structures required retrofit, and new buildings needed to be designed taking multiple loading cases into consideration (Mays, 2005). At the 2005 Solutions to Coastal Disasters conference, Dr. Timothy Mays presented two case studies: one of a new public school building, and one of a retrofit and addition to a medical center. From these case studies, it was demonstrated that design components for various single hazards can be combined in an economical manner to restrain building response for multiple load types.

For the design of Daniel Island Elementary and Middle School, the irregular shape of the building with two wings and large open spaces for the gymnasium and cafeteria led to the partitioning of the building using seismic separation joints. The isolation of the wings

reduces the damage from conflicting seismic responses of each section. Seismic loads were greater than wind loads for this structure, and resulted in the usage of separation joints, however the wind load controlled for the design of the exterior masonry shear walls. An additional concern with regards to multi-hazard loading was the design of the gymnasium and cafeteria. The gymnasium's 2-story exterior wall was four inches thicker than other walls in the structure to resist the increased base moment from wind loading, and a combined reinforced masonry-steel frame was required for the seismic lateral load resisting system (Mays, 2005). Figure 1 presents the finite element model for the masonry-steel frame. Inclusion of masonry walls in only the second story increases the stiffness of the wall for wind resistance, but limits the stress concentrations in the frame due to wall-frame interaction in earthquake events. The manner in which the engineers approached the design of the school was by judging the controlling load for building elements separately instead of designing the entire structure for only one load or the other. By breaking the structure down into specific elements, the completed design can resist multiple hazards and has components like exterior shear walls that resist wind loads and interior combined reinforced masonry-steel frames to resist seismic loads.

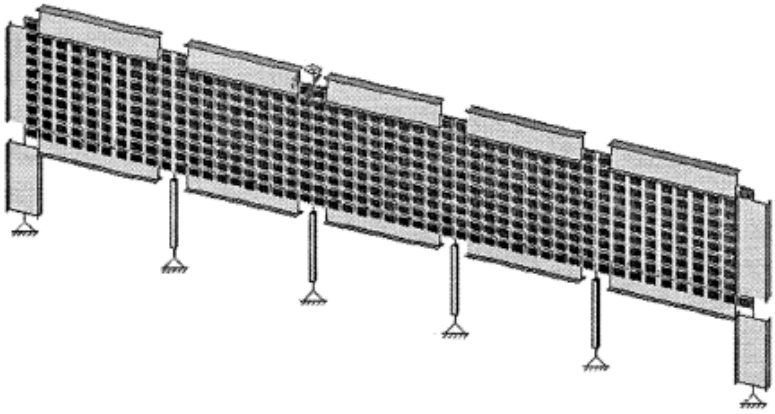

Figure 1. Finite Element Model of Combined Reinforced Masonry Steel Frame Seismic Resisting System (Mays, 2005)

For the second case study, the McLeod Regional Medical Center was not a multi-hazard design, but a retrofit of a wind designed building for new seismic load requirements. The adoption of the IBC in 2004 required the medical center to be designed for earthquake

loads three times greater than the loads it was initially designed for. Due to the increased loads, the lateral load resisting system of reinforced concrete shear walls was insufficient and needed to be retrofitted. The lateral load resisting system was reinforced with thin steel plates bolted to the shear walls. The base plates of the structure were also detailed to resist the increase in overturning moment from seismic loads (Mays, 2005). The only multi-hazard design procedures exhibited by this case study was that the building was converted from a wind-resistant structure to a seismic resistant structure through the stiffening of shear walls and shoring up of base connections.

Through these two examples, Mays presented detailed design concerns for each particular structure. The case studies are useful in demonstrating the procedure and points of interest in multi-hazard design, but the buildings are too irregular for their design characteristics to be applicable on a wide scale. Although this thesis focuses on the specific case of a 47 story steel frame building, the structure is regular enough that the results of the analyses can be applied to a range of mid- to high-rise buildings.

2.3 Guidelines for Multi-Hazard Design in Low-Rise Structures

Each of the preceding studies and papers reviewed provided arguments for the necessity of multi-hazard design and a few recommended possible avenues of research to improve the design of such buildings; however none set clear recommendations that can be applied to current construction practices. Only Dr. Rima Taher, who wrote a paper detailing suggestions for improving building construction for Architecture for Humanity after the Haiti earthquake in 2010, laid out a set of general guidelines for multi-hazard design. Many of Taher's recommendations relate to building shapes and construction practices for low-rise structures no taller than a couple stories, but the purpose of his research is similar to that of this thesis: to identify specific areas of improvement in structural design to aid in resisting the effects of both wind and seismic hazards (Taher, 2010).

As the function of Taher's 2010 paper was to provide a simple-to-understand list of guidelines, many of his suggestions were not fully detailed in terms of structural engineering methods. Nevertheless, the general recommendations relating to building

forms, roof shapes and slopes, construction materials and methods, foundations, jobsite safety, and sustainability are useful for furthering the use of multi-hazard design in common practice (Taher, 2010). While all the guidelines set by Taher are useful, the sections concerning building forms and roof shapes are the most relevant to multiple-hazard design, the first addressing seismic resistance, and the second addressing wind resistance.

With regards to building forms, the guidelines include:

1) Use regular building shapes without changes in geometry or stiffness, and/or seismic isolation of sections.
2) Limit the inclusion of large openings in diaphragms and shear walls.
3) Avoid placing large loads at higher building levels.
4) Use diagonal or chevron bracing (Taher, 2010).

The building form guidelines are generally for seismic resistance, with the first recommendation used to limit torsion and large conflicting deflections in building sections, and the second to maintain consistent load transfer through the building. The third is to prevent excessive loading on the top floor that would result in greater overturning moment, as seismic loads are proportional to mass. Additionally, the use of bracing in lateral load resisting systems was suggested to increase stiffness in first floors to prevent a soft story. In terms of limiting wind effects, optimal roof shapes were suggested.

Designing for wind resistance, Taher's guidelines for roof shapes include:

1) Having hip roofs with four sloped sides is better than two-sided gable roofs in hurricane events.
2) Use the optimal roof slope of approximately 30 degrees.
3) Include openings in negative wind pressure regions on the roof.
4) Structurally isolate the two parts of double-span roofs.
5) Use roof edge treatment systems (Figure 2).
6) Limit lengths of roof overhangs (Taher, 2010).

The use of hip roofs, optimal roof slopes and roof openings reduces the uplift forces due to wind pressures and limits the imbalance of pressure between the interior and exterior faces of the roof. Structural isolation of the two halves of double-span roofs is necessary to prevent progressive collapse. With regards to the roof edges, treatments developed by the Centre Scientifique et Technique du Bâtiment (CSTB) center in France reduces local pressures by disturbing air flow at edges.

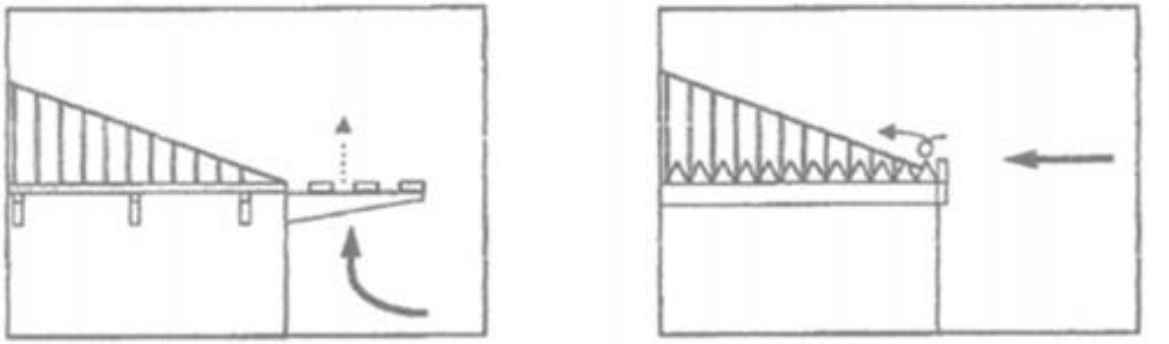

(a) Horizontal Grid Overhang **(b) Notched Frieze Along Perimeter**

Figure 2. Roof Treatment Systems suggested by CSTB (Taher, 2010)

These guidelines are certainly useful for the construction of low-rise structures, however the concerns for high-rise structures in wind events are different, and therefore these wind resistance suggestions would not be applicable for mid- to high-rise structures.

2.4 Risk in Multiple Hazard Regions

In an article written for the Journal of Structural Engineering in March of 2010, Dr. Dat Duthinh and Dr. Emil Simiu of the National Institute of Standards and Technology (NIST) presented a study of the increased risk of limit state exceedance for regions subjected to multiple hazards when compared to regions with risk of only one hazard (Duthinh and Simiu, 2010). The premise upon which Duthinh and Simiu base their 2010 research on is that the United States' ASCE 7-05 design code treats regions affected by wind and earthquake separately, considering only the dominant loading in the design (ASCE, 2006). This premise is the same as the motivation for this thesis. However, the study performed at

NIST examines the effect of multiple hazards on the probability that limit states would be exceeded and not specifically on the structural behavior of buildings.

Duthinh and Simiu's argument is that since the ASCE 7-05 standards includes considerations for risk due to hazards based on a region's susceptibility to each hazard implicitly, neglecting to consider the sum of the risks for region for two hazards is an oversight. From a probability standpoint, they argue that the risk of wind loads greater than design wind loads developing and the risk of seismic loads greater than design seismic loads developing should be combined to determine the total risk of limit state exceedance. Even though the two hazards result in different types of loading and different types of damage, a structure within a region with overlapping hazards is still at risk for both and should be designed taking the increased risk into consideration. There have also been arguments that since the probability of both hazards occurring simultaneously is negligible, only the greater demand needs to be satisfied. This is invalid because while the physical stress on the structure does not increase for a multi-hazard region, limit states specified by the code are not solely dependent on the load demand, but also depend on the probability of the load occurrence. To resolve this problem of increased risk for multi-hazard regions, Duthinh and Simiu proposed to modify ASCE 7-05 standards so that areas with both wind and earthquake hazards can be designed separately with corrected limit states so the risks in that region are similar to areas subjected to only one hazard. Since the mean recurrence interval for the combined events is shorter than that of the separate events, the study proposed to increase the load factors for both wind and seismic design loads to maintain a consistent level of safety across regions (Duthinh and Simiu, 2010).

In a subsequent publication in 2011, Crosti et al. expanded on the 2010 study by quantifying the risks of a specific value of drift for structures in multi-hazard regions. Through a case study on the behavior of a 10-story steel frame, the effects of multiple hazards on the mean recurrence interval (MRI) as well as the effects of different structural configurations were evaluated and compared. The second portion of the study is a comparison of the structural behavior of two connection types: a welded unreinforced flange, bolted web (WUF-B) and a reduced beam section (RBS). For both structural

configurations, the MRI of each individual hazard was determined, and then used to calculate the multi-hazard MRI. The individual MRIs were determined based on the ASCE 7-05 design 3-second gust wind speed maps and Maximum Considered Earthquake (MCE) maps and then adjusted by accounting for subsequent importance and safety factors. Using basic probability calculations with the equation shown, the MRI of the combined hazards was then determined (Crosti et al., 2011)

$$P[\max(\delta_1, \delta_2) \leq \delta_L] = P(\delta_1 \leq \delta_L)\, P(\delta_2 \leq \delta_L) \quad (1)$$

where

δ_1 = drift for event 1 (wind design)

δ_2 = drift for event 2 (seismic design)

δ_L = limiting drift

The results of the study with the return periods for seismic, wind, and multi-hazard structures in the conducted case study were compiled in the table below.

Table 1. MRI under Single and Multiple Hazards (Crosti et al., 2011)

		Mean Recurrence Interval, MRI		
Connection Type	Lateral Drift (m)	Seismic (years)	Wind (years)	Wind or Seismic (years)
WUF-B	0.292	2,500	1,830	1,060
RBS	0.322	2,500	1,720	1,020

As shown in the table, the MRI for a structure subjected to multiple hazards is significantly lower than the structure under either of the single loads independently. While it is reasonable to expect that the MRI is lowered for multiple hazards, it is important to note that this is a conservative estimate. This is because the multiple-hazard MRI is based on the assumption that both events are completely independent of one other, and although the input loading from the wind and seismic hazards are independent, the effects of the loads, i.e. the damage to or deterioration of the structure due to the hazard, are not (Crosti et al.,

2011). Based on the conclusions of the research of Crosti, Duthinh and Simiu on the matter of increased risk in multi-hazard design, it is clear that ASCE 7-05 needs to be adjusted in order for structures under the combined hazards of wind and earthquake to meet the levels of safety set for the design for single hazards.

2.5 Summary

With the field of multi-hazard design still in its first decade, there are few studies solely based on the subject; but, from the ones conducted thus far, it is clear that further investigation is necessary. Ettouney and his co-authors in the three papers they published in 2002, 2005, and 2006, discussed the growing concern for the design of structures for blast loads. With an understanding that to design structures solely for blast resistance and ignoring the effects of natural hazards would be negligent, but that combining multiple hazards in a load case would be overly conservative, Ettouney was among the earliest proponents for the necessity of multi-hazard design.

In case studies of structures designed and retrofitted in Charleston, South Carolina, Mays in 2005 explained the still informal process of multi-hazard design, demonstrating that the combination of wind and seismic design components is both attainable and effective. In 2010, Taher created a more generalized set of recommendations regarding the design of low-rise structures to resist multiple types of loading. Particularly concerned with the design of houses in underdeveloped countries where design standards are rarely enforced, Taher's research focused on setting guidelines and recommendations for construction practices that would assist in the fortification of non-designed buildings for multiple hazards.

Perhaps the most similar to this thesis, Simiu, Duthinh and Crosti in 2010 and 2011 attempted to make suggestions to changing ASCE standards to account for the effects of multiple hazards. However instead of investigating the structural behavior of buildings, they contended that since code defined limit states consider the probability of occurrence of the hazard, the increased risk to buildings in multiple hazard regions must be accounted

for. Their conclusion was that by redefining design loads through the MCE seismic maps and wind speed maps so that they were adjusted based on probability of the region being exposed to multiple hazards, multi-hazard design can be achieved. Though the authors of the presented literature all approach the issue of multi-hazard design differently, they are all in agreement that the current procedure of designing for only the controlling load case is no longer sufficient for structures subjected to more than one hazard.

CHAPTER 3: HISTORY AND CHARACTERISTICS OF HURRICANES AND EARTHQUAKES

In order to fully develop a method to multi-hazard design, a complete understanding of hurricanes, earthquakes, and their characteristics must be developed. This chapter explores the factors that influence each hazard in order to understand how design loads and limit states are defined, beginning with a survey of damage to mid- to high-rise structures in previous wind and seismic events. Although hurricane level winds rarely cause catastrophic structural failure in mid- to high-rise buildings, considerations must be made for occupant comfort, as persistent high winds may cause substantial lateral deflections. The serviceability limit state is often the controlling condition for wind design; regardless of whether or not the building is structurally sound, if the building is not serviceable, it is not marketable and therefore not economical. Comparatively, since earthquakes are relatively rare events when compared to annual hurricane seasons, serviceability is less of a concern. Life safety balanced with the economic costs with regards to restoration is often what controls seismic building design. A thorough comprehension of the individual hazards is necessary to the effectual design of a structure for multiple hazards.

3.1 Building Behavior in Previous High Wind Events

Hurricanes, also known as typhoons, are large rotating storm systems with a low-pressure center that form over water in the Atlantic Ocean off the east coast of the United States and Gulf of Mexico, or in the Pacific Ocean off the coast of eastern Asia. These storms are characterized by high winds and heavy rains, and both can cause significant damage to built structures. Flooding due to hurricanes can be a significant hazard, which was demonstrated in Hurricane Katrina where the most casualties were caused by the flooding in New Orleans, Louisiana after the levees failed. Thus, although high winds are not the only damaging characteristic of hurricanes, the focus of this section is on the behavior of tall buildings under wind loads and the effects of flooding and storm surges will be ignored when categorizing previous wind events. This is in order to establish the influence of high wind on building behavior.

Because hurricanes cause limited structural damage to high-rise buildings, the focus of damage assessments and reconnaissance studies is typically on the greater and more widespread damage to low-rise structures. Nevertheless, even though life safety is not a primary concern in wind design of high-rise structures, the design of structures for high wind is important from a serviceability and economic standpoint. In addition to limiting drift for occupant comfort, designing the structure and cladding to withstand wind pressures is important as wind speeds from hurricanes increase with height. The significant pressure differences between the interior and exterior of high-rises result in the most common form of damage in tall buildings, which is blown-out windows. Not only does the glass become dangerous debris for surrounding structures, but with the windows gone, high winds can cause significant damage to the interior of the building. Though they are non-load-bearing elements of the structure, damage to partitions and ceiling features can be costly to repair and replace. Examples of damage to buildings due to high winds in previous hurricane events in the last twenty years are shown through the photographs below.

Figure 3. Burger King Headquarters' CEO office in Miami after Hurricane Andrew (NHC, 2010)

The figure above is from Hurricane Andrew, a Category 5 hurricane on the Saffir-Simpson Hurricane Scale (SSHS) that made landfall near Miami, Florida on August 24th, 1992. The third costliest hurricane with $29.5 billion in damage (unadjusted for inflation) Hurricane Andrew is an example of a hurricane event that had significant wind speeds and resulted in costly destruction (Blake et al. 2011). With the eye of the storm passing less than 20 miles south of downtown Miami, the city recorded a maximum sustained 1-min surface wind speed of 62 m s^{-1}, or 138 mph, at landfall (Powell and Houston, 1996). Since wind speeds

tend to increase with height, the wind speeds for high-rise buildings can be assumed to be greater than 138 mph (NHC, 2010). Figure 3 shows the damage to the interior of the Burger King Headquarters due to high winds. Though the majority of the $10 million in damage to the headquarter building was due to a 16.9ft storm surge (Rappaport, 1993), high winds also caused a significant amount of damage.

With one of the highest wind speeds of hurricanes in recent history, the substantial wind damage caused by Hurricane Andrew was expected. However, the same type of damage, where windows are blown out for mid- and high-rise structures were evident in other hurricanes where wind speeds were not as high. Figure 4 displays examples of damage caused in different category hurricanes; the same form of damage is present for hurricanes greater than Category 3.

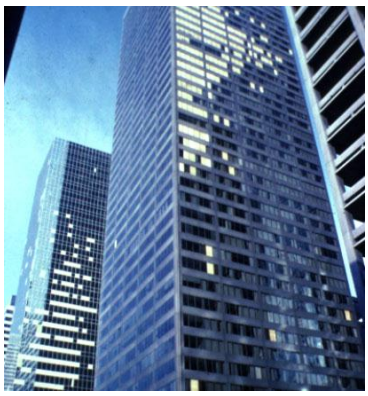

(a) Hurricane Alicia (Category 3) – Houston, TX in 1982

(b) Hurricane Andrew (Category 5) – Miami, FL in 1992

(c) Hurricane Wilma (Category 5) – Miami, FL in 2005

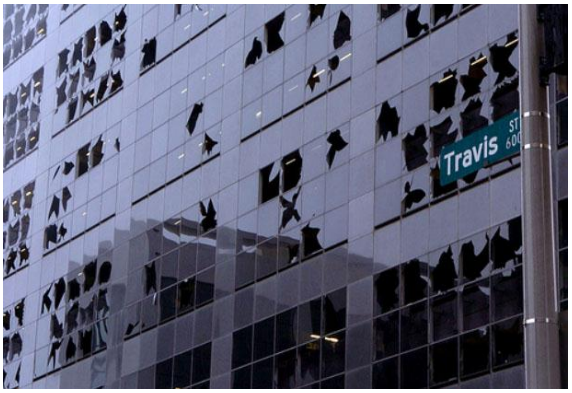

(d) Hurricane Ike (Category 4) – Houston, TX in 2006

Figure 4. Wind Damage to Mid- and High-Rise Buildings (Beers, 2011)

Although the predominant damage caused to high-rise buildings in hurricanes is not structural, the economic and social impacts of high wind events are still of great consequence.

3.2 Building Behavior in Previous Earthquake Events

Damage to buildings from earthquakes is often due to the primary effect of structural failure due to ground acceleration. From observations of previous earthquakes, however, it is clear that ground shaking is not the only damaging characteristic of earthquakes. Depending on the location of the earthquake, as well as the magnitude, earthquakes can lead to secondary effects such as tsunamis or fires. Tsunamis are large waves caused by the displacement of water when a subduction earthquake occurs below an ocean, and can cause significant damage from both the impact of the wave and the subsequent flooding. The tsunami from the 2004 Indian Ocean earthquake off the western coast of Indonesia resulted in nearly 230,000 confirmed casualties; and, the tsunami due to the 2011 Tohoku Earthquake caused more damage than the ground shaking did (Bertuca, 2011). Ruptured gas lines or fallen stoves combined with broken water lines for fire hydrants due to ground displacement leads to uncontrollable fires that can burn for days. For example, the Great San Francisco Earthquake in 1906 resulted in a fire that burned for three days and, in the 1923 Great Kanto Earthquake in Japan, more casualties were due to fires than building collapse (Goltz, 1995). The secondary hazards resulting from earthquakes are by no means minor, however, for the purpose of this study the focus of this section will be on the response of buildings to only the primary ground motion effect of earthquakes.

While the specific mode of failure of tall buildings varies significantly with duration and characteristics of the load, there are certain collapse mechanisms that engineers design against. Extensive study in the field of earthquake engineering and lessons from previous events in the last few decades have led to improved seismic design and reduced the amount of significant structural damage to tall buildings. Common forms of structural damage due to seismic events include X-shaped cracks in walls, cracking of concrete, reinforcement pull-out, buckling or shear failure of beam and column members, and connection

deformation (Elnashai and Di Sarno, 2008). In addition to local failures, there can be frame failures such as soft stories where a single floor of the building collapses due to the reduced stiffness of that level when compared to other levels. Soft story collapse is particularly common in low- to mid-rise buildings and often occurs in the first floor where commercial spaces require greater floor heights or column spacing, although it can occur in other floors with these similar characteristics. Figure 5 includes examples of soft story collapse in various earthquakes.

(a) 1995 Kobe Earthquake (Braile, 2003)

(b) 1971 San Fernando Earthquake (Faison et al. 2004)

(c) 2001 Gujarat Earthquake (SED, 2011)

Figure 5. Soft Story Collapse

Building collapse can also occur in the form of progressive failure, "pancaking," and overturning due to inadequate foundations or liquefaction. Progressive failure develops when the failure of a single section of a structure leads to the collapse of a significant portion of the building due to lack of redundancy. In the 2001 Gujarat Earthquake, the left side of an eleven story apartment building was completely destroyed when the first floor soft story was heavily damaged as shown in Figure 6. The "pancaking" of floors is the most typical mode of failure and is caused by column elements failing before beam elements. The weight of upper floors landing on the ones below them leads to the building collapse. Figure 7 displays two examples of this behavior.

Figure 6. Progressive collapse of left side of building (SED, 2011)

(a) 2009 Sumatra Earthquake (AP, 2009)

(b) 2010 Haiti Earthquake (Lorant, 2010)

Figure 7. Pancake collapse of buildings.

Taller buildings can also fail due to overturning, though it is not as common as the pancaking mode of failure. The overturning of the entire building onto its side without initial catastrophic damage to the intermediate levels of the building is relatively rare; however, it can occur due to a few causes. First, weak foundation to superstructure connections can be easily damaged in an earthquake, so that ground motions result in uplift of the superstructure at the foundation connection, which, if large enough, can lead to complete overturning of the building (Jayachandran, 2009). Discontinuations in the support system on one side of the structure, close to the base of the building, as exemplified by the 15 story Alto Rio apartment building in Concepción, Chile (Figure 8) from the 2010 Chile Earthquake can also be a cause for overturning (MAE Center, 2008).

Figure 8. Alto Rio condominium in Concepción (MAE Center, 2010)

Another cause is liquefaction where increased pore water pressure due to the earthquake results in the soil beneath structures losing stiffness, allowing buildings to sink. Long duration earthquakes combined with saturated soils increases the possibility of liquefaction occurring (Elnashai and Di Sarno, 2008). Although liquefaction often results in different types of structural damage and not always complete collapse, during the 1964 Niigata Earthquake, multiple apartment buildings suffered overturning due to liquefaction as shown in Figure 9.

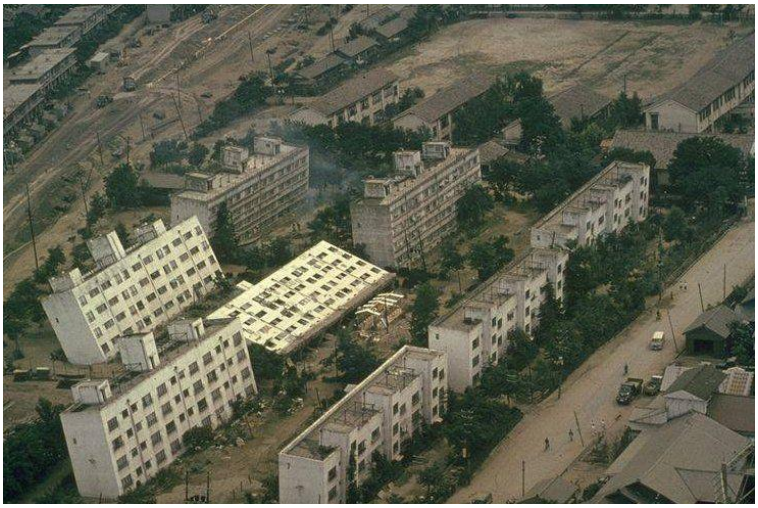

Figure 9. Collapse due to Liquefaction (Isaradharm, 1997)

In the most recent 2011 Tohoku earthquake in Japan, all of Tokyo's high rise buildings escaped without any structural damage. Due to Japan's stringent seismic design code, which requires time-history analysis and engineering peer review for buildings over 60m, and proper design and construction practices, no structural damage was reported in any of the tall office and apartment buildings in downtown Tokyo. There were reports of non-structural damage, as significant side to side swaying of high-rises during the earthquake was observed, but other than the loss of serviceability due to damage to building systems like water and electricity, and entangled elevator cables, the impact of the Tohoku earthquake on tall buildings was minimal (Taylor, 2011). Compared to the response of mid- and high-rise buildings in previous earthquakes, the behavior of Tokyo's high-rises in this case was viewed as a success in structural engineering, especially when the input motion is taken into consideration.

The specific details with regards to earthquake characteristics will be further explained in ensuing sections, but for the Tohoku Earthquake, a subduction zone earthquake, its long period-long duration traits often cause greater damage to high-rises than low-rises (Taylor, 2011). This is because the high period of the earthquake resonates with the natural periods of tall buildings. Larger durations are also expected to result in greater damage as the structure is subjected to high accelerations for greater periods of time (Lorant, 2010). Figure 10 compares the Tohoku earthquake's ground motion to previous earthquakes.

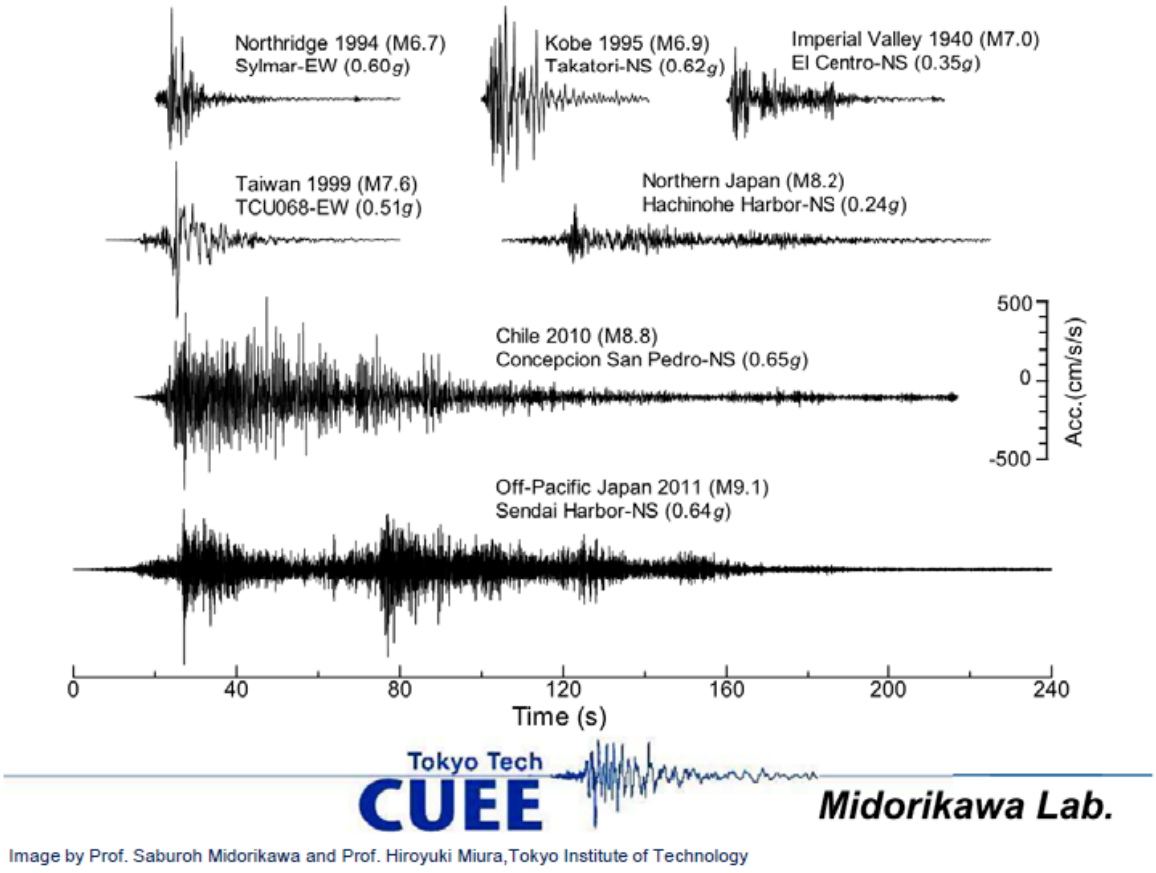

Figure 10. Ground Acceleration Record Comparison (Taylor, 2011)

Prepared by Professors Saburoh Midorikawa and Hiroyuki Miura of the Tokyo Institute of Technology, the figure shows the Tohoku ground acceleration record recorded at Sendai Harbor compared to other notable earthquakes. The fact that all of Tokyo's high-rises avoided structural damage, given the type of input motion, is a noteworthy feat that demonstrates the substantial advances in earthquake engineering in recent decades.

3.3 Wind Load Characteristics

The characteristics of wind loads on a local scale are always consistent; the movement of air has kinetic energy which is transferred to structures via air pressure upon contact with structures. On an overall structure scale, the manner and scale in which wind loads affect a building depends heavily on multiple factors, some which are considered in design codes explicitly, and others which are included implicitly through scaling factors. The factors

that influence wind loads include, air density, wind velocity, wind direction, structure shape, and structure stiffness (Yang, 2006).

Of the five factors that are considered in the calculation of wind loads, air density is the only one that is considered as constant across all structures. The factor is included in the wind design calculation simply through the use of Bernoulli's equation for fluid flow as shown in the equation below.

$$q = \tfrac{1}{2}[\rho V^2] \tag{2}$$

where

q = static wind pressure

ρ = mass density of air

V = wind velocity

Within the ASCE 7-05 code, the static wind pressure (q_z) is defined by a version of Bernoulli's equation that takes air density as a constant. For a static wind pressure in English units (psf) and input wind velocity in miles per hour, the coefficient representing the $\frac{1}{2}\rho$ portion of Bernoulli's is 0.00256. While it does fluctuate with temperature, humidity and altitude, the changes are small enough that further correction factors are not required. Below is ASCE code equation for velocity pressure which varies along the height of the structure (z).

$$q_z = 0.00256 K_z K_{zt} K_d V^2 I \tag{3}$$

where

q_z = velocity pressure at height z above ground, lb/ft^2

K_z = velocity pressure exposure coefficient at height z

K_{zt} = topographic factor

K_d = wind directionality factor

V = wind velocity, mph

I = importance factor

In addition to the constant air density, the code definition of static wind pressure also has multiple coefficients that adjust for differences in exposure, topography, direction, and building importance. Given the complexity of actual wind movement, the wind design chapter of the ASCE 7-05 standards uses a simplified method − Section 6.5 Method 2-Analytical Procedure − to evaluate the contribution of each factor. Each of the five factors influencing design wind loads are incorporated into the code through the use of the coefficients in the ASCE velocity pressure (q_z) or through the gust effect factor (G).

The next two components that contribute to wind load definition are wind velocity and wind direction. Clearly, higher wind velocities result in greater loads, as the kinetic energy of the moving air is directly related to the square of the velocity. Wind direction on the other hand is, for the most part, unpredictable. Since changes in direction alter how wind load is applied, for a conservative building design, wind direction in design wind load is represented by loads calculated for the weak direction of the building. Within ASCE 7-05, wind velocity and direction are accounted for through multiple coefficients and factors.

Wind velocity and direction are somewhat linked, with respect to how they are included in the code and how the physical loads are shaped. For wind velocity, there are multiple elements including geographic location, topography and building height that govern its magnitude. The geographic location of the building is the principal element that determines wind velocity. The basic wind speed (V) is determined using maps where the design 3-second gust wind speeds, 10m above the ground for the standard exposure, Exposure C, are labels for the map contour lines. The height and exposure where wind speed is measured is defined, not only to create a standard across geographic locations that represent the wind speed with 2% probability of exceedance per year, but also to have a standard that can be easily adjusted for different heights and exposures. For wind direction, an element that controls wind direction in addition to velocity is building exposure.

A topographic factor (K_{zt}) accounts for how wind velocity increases for buildings on isolated hills and ridges. Building height also influences wind velocity, as it increases with height, as displayed in Figure 13. For basic wind load calculations, the exposure, or the

influence of surrounding structures on the building being designed, is defined according to four categories. These categories, also shown in Figure 11, range from flat, unobstructed areas in Exposure D, to suburban and urban areas in Exposures B and A (ASCE, 2006). The exposure categories are applied in the wind load calculations through the use of different velocity pressure exposure factors (K_z) for different exposures.

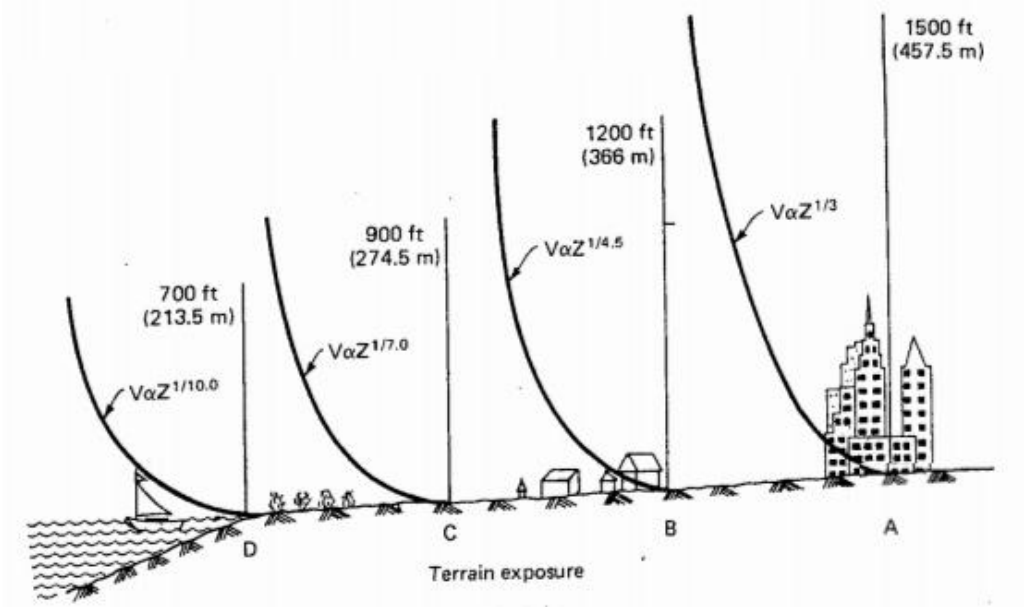

Figure 11. Variation of wind velocity with exposure and height (Yang, 2006)

While exposure does affect wind direction, it is difficult to account for the variations simply based on the definition of "urban" as in the ASCE standards. As changes in wind direction do not have as significant an impact as changes in wind velocity because of the conservative design of buildings, the directionality factor (K_d), which account for changes in direction due to building type, is only required for certain load combinations. Only for extremely sensitive or important structures like iconic skyscrapers, should the exact effects of the case specific exposure be evaluated. In wind tunnel tests, the inclusion of models of surrounding buildings and their locations relative to the building being tested are extremely important for the accurate evaluation of wind loads on the structure. Figure 12 demonstrates how the distance between a building, represented by the square object, and an obstructing building, represented by a small cylindrical rod, can alter the air flow around the second, square building.

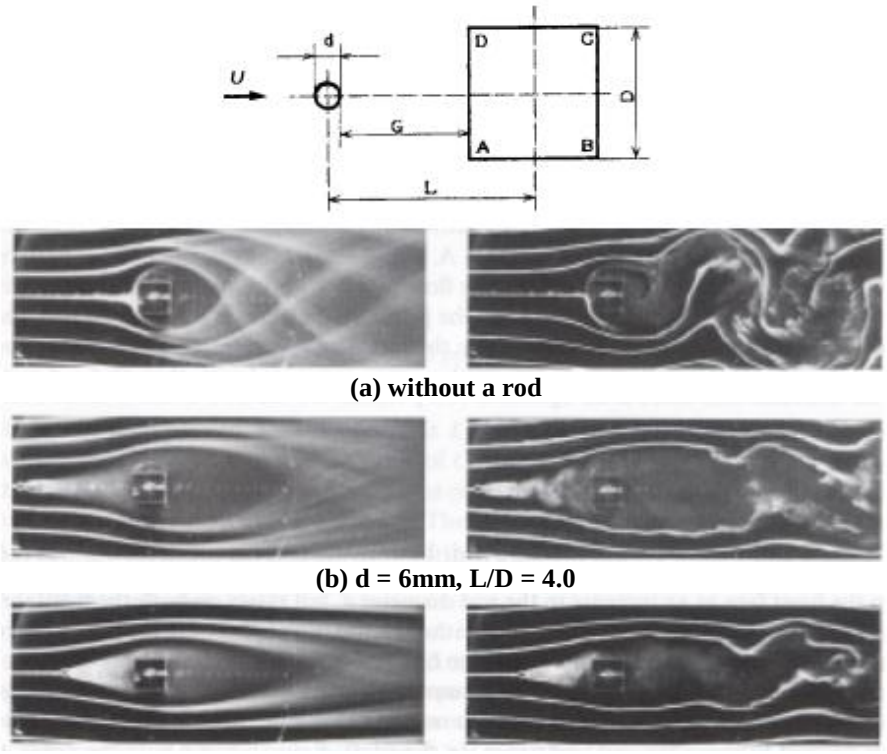

(a) without a rod

(b) d = 6mm, L/D = 4.0

(c) d = 6mm, L/D = 2.67

Figure 12. Changes in flow patterns around square object due to small rod upstream (Buresti, 2000)

Structural shape, with regards to both the general profile in terms of the length-to-width aspect ratio in the direction of loading and the height, along with more specific building and façade details, can significantly change the pattern of wind loading due to changes in turbulence and air flow around the building form. Bluff-body aerodynamics is the branch of study that investigates the behavior of air around a non-streamlined object. As shown in Figure 13, bluff-body objects cause separated air flows that do not follow the surface of the object and result in vortex generation. The vortices created differ for varying shapes and direction of air flow; different vortices cause different magnitude and patterns of wind load on the object. Since streamlined-body aerodynamics is dependent on direction of air flow and the direction of wind is completely variable for any structure at any given time, all buildings are considered to be bluff-bodies (Buresti, 2000).

The air flow around a three-dimensional bluff-body is exceedingly complex as demonstrated through the diagram in Figure 14, and the exact forces on the objects can only be determined through the use of the Navier-Stokes equations or air tunnel

experimentation (Buresti, 2000). Requiring only the mean roof height (h), horizontal dimension of the building normal to wind direction (B), and horizontal dimension of the building parallel to wind direction (L) (ASCE, 2006), the code accounts for the basic structure shape without requiring complicated analyses.

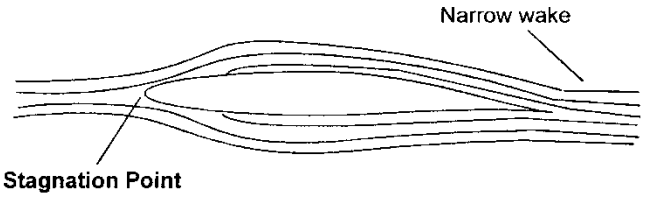

(a) Streamlined-body aerodynamics

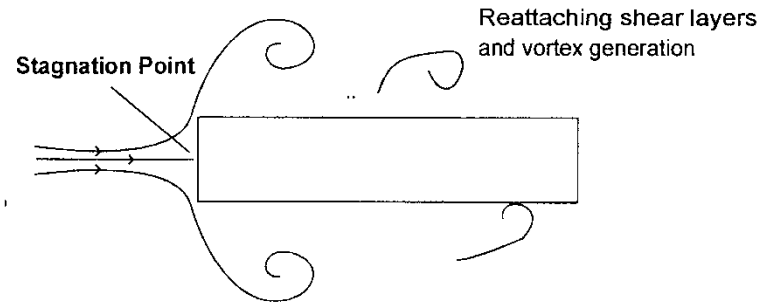

(b) Bluff-body aerodynamics

Figure 13. Comparing bluff- and streamlined- body aerodynamics (Holmes, 2003)

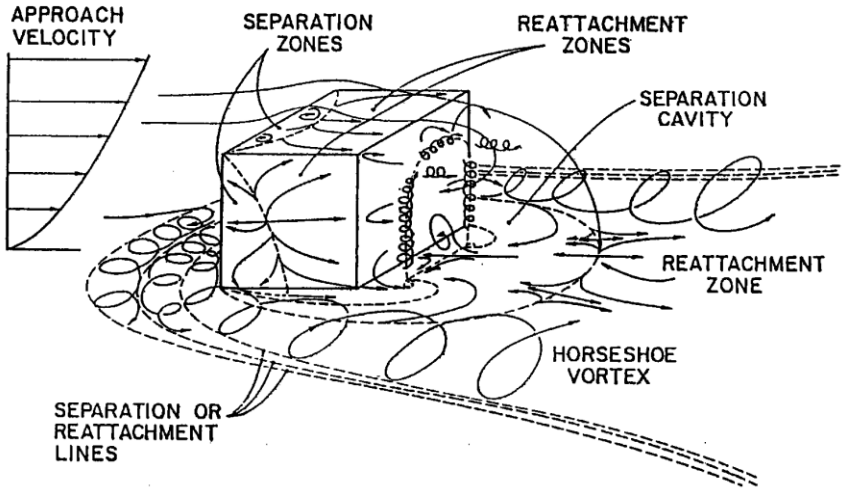

Figure 14. Schematic flow field around a three-dimensional bluff body (Buresti, 2000)

For buildings of great height or importance, wind tunnel testing is used to obtain a more precise understanding of the wind loads. In the case of the Taipei 101, built in Taipei, Taiwan and completed in 2004, the wind tunnel testing led to the determination that by adjusting the details of the shape of the building's corners, the crosswind excitation could be limited. Crosswind excitation is primarily caused by vortex shedding, with the vortices exerting horizontal loads on the sides of the building, alternating from one side to the other (Yang, 2006). By changing from sharp to saw-tooth notched corners, which interrupt vortex formation, the wind load was considerably reduced (Joseph et al. 2006). The specific geometry of buildings on both local and global scales greatly effects wind load.

It is also important to consider the structure stiffness when evaluating the wind load. The manner in which the building deflects due to external wind pressure alters the creation of turbulence in the air flow; decreasing stiffness allows for more severe vortex shedding, and therefore, greater wind pressure and crosswind excitation. In addition to increased crosswind loads from vortex shedding, reduced stiffness also results in greater design wind loads due to greater dynamic response. Resonance of the building with the frequency of vortex shedding begins to occur as the higher building natural frequency is decreased and approaches the lower frequency of shedding (Boggs and Dragovich, 2008). In order to limit both the magnitude of load, as well as the response of the building with regards to tip deflection, greater stiffness is required.

As building stiffness and shape are both factors that greatly influence vortex generation, they are closely related in their inclusion in ASCE 7-05. In the Analytical Method, both factors are accounted for through the inclusion of the structure's natural frequency and dimensions in the gust effect factor (G) (ASCE, 2006). While the previously defined velocity pressure (q_z) is the component of design wind load that considers the characteristics of the wind, the gust effect factor (G) incorporates the characteristics of the structure and its dynamic response into the design wind load.

Although it is not a physical attribute of the wind or the structure, the importance factor (I) is essential in the scaling of the design wind load. The remaining component of the

velocity pressure equation, the importance factor assigns an additional factor of safety based on the desired risk to buildings of different natures of occupancy and use. The factors that influence wind loads introduced in this section do not present all the details and variability in actual wind behavior, but this explanation of air density, wind velocity, wind direction, structure shape, and structure stiffness, and how they are represented in design codes is a sufficient foundation for multi-hazard design.

3.4 Earthquake Load Characteristics

In order to acquire a complete understanding of the characteristics of seismic loads and how they are evaluated for the purposes of design, the sources of an earthquake must first be established. Defined as the ground shaking due to rapid energy release from the Earth's crust, earthquakes can be activated by natural or man-made events. Naturally instigated earthquakes are caused by the movement of tectonic plates against each other; for inter-plate earthquakes, two plates move against each other until the boundaries catch due to some obstruction, building up stress until it is released in the form of an earthquake. Earthquakes within plates, or intra-plate earthquakes, can occur naturally due to compressive stress transferred from plate boundaries, but they can also be prompted by human activities, such as mining (Elnashai and Di Sarno, 2008). Recently, it has been suggested that small earthquakes in the Ohio region are linked to the process of hydraulic fracturing to extract natural gas (Joyce, 2012).

Whether natural or man-made, ground motion due to earthquakes is entirely unpredictable, with regards to when it occurs, where it occurs and how it occurs. At most, hazard estimations based on location relative to known fault lines and previous earthquakes can be used to predict the potential seismic load for a structure. There are also many intra-plate fault lines that are yet to be discovered and located. Because of this variability, a significant component of the seismic design code is probability and risk based, and cannot be directly translated to physical characteristics of the load. While complex and important structures are often designed using time-history analysis in order to better account for earthquake load effects, the ASCE 7-05 standards only requires the use of simplified

methods. For the design of the model in this study, the seismic design load is calculated using the Section 12.8 Equivalent Lateral Force Procedure within ASCE 7-05. Though not explicitly stated in code standards, the primary factors that influence earthquake load on a structure are the earthquake magnitude, source mechanism, distance to the source, local site conditions, building stiffness, building mass and lateral load resisting system.

One of the most irregular aspects of earthquakes, magnitude is a measure of the size and strength of an earthquake. There are several scales that have been used in the past, however, the current standard and most popular scale is the moment magnitude (M_w). Unlike other scales which typically determine the size of an earthquake based on the amplitude of ground motion waves, the moment magnitude is a function of the size and movement of the fault rupture (Elnashai and Di Sarno, 2008). By that definition, the moment magnitude is a measure of the energy released by the fault which is a more direct and accurate scale for the strength of an earthquake. Since a greater amount of energy generated by an earthquake is directly related to a greater level ground shaking and therefore loading on a structure, the magnitude is one of the most important characteristics of an earthquake with regards to building design.

Earthquake source mechanisms, or the manner in which tectonic plates move with respect to one another, also contribute to variability in earthquake load. Different mechanisms produce different seismic waves and therefore different ground motions. There are dip-slip faults where plates move vertically against one another, strike-slip faults where plates move laterally against one another, and those in between which can be either normal faults or reverse faults. Normal and reverse faults are dip-slip faults, which move against each other along a non-vertical plane. If the overhanging plate moves down, it is a normal fault, and if it moves up, it is a reverse fault. In all cases, earthquakes occur, not due to the gradual sliding of the plates against each other over time, but due to sections of the plates getting caught and releasing the stress build-up when the "caught" sections fail. The source mechanism when this energy release occurs determines if the energy is dispersed in more vertical seismic waves or horizontal seismic waves.

The distance between a building site and the source is also a critical factor, as the shorter the distance, the greater the ground motion expected at the site. This is due to the way earthquake stress waves disperse from the source or epicenter. While the waves propagate through the ground away from the source, they release energy in the form of ground motion; so the further a source is from the site, the less ground motion is experienced due to the seismic waves losing energy as they travel.

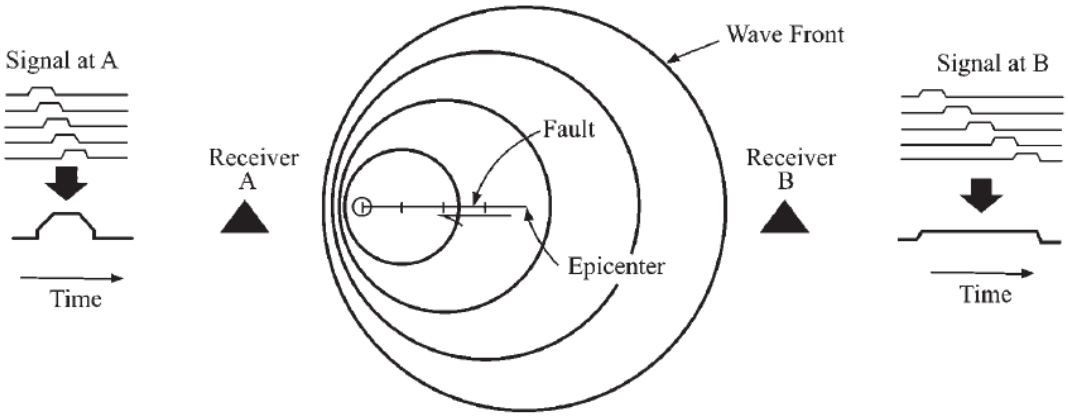

Figure 15. Directivity effects on sites in different locations (Elnashai and Di Sarno, 2008, adapted from Singh, 1985)

An additional feature of ground motion that is also related to the position of the site relative to the source is from the directivity of the earthquake. Above, Figure 15 illustrates the effect of directivity. The directivity, or direction the fault rupture occurs relative to the site, has a considerable effect on the ground motion because of the staggering of earthquake stress waves as the rupture expands. If the directivity of a fault rupture is towards the site, the staggering of the stress waves combined with waves' own velocity results in the waves arriving at the site near simultaneously and therefore having larger amplitude of motion. In the opposite direction, the waves are more spaced out leading to a longer period instead (Elnashai and Di Sarno, 2008).

The contributions of earthquake magnitude, source mechanism, and distance are the most variable components of earthquake loads, but are simplified within ASCE 7-05 so that they only affect the magnitude of the seismic design load through response acceleration contour

lines as defined in the ASCE Maximum Considered Earthquake (MCE) maps. The MCE maps are the result of a complex amalgamation of expected earthquake magnitude, distance from known faults, mechanisms of those faults, and probability of earthquakes occuring. The resulting estimations are the expected peak ground acceleration (PGA), which is defined as the maximum acceleration of ground motion, at a location. Those values are then converted to the spectral response accelerations that are displayed on the maps. These are not the PGA, but the maximum response acceleration of buildings with short natural periods, and natural periods of 1 second (ASCE, 2006). Site coefficients including the mapped MCE spectral response acceleration at short periods (S_S) and at a period of 1s (S_1) are the only coefficients within design seismic load calculation using the equivalent lateral force procedure that considers the first three earthquake characteristics.

Of the non-structure related factors that govern the characteristics of an earthquake load, soil condition is the only one that isn't dictated by the MCE maps. Soil conditions of the regions between the earthquake source and the site of interest can cause changes in the seismic waves through reflection and refraction off rock layers, but the variation in soil condition between the two points of interest is too substantial to be properly accounted for. The situation for which soil condition has the most significant effect on earthquake loading on a structure is at the structure site. Depending on the soil type upon which the structure's foundation is built, the building may experience a range of frequencies of motion. Rock and stiff soils better transfer high frequency motion, while softer soils transfer low frequency motion. This amplification effect of the soil is why the soil type must be carefully chosen specific to the structure; tall buildings with long natural periods should not be founded on soft soil as the amplification of low frequency motion would lead to greater earthquake loads due to a site resonance effect (Elnashai and Di Sarno, 2008).

Soil properties are used to define site classes, ranging from Site Class A to Site Class F with A being hard rock and F being extremely soft clays in ASCE 7-05. The typical site with stiff soil is considered to be Site Class D. In order to include the site classes in the load calculations, short period site coefficient (F_a) and 1s period site coefficient (F_v) are specified in a table where they are dependent on both site class and strength of the MCE.

These site coefficients are then used to adjust for the amplification to the spectral response accelerations (S_S and S_1) due to soil condition. The resulting spectral response accelerations are then corrected to be usable as design spectral acceleration parameters (S_{DS} and S_{D1}) in the equivalent lateral force procedure (ASCE, 2006).

The remaining factors that influence the magnitude and distribution of earthquake loads for the equivalent lateral force procedure all pertain to the design and features of the structure itself. Building stiffness and mass are the paramount factors, as both contribute to the natural frequency of the structure and the resonance of ground motion of similar frequencies is what essentially determines the effect of an earthquake on a structure. High-rise buildings, which have less stiffness than low-rise buildings, are generally subjected to lower earthquake forces because of the limited amount of low frequency ground motion relative to the more common high frequency seismic waves. Mass is also a major component of magnitude of earthquake load because the ground motion only applies an acceleration to the base of the structure. The resultant force on the building that is generated is directly related to the mass of each floor as expressed by Newton's second law of motion. The greater the mass, the greater the influence of the applied acceleration is (Elnashai and Di Sarno, 2008).

Both building stiffness and building mass are incorporated into the code based load calculations through the seismic response coefficient (C_s). The seismic base shear (V) is the total design lateral load applied to the structure and is equivalent to the seismic response coefficient multiplied by the building total weight. The building weight includes the effect of mass, while stiffness is included in the calculation of the seismic response coefficient. With a set of equations shown on the following page, the design spectral parameters are scaled depending on structure natural period (T), the response modification factor (R), and occupancy importance factor (I). Both the response modification factor and importance factor are dependent on the remaining earthquake load factor: the lateral load resisting system. While a structure may have identical general properties, differences in lateral load resisting systems result in changes in local behavior. Different systems also

have varying levels of reliability and the response modification and importance coefficients are tabulated to account for these differences.

$$C_s = \frac{S_{DS}}{\left(\frac{R}{I}\right)} \tag{4a}$$

$$C_s = \frac{S_{D1}}{T\left(\frac{R}{I}\right)} \quad \text{for } T \leq T_L \tag{4b}$$

$$C_s = \frac{S_{D1}T_L}{T^2\left(\frac{R}{I}\right)} \quad \text{for } T > T_L \tag{4c}$$

$$C_s = \frac{0.5S_1}{\left(\frac{R}{I}\right)} \quad \text{for } S_1 \geq 0.6g \tag{4d}$$

$$C_s \geq 0.01 \tag{4e}$$

where

C_s = seismic response coefficient

S_{DS} = short period design spectral acceleration

S_{D1} = 1s period design spectral acceleration

T = structure natural period

T_L = long-period transition period

I = importance factor

S_1 = MCE 1s-spectral acceleration

Once the seismic base shear is determined, the total lateral load is distributed along the height of the building based on the mass at each floor and the height at which the mass is located. The higher a mass is, the greater the equivalent lateral load applied at that height is, resulting in a load distribution that is an inverted triangle and has the greatest loads at the roof level and decreasing until the load is zero at the base.

A final consideration in seismic design is the Strong Column-Weak Beam (SCWB) theory. Although it does not directly relate to limiting structural response in the event of an

earthquake, the application of SCWB, is useful to obtain a safer failure mode. This theory states that the capacity of columns and beams should be adjusted so that beams fail before columns, which is essential to limiting progressive failure and preventing the collapse of the entire structure. Like the section on wind characteristics, this section does not give a comprehensive explanation of the details of earthquake load characteristics, but instead provides a sufficient guide so that the relationships between central characteristics and design earthquake loads can be clearly understood.

CHAPTER 4: MODEL DEVELOPMENT

The examination of the specific variations between wind and seismic designed structures requires the development of two detailed analytical models. The procedure of this study begins with the design of a two-dimensional (2D) frame for gravity loading only, followed by the formation of two separate models: one adhering to ASCE 7-05 Section 6.5 for wind design loads and limit states, and one to Section 12.8 for earthquake design loads and limit states. Once the two models are established, the analysis of each model under the two loading conditions will be performed. The model-load combinations are titled by model type then load type (i.e. W/EQ is the designation for the wind model under earthquake load case). By comparing the structural response for the four model-load pairs, specific design aspects that contribute to differences in behavior can be identified.

4.1 Model Background

To assess the behavior of a mid- to high-rise structure under various loading conditions, an analytical model of such a structure must be developed. For this purpose, a standard existing building needed to be used as the basis for the structural model. The particular building chosen for this study is a 47-story office building in downtown San Francisco, California. Built in 1978, it is a rectangular steel frame building with floor dimensions of 122 feet by 180 feet. It has a composite floor system with 2.5 inch concrete over metal deck and a lateral force resisting system that consists of moment resisting frames in both directions with eccentrically braced frames in the center bays.

Though the structural layouts and floor plans for this particular building are unavailable, it was used as the basis for the model because of its simple rectangular geometry and its inclusion in the CSMIP-3DV program. The program, developed by Dr. Farzad Naeim of John A. Martin & Associates, Inc. in association with the California Geologic Survey (CGS), is a software system that uses a network of sensors installed in existing structures to investigate the response of those buildings to actual earthquake events. The intended application of the CSMIP-3DV software for this research was to use the sensor data from the 47-story San Francisco office building to derive a form of dynamic wind loading for

the structure, as databases for dynamic time history records for wind loads do not exist as they do for earthquake loads. Unfortunately, the program does not provide enough information to do so, as the sensors were not sensitive enough to record the response of the structure to wind loads. Figure 16 is an image of the office building that the analysis model is based on.

Figure 16. 47-story office building in San Francisco, CA (Naeim, 2011)

Although the attempt to develop a time history record for wind loading was unsuccessful, the program still provided sufficient information about the building layout so that a structural model of a representative plane frame could be created in a structural analysis platform.

4.2 Frame Geometry and Material Properties

The structural analysis program used for this study was Zeus Nonlinear (ZeusNL), which was developed at the University of Illinois at Urbana-Champaign for the purpose of predicting behavior of two-dimensional and three-dimensional frames under both static and dynamic loading. Although specifically created for simulating frame response under

seismic loading, the capability of the program for multiple types of analyses makes it ideal for comparing the behavior of a 47-story plane frame when subjected to wind and earthquake loading.

Generally following the geometry of the San Francisco office building, the analysis models are 2D space frames which include frame and equivalent slab contributions, but no other infill considerations. The steel frame is 141 meters high with 47 stories at 3 meters each and has a width of 36 meters with 4 bays at 9 meter spacing. Modeling the lateral load resisting system in the building's weak axis allows for a conservative estimate of member sizes throughout the building. The number of bays was not specified in the building information obtained and a concentrically braced frame was used in the second bay instead of an eccentrically braced frame as in the physical building; the model is not a direct representation of the building. Although the San Francisco office building was used as a template for the model, the purpose was not to model an existing building, rather it was to create a realistic frame to represent standard mid- to high-rise structures.

The entire frame is modeled using a single steel material property. Modeled as bilinear elasto-plastic with 0.5% kinematic strain hardening, the steel is classified as ASTM A992 structural steel and has a Young's modulus of 200,000 N/mm^2 and yield strength of 345 N/mm^2. This model allows for the simulation of strain hardening and non-linear behavior of steel, but is less complex than the Ramberg-Osgood or Menegotto-Pinto material models. The modeling of the material property as non-linear is essential for this specific study, as buildings often respond in an inelastic manner to powerful earthquakes.

As previously mentioned, the beam sizes consider the contribution of the slabs and are uniform throughout the frame. The column sizes, however, change every ten floors and decrease as height increases. For both the wind and earthquake models, the initial column sizes were scaled to maintain a constant squash ratio – basic load to capacity estimation. However, this was impossible to maintain for the earthquake model because the Strong Column-Weak Beam (SCWB) theory was considered in its design.

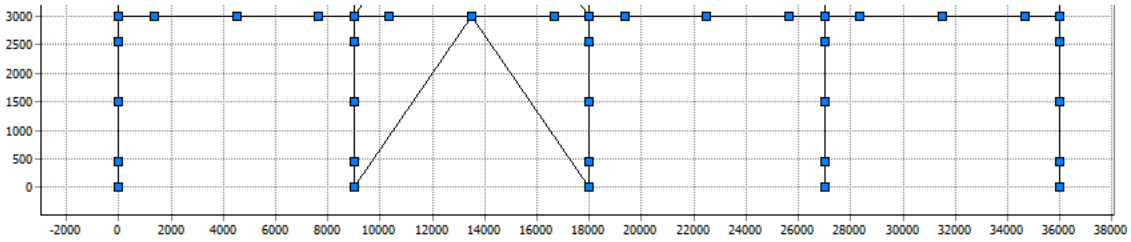

Figure 17. Model of first story in ZeusNL

Figure 17 shows the geometry of the first story of the model. Each of the higher floors has the same geometry, however column sizes may differ. The brace elements were kept the same for both models and were connected to the moment frame with joint elements. The joint elements in ZeusNL allow for the specification of limiting load and moments to represent joint behavior between pure fixed and pure pinned connections. In this case, the joint elements allowed for the loads to be carried mostly in tension and compression, but retained some moment resistance to more closely model a physical pinned connection.

4.3 Design Loads

With initial geometry defined, the design loads specific to this model were required in order to select the appropriate section sizes for the gravity model and subsequent wind and earthquake models. First, the controlling load combinations for wind and earthquake were chosen in order to determine the applicable load factors for each load type. From the load cases listed below, it was found that the gravity load factors were uniform for both lateral loads.

Table 2. Controlling Load Cases

Lateral Load	Load Case
Wind	1.2DL + 0.5LL + 1.6W + ~~0.5(Lr or S or R)~~
Earthquake	1.2DL + 0.5LL + 1.0E + ~~0.2S~~

The gravity loads, calculated from either ASCE recommendations or estimations for material weight, were found to be $W_{Wind\text{-}Vertical} = W_{Earthquake\text{-}Vertical} = 68.624$ kN/m based on

a 9 meter frame spacing. These values do not include the beam and column self-weight. After a preliminary frame model consisting of sections sized solely for gravity loads was established, an iterative process was used to calculate the design wind and earthquake loads. In both cases, the iterations involved the following steps:

1. The estimation of member sizes
2. Determining the first mode natural frequency
3. Calculating the corresponding lateral loads based on that natural frequency
4. Re-evaluating member sizes so the frame response under design load is within limit state conditions
5. Verifying the first mode natural frequency

The first iteration for wind design used the member sizes and first mode natural frequency required for the gravity load only condition, while the first seismic design iteration estimated the natural frequency to be T = 0.1N = 4.7 s, where N is the total number of floors. Only after adjusting column and beam sizes to eliminate the differences in natural period for each step could the design lateral loads be calculated.

The Method 2- Analytical Procedure found in Section 6.5 of ASCE 7-05 was used for the wind design load calculations and the wind load parameters, which were outlined in Chapter 3, were assigned for the specific characteristics of the model. The limit state for wind design is to limit the roof deflection to Δ_{lim} = H/400, where H is the total height of the building. As there are not codified standards for limiting drift for wind design, the limit state used in this study is based on a rule of thumb estimate for occupant comfort.

Though the natural frequency shifted depending on section size, the remaining factors were solely dependent on building geometry and location. Due to the building's location in downtown San Francisco, the design wind speed was determined to be V = 85 mph and the exposure was set as Exposure B. Using those and other coefficients, the final iteration resulted in a first mode natural period of T_1 = 6.146 s, a velocity pressure of $q_z = 752.3K_z$ N/m^2, and a gust effect factor of G = 0.883 which resulted in an average design pressure of

$p = 1.866\ kN/m^2$ (38.97 psf) over the face of the building. Recall from the previous discussion of load cases that the wind load needs to be scaled by a factor of 1.6 in order to meet the appropriate load combination.

For the calculation of earthquake loads, the Equivalent Lateral Force Method of Section 12.8 of ASCE 7-05 was used. Similar to the design wind load, the characteristics that control the scale and distribution of the seismic loads were explained in Chapter 3. Dissimilar to the design wind load process, however, is the definition of the controlling limit state. Although it remains a function of the roof deflection, the limiting value could be defined by multiple failure modes from the most stringent where the structure is expected to be serviceable immediately following an earthquake, to the life-safety limit state where the central purpose of the structure is to prevent building collapse. For the interests of this study, the limit state was judged to be at 0.5% building height based on the acceptable drift for damage to partitions.

With regards to the seismic design load contributing coefficients, the spectral response accelerations, $S_S = 0.1.5g$ and $S_1 = 0.9g$ were ascertained based on the MCE maps for San Francisco. Those values were then adjusted for Site Class D, which is the standard site condition specification unless geotechnical data proves otherwise. For the final iteration for seismic design load, the loads were based on $T_1 = 4.619s$. This resulted in a seismic response coefficient of $C_s = 0.0563$, calculated using equation 4d from Chapter 3. Once the equivalent lateral load is determined, there is no need for additional scaling, as the load factor for earthquake loads in the controlling load case is 1.0E.

4.4 Model Comparison

Considering the differences in the magnitude and distribution of the design loads for wind and earthquake, it is clear that there are differences in the two models. A brief comparison of the two will be presented in this section. With regards to load distribution, since the application of equivalent lateral seismic loads is based on the mass at each floor and the height at which the mass is located, the distribution of design seismic loads is vastly

different than that of design wind loads. While the lateral loads increase slightly as height increases for wind load due to greater wind speeds at greater heights, it is still a relatively uniform load through the height. On the other hand, seismic loads are much like a triangular distributed load with the maximum loading at the roof level. There is also a significant difference in the equivalent lateral load for both designs: the earthquake load is nearly three times greater than the wind load and it is applied at a greater height which results in a larger base moment. A comparison of the design loads for the wind and earthquake models are shown in Fig. 18.

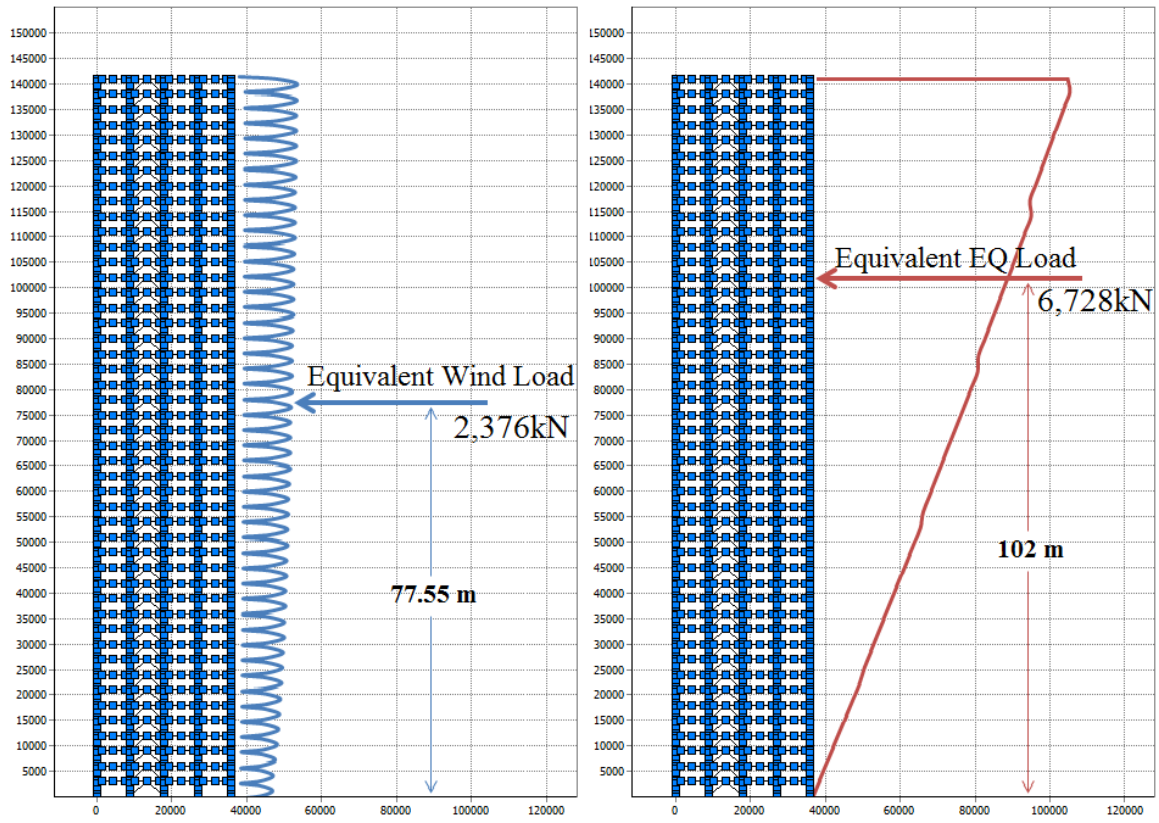

Figure 18. Comparison of magnitude and distribution of loads

Due to these differences in load, there are obvious disparities in the requirements for the two structural systems. In terms of section sizes, the beam sections are similar for the models with the wind model requiring W16X40 beams and earthquake model requiring slightly larger sections at W16X50. The columns, however, are considerably larger for the earthquake model; the earthquake base columns are nearly 250% larger in area than the

wind model base columns. Exact member sizes and geometry can be found in Appendix A. Details, such as axial load capacity and column squash, are also included in Appendix A.

Because of variation in section sizes, there is an 11% difference in weight with W_t(Wind Model) = 123,405 kN and W_t(Earthquake Model) = 138,878 kN. The substantial change in weight from the wind to earthquake model reflects the increased demands of seismic design. Simply based on the deflection limit, the wind model should have greater stiffness since Δ_{lim}(Wind Model) = 353mm is twice as large at Δ_{lim}(Earthquake Model) = 705mm. But since the magnitude and height of the earthquake load is much greater than the wind load, it is reasonable that the earthquake model requires a greater stiffness and therefore larger beams and columns. A comparison of the first mode frequency – T_1 = 6.146s for wind and T_1 = 4.619s for earthquake – reinforces the fact that the wind model is more flexible. Further exploration into the similarities and differences between the earthquake and wind models will be done in the following chapter, where the descriptions of analyses performed and results of the study will be presented.

CHAPTER 5: DYNAMIC LOAD DEFINITION

Representing seismic and wind loading as static design loads calculated using code parameters is acceptable for determining basic characteristics and behavior of the model, but the use of wind and seismic acceleration time histories as dynamic loads yields greater insight into the model response. Unfortunately, dynamic time history analysis is less common in wind design than seismic; while there are a number of extensive databases of earthquake ground motion records, there are no equivalent sources for dynamic wind load records. Detailed analysis of structural response to wind loading is typically done with wind tunnel testing and not through response-history analysis. With no affordable method of dynamic response analysis for wind loads available for this study, only seismic loads were considered for this more comprehensive analysis.

5.1 Selection of Ground Motion Records

Given the variability of seismic loading, it is necessary to take into account the effects of several different earthquakes when studying the response of the models in a response-history analysis. While artificial records could have been produced to create accelerograms that consider non-physical code requirements, they generally have long durations which result in greater damage than actual earthquakes (Elnashai and Di Sarno, 2008). Since natural records are widely available for the region of interest, a set of records that correspond with the anticipated loading scenario can be compiled. By selecting a set of different records based on the parameters of the building loading situation − including the site soil conditions and distance from fault − the amount of uncertainty due to variable loading can be reduced while maintaining the desired loading conditions. The set of records used for this study were chosen from the PEER Strong Motion Database which is maintained by the University of California, Berkeley (PEER, 2010).

Beginning with a collection of all records for earthquakes in California, the selection of records was filtered using different limiting conditions until only nine remained: San Fernando (1971), Imperial Valley (1979), Morgan Hill (1984), Chalfant Valley (1986), Superstition Hills (1987), Loma Prieta (1989), Big Bear (1992), Landers (1992), and

Northridge (1994). Table 3 lists each of the conditions that were met by most of the chosen records; the Big Bear Earthquake fell outside the parameters in a single category, distance from source, due to lack of stations within the defined range, but was still included to maintain a robust sample size of records.

Table 3. Parameters for Ground Motion Record Selection

Parameter	Limits
Location	California, USA
Lowest Usable Frequency	$f \leq 0.25$ Hz
Fault Mechanism	Strike-Slip or Reverse
Magnitude	$6.0 < M_w \leq 7.5$
Distance	20 km $< R_{rup} \leq$ 25 km
Soil Type	180 m/s $< v_{s30} \leq$ 360 m/s

The first parameter listed limits the location of the earthquake record to California in order to account for regional differences. Records from California may include certain unquantifiable traits that are present in all earthquakes in that area due to similarities in fault mechanism, topography, and regional soil conditions. Because of these differences in earthquake characteristics, modifications of records cannot be made so that they are interchangeable for different regions. A comparison of eastern North America (ENA) and California ground motions proved that high frequency seismic waves propagate further in ENA than in California (Atkinson and Boore, 1997).

Lowest usable frequency is an important parameter as it ensures that there are sufficient low frequency ground motions to induce structural response for mid- to high-rise buildings which tend to have longer natural periods. While low frequency ground motions are necessary to promote greater response from long-period structures, there are potential errors in the recording of long-period ground motion due to the digitization of analog records (Elnashai and Di Sarno, 2008). These errors are unavoidable, as there have not been many large magnitude earthquakes in California in the few decades since the use of digital accelerographs became the common mode of recording ground motion.

The remaining factors that limit record selection consider the contributions of source, path, and site effects of the recording station. The source, path, and site effects alter the recorded ground motion, therefore they must be considered in record selection (Elnashai and Di Sarno, 2008). A shear wave velocity range that is representative of soft soil has been applied in order to maintain a consistent level of site effects. To ensure that the records are recorded at stations with soil types similar to that used in the design of the model, stations with soft soils that correspond with Site Class D were used. As stated in Chapter 3, the typical site is considered as Site Class D. A detailed list of the natural earthquake records chosen, including their characteristics, can be found in Appendix B. Figure 19 presents a comparison of the elastic acceleration response spectra of the nine records to demonstrate the similarities and differences in the records.

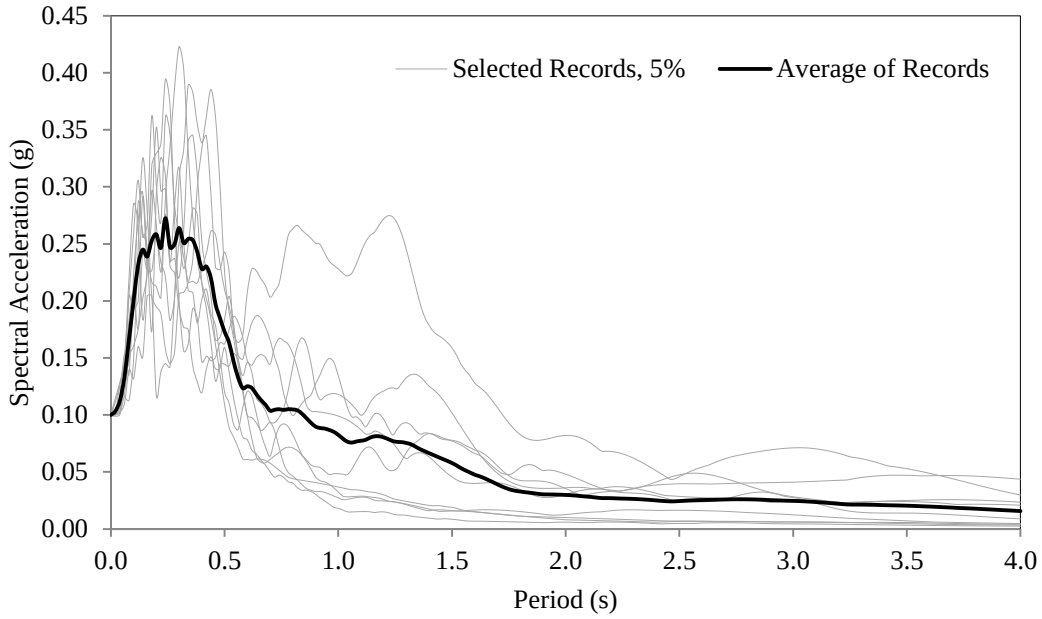

Figure 19. Elastic Response Spectra for the selected earthquake records for a damping value of 5%

The outlier of the records, with an extended region of high spectral acceleration until a period of 1.2s, is that of the Superstition Hills Earthquake in 1987. A study of the time history accelerograms reveals that the Superstition Hills Earthquake has a greater duration of high acceleration, long period ground motion than the other selected earthquakes. Figure 20 on the following page compares the ground motion for Superstition Hills with that of

the Landers Earthquake. The remaining records are included in the complete set of time history records that can be found in Appendix B. Of all of the chosen records, Landers was used for this comparison due to its close approximation to the average response spectra.

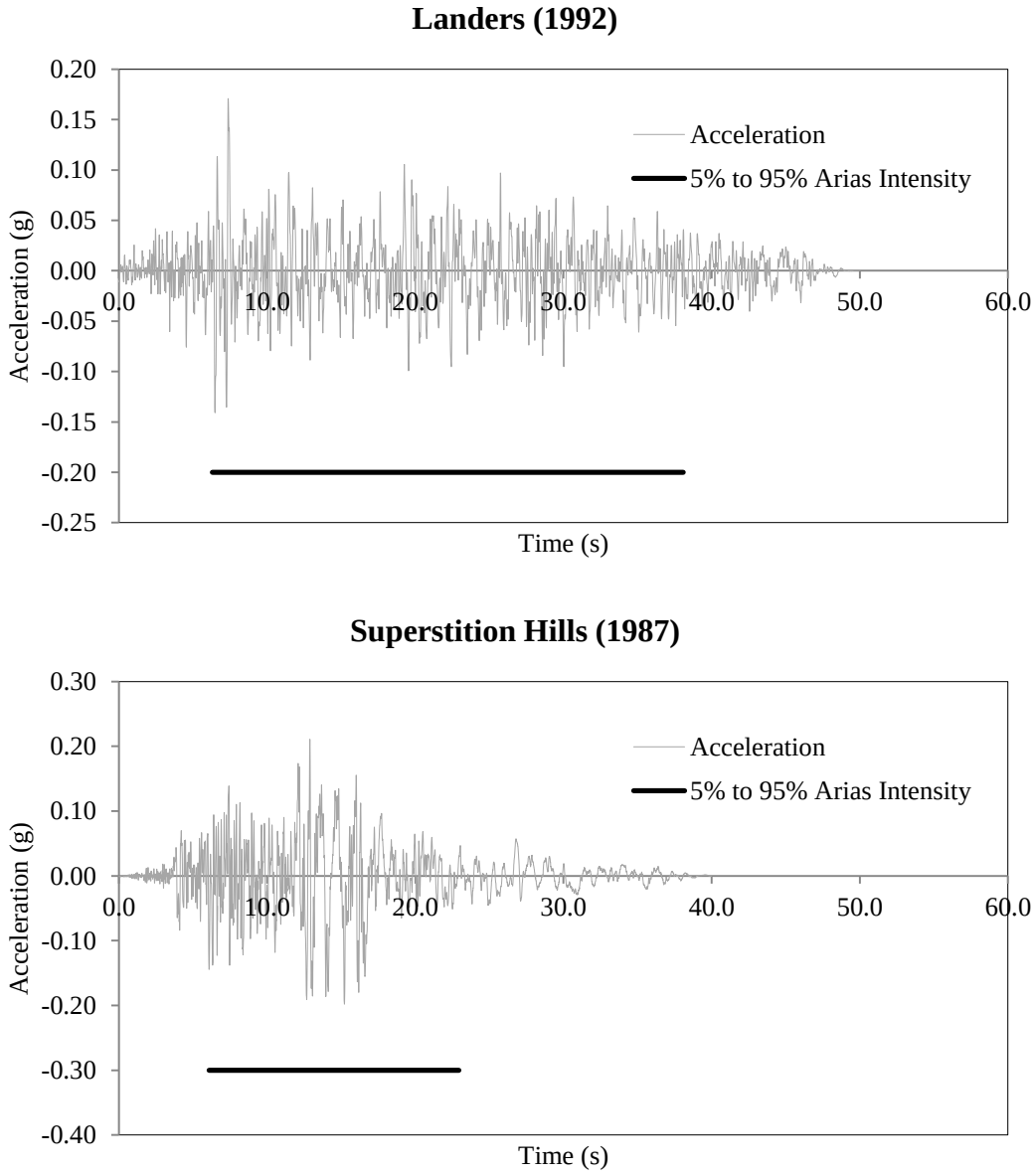

Figure 20. Comparison of Superstition Hills and Landers Earthquakes

While Landers has a greater duration under the assumption of 5% to 95% Arias Intensity, which is an estimation of the energy accumulation in an earthquake, Superstition Hills has a clearly displayed range of low frequency ground motion from approximately 12.4s to 16.2s. This region of low frequency ground motion is what causes the greater spectral

response for higher period structures. This atypical ground motion causes significant differences in behavior, which will be presented and discussed in Chapter 6.

5.2 Scaling of Records

The selected records were scaled using peak ground acceleration (PGA) so that each record has been scaled to a PGA of 0.1g, 0.3g, 0.5g, and 0.7g. With each record scaled to four different PGAs, there were a total of 36 records used for the analysis of each model. Because mid- to high-rise buildings are long period structures, they are more sensitive to changes in displacement and velocity than acceleration. Given this sensitivity, the scaling of records using peak ground velocity (PGV) or peak ground displacement (PGD) may have resulted in a lesser dispersion of the response spectra (Elnashai and Di Sarno, 2008). However, the conventional definition of earthquake loads in ASCE standards is based on PGA; thus, a PGA based scaling method was chosen in order to maintain a consistent definition of earthquake loads that is compatible with the code definition.

CHAPTER 6: RESULTS OF ANALYSIS AND DISCUSSION

Analyses performed with frame models are useful in determining the similarities and differences between wind and seismic design. Although the 2D frame models used to assess the behavior of mid- to high-rise structures under wind and earthquake loads may not be a precise measure of an actual building's response due to the exclusion of infill considerations, they provide a realistic prediction of structural response. For that purpose, a number of different types of analyses were performed. Eigenvalue analysis was used for both model development and assessment. Static pushover analysis was valuable for the assessment of global capacities, such as the stiffness, strength, and ductility of each structure. The final type of analysis, dynamic time history analysis, was useful in evaluating the local and intermediate level characteristics of structural response under realistic simulated earthquake loading.

6.1 Eigenvalue Analysis

One of the essential characteristics of a building that governs structural response due to lateral loads is the building's fundamental period. The magnitude to which an earthquake affects a building is essentially controlled by the correlation between the structure natural frequency and frequency of the earthquake ground motion. The greater the correlation between the two, the greater the earthquake loads are amplified to create larger response in the structure. Tables 4 and 5 contain the first five modes of vibration for the wind model and the earthquake model respectively.

Table 4. Modes of Response for Wind Model

Mode	Period (s)	% Mass Participation
1	6.1458	68.990
2	1.9339	15.379
3	1.0219	4.988
4	0.6733	2.722
5	0.4965	1.293

Table 5. Modes of Response for Earthquake Model

Mode	Period (s)	% Mass Participation
1	4.6189	65.501
2	1.4603	14.305
3	0.7530	5.268
4	0.4731	3.424
5	0.3411	2.002

The tables also include the mass participation of each mode, which is useful in gaging the contribution of each mode to the structural response. The natural frequencies and mass participation values listed in Tables 4 and 5 were determined using Eigenvalue Analysis in ZeusNL and modal analysis respectively. The first mode natural frequencies were verified using Rayleigh's method with the following equation:

$$T = 2\pi\sqrt{\left[\sum_{i=1}^{N} W_i\,\delta_i^2\right] \Big/ \left[g\sum_{i=1}^{N} F_i\,\delta_i\right]} \qquad (5)$$

where

W_i = story weight of the i^{th} story

δ_i = lateral displacement due to load pattern at story i

F_i = force at story i

Table 6. Comparison of First Mode Periods for Eigenvalue and Rayleigh Methods

Model	Load	Eigenvalue Analysis (s)	Rayleigh (s)
Wind	Wind	6.1458	6.7779
	Earthquake		6.7901
Earthquake	Wind	4.6189	4.8211
	Earthquake		4.8261

Using the lateral load distribution and corresponding displacements for wind and earthquake load for both models, the Rayleigh calculated periods were calculated and the values are compared to those from the eigenvalue analysis in Table 6. As shown, the first natural frequencies from the eigenvalue analysis are similar to calculated values, verifying the results.

The modal participation factors for the two models were determined using modal analysis, where eigenvectors were extracted from the ZeusNL Eigenvalue Analysis, and mass matrices were derived with the assumption of lumped masses at each floor. By using lumped masses instead of considering the distribution of mass along the two dimensional frame, the mass matrix can be simplified to a diagonal matrix with dimensions equal to the number of stories for easier computation. Once the mass matrix was defined, the eigenvectors representing the lateral deflection at each floor were compiled in the modal matrix, Φ. The eigenvectors in the modal matrix were scaled so that the generalized mass, M_i, as defined in equation 6b would be equal to one. Calculations using the set of equations below determined the modal participation factors. Iterative analytical processes such as adaptive pushover analysis that adjust lateral load distribution during analysis according to modal shapes in each step are more accurate than the modal analysis used, however the size of the model exceeds the capacities of the analysis program and computer processor.

$$\Phi = [\varphi_1 \ \varphi_2 \ ... \ \varphi_n] \tag{6a}$$

$$M_i = \Phi_i^T \mathbf{M} \Phi_i \tag{6b}$$

$$\Gamma_i = \frac{L_i}{M_i} \tag{6c}$$

where

Φ = modal matrix

M_i = generalized mass for the i^{th} mode

M = lumped mass, mass matrix

Γ_i = modal participation factor for the i^{th} mode

$L_i = \Phi_i^T \mathbf{MI}$

I = vector of influence coefficients, taken as a unity vector

Due to the concentration of mass responding in the first five modes for both structures, it is important to consider the spectral acceleration at each value. While the mass participation data indicates that the structure typically responds in the first mode, the limited amount of low frequency ground motion present in most earthquakes result in low spectral accelerations for longer periods. This means that even if the structure response is predominantly in the first mode, the applied loads from earthquakes are often too minor to cause significant deflections. Instead, the greater spectral accelerations associated with lower period modes cause a larger response with a smaller mass participation.

When comparing the natural frequencies and modal participation factors of the wind and earthquake models, there are two important distinctions. First, the natural period of the wind model, $T_1 = 6.15s$, is significantly longer than that of the earthquake model, $T_1 = 4.62s$. Second, although the modal mass participation is slightly greater for the wind model than the earthquake model with first mode mass participation percentages of 68.99% and 65.50% respectively, the values are similar enough that it can be stated that the modal response is the same for both structures.

The differences in natural periods indicate that wind designed structures are more flexible than the structures designed for earthquakes. The greater flexibility of the wind model is in part due to the lower strength requirements of wind design compared to seismic design and in part due to decreased wind loading from vortex shedding for low frequency structures. For wind designed buildings, having a longer natural period can be a benefit or a detriment to the building response in earthquakes depending on the situation. The greater difference between soil natural frequency and structure natural frequency limits the amplification of ground motion that corresponds to resonance response; for the same ground motion, a wind designed building will have lesser earthquake lateral loads than an earthquake designed building. This is balanced by the fact that the increased flexibility in the wind model allows for increased deflections for equivalent loads.

The similar mass participation for both models in the first five modes supports the previous conclusion that for identical ground motions, wind designed buildings are subjected to

lower lateral loads than earthquake designed buildings. With comparable levels of mass participation in each mode, the lower spectral accelerations associated with the wind model's higher natural periods result in smaller lateral loads. The marginal differences in modal participation between the two models further decreases the lateral loads due to earthquake ground motion for the wind model. Figure 21 depicts the earthquake spectra for the 1992 Landers Earthquake, using 5% damping and scaled to a PGA of 0.1g. The corresponding spectral accelerations for the first five modes of each model are also indicated in the figure.

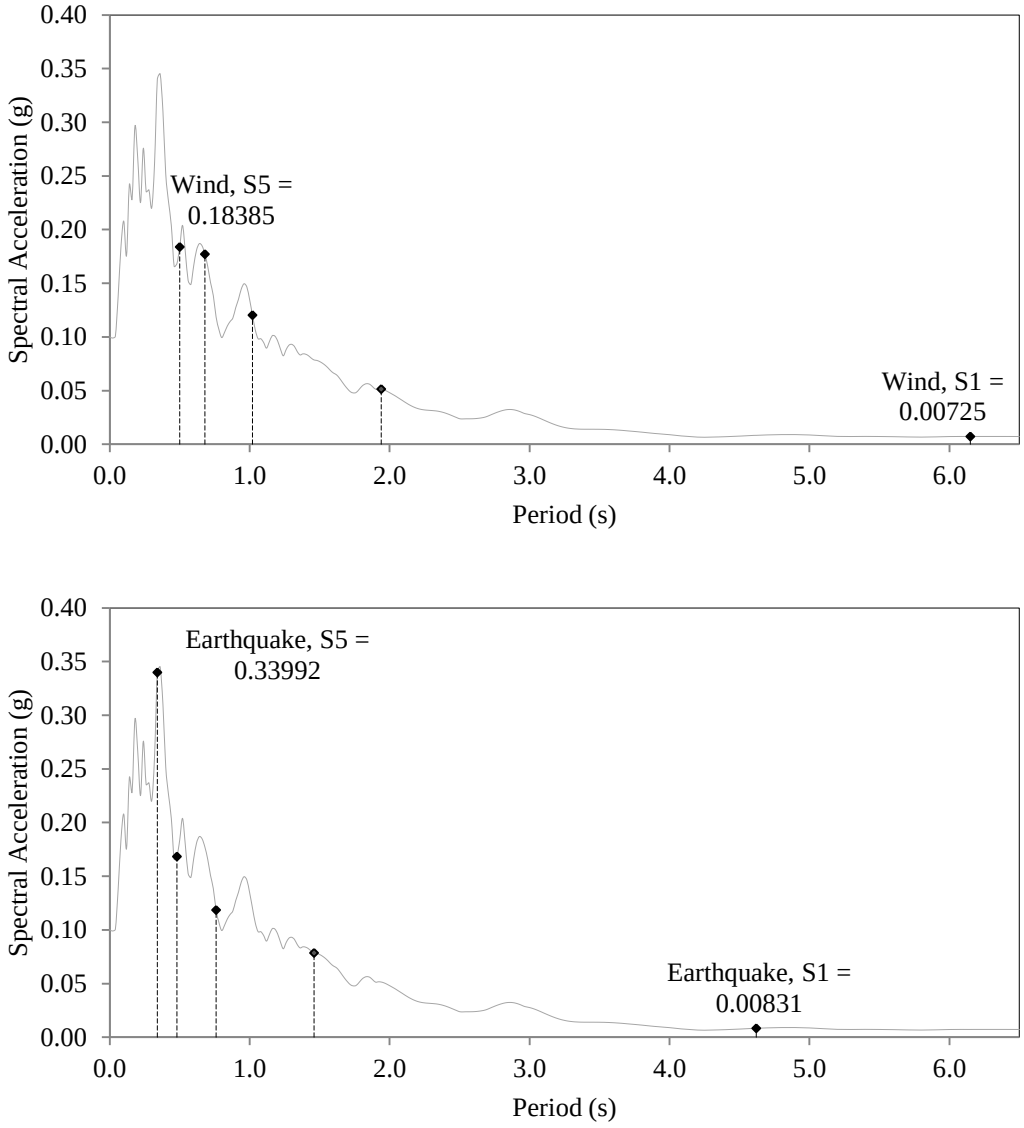

Figure 21. Landers Earthquake Spectra with mode spectral accelerations for both models

Based on the maximum and minimum spectral accelerations associated with the first five modes of each model, it is expected that the actual maximum accelerations experienced by the models fall between their respective limits. The wind model maximum acceleration was determined to be 0.115g, which is between 0.00725g and 0.18385g and the earthquake model maximum acceleration was determined to be 0.167g, which is between 0.00831g and 0.33992g. Both the range of spectral accelerations and the determined value of maximum acceleration are greater for the earthquake model than the wind model; therefore, the conclusion that the same ground motion results in greater loads for earthquake designed buildings than wind designed buildings is reaffirmed by the larger maximum acceleration experienced by the earthquake model.

6.2 Static Pushover Analysis

Static pushover analysis performed using the distribution of design wind and earthquake lateral load provides insight into the behavior of the structure in the first mode. Although structural response is in a combination of modes as shown in the earlier section, static pushover analysis is useful to observe the global characteristics of the two models. Some information about local and intermediate behavior can also be ascertained from static pushover analysis. However, due to the use of design load distributions that are not exactly the same as physical loads and the absence of cyclic loading as in the actual lateral loads, the local and intermediate response can be more accurately assessed with time history analysis. Static pushover analysis is particularly useful for this research because of the lack of availability of dynamic wind load records for time history analysis. Insight into the inherent wind resistance of earthquake designed structures is provided mostly through static pushover analysis.

In this study, there are four setups, one for each of the load and model combinations: wind model-wind load (W/W), wind model-earthquake load (W/EQ), earthquake model-wind load (EQ/W), and earthquake model-earthquake load (EQ/EQ). All four analysis systems are analyzed using displacement control of the node at the roof level of the 5^{th} column line.

Displacement control is used to be able to assess post peak response. Under each of the loading conditions, which take into account changes in the magnitudes of load due to the different natural frequencies of the wind and earthquake model, the load and model response corresponding to each displacement step is determined. Figure 22 displays the base shear plotted against roof drift for all four model-load scenarios.

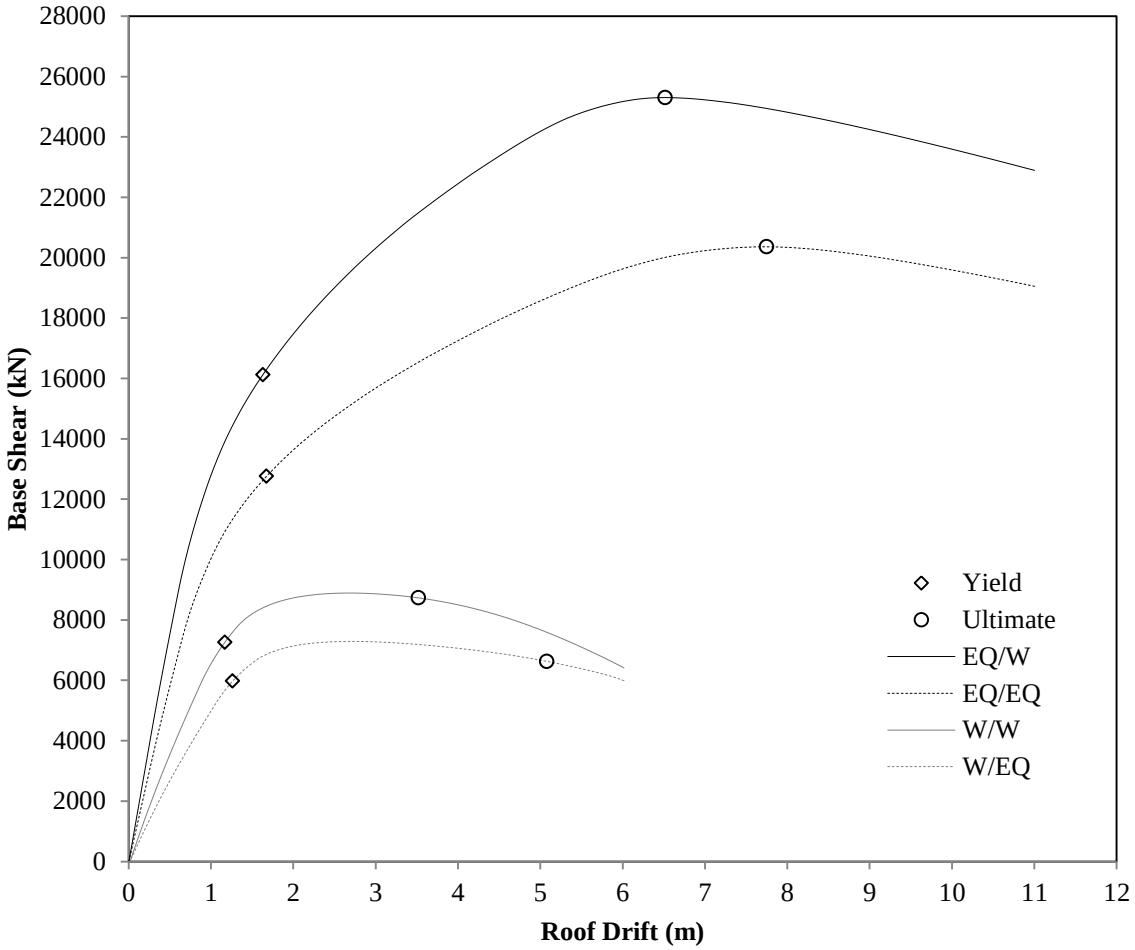

Figure 22. Static Pushover Curve comparing base shear and roof drift for all model-load scenarios

From this figure, it is clear that the earthquake model has significantly greater stiffness, strength, and ductility than the wind model regardless of load applied. The yield points are based on equivalent elasto-plastic yield, while the ultimate point is based on the peak load for earthquake and first base column yield for wind. While it may appear that the wind model should have more stiffness because the deflection limit for wind is more stringent than that for earthquake design – Δ_{lim} = H/400 = 352.5mm for wind compared to Δ_{lim} =

0.005H= 705mm for earthquake – the much larger strength requirement of the earthquake model necessitates a higher stiffness. Table 7 presents a summary of the global characteristics: stiffness, strength, and ductility, of each of the four model-load scenarios from static pushover analysis.

Table 7. Global Characteristics from Static Pushover Analysis

	W/W	W/EQ	EQ/W	EQ/EQ
Stiffness				
Stiffness, k (kN/m)	7,581	5,728	15,516	11,994
Strength				
Base Shear, V_{max} (kN)	8,892	7,290	25,304	20,361
Ductility				
Yield Displacement, Δ_y (mm)	1.167	1.263	1.631	1.675
Ultimate Displacement, Δ_y (mm)	3.519	5.079	6.515	7.747
Displacement Ductility, μ	3.015	4.021	3.994	4.625

With the tabulated values for global characteristics, certain observations can be made. First, the stiffness of the earthquake model is over double the stiffness of the wind model. This relationship holds true for both loads. Second, the earthquake model has nearly three times greater strength in terms of base shear than the wind model. Finally, although the variation is not as large, the earthquake model still maintains a higher ductility. All of these global characteristics are attributed to the substantial bulk of the sections used in the earthquake design compared to the wind design. Because the earthquake design is controlled by strength, the earthquake model's base shear capacity being close to three times the base shear capacity of the wind model is directly linked to the design earthquake load being almost three times the design wind load.

Although the differences in stiffness, strength, and ductility between the earthquake and wind models are well-defined from the static pushover data, the changes in global response characteristics between loads for each model are not as obvious. Due to the different

distributions of lateral load for design earthquake and design wind, there are slight differences in the static pushover curves. First, the earthquake load leads to approximately 20% less stiffness than the wind load for both models. This difference is due to the smaller differences in load from floor to floor for the wind load. Stiffness, by definition, is the rigidity of an object and is measured by the amount of deflection for a given load. Therefore, it is understandable that for an equal load, a greater variation of the load from floor to floor from earthquake loads leads to more significant inter-story and global roof drifts. As stiffness is inversely related to deflection, the larger roof deflection associated with the earthquake load results in lower stiffness.

Second, with regards to strength, both models have more capacity for base shear when subjected to wind load than earthquake load. This behavior is related to the action of the design wind load at a lower elevation than the design earthquake load. The triangular load distribution from the equivalent lateral force procedure for seismic design means that the earthquake load acts at approximately 0.67H while the rectangular wind load acts at approximately 0.5H. The lower location of the equivalent wind load results in a lower base moment than an equal magnitude of earthquake lateral load. Since base shear begins decreasing as moment capacity is exceeded at the base of the structure, it is reasonable to deduce that for a single model, the moment capacity at the base is the same at maximum base shear regardless of load. Stemming from that assessment, to reach the same base moment, the wind load needs to be greater than the earthquake load in magnitude to make up for the smaller lever arm.

Lastly, the ductility of the models under each load varies slightly with wind loads resulting in slightly smaller values for displacement ductility. Unlike the other two characteristics, where the wind load yielded higher values for strength and stiffness, the opposite occurs for this characteristic. It occurs because although the roof drift at yield is constant for each model regardless of load, the drift at which ultimate deflection occurs varies. The larger value of ultimate roof drift for earthquake loads is likely because even with decreased stiffness and strength, the distribution of earthquake loads result in more plastic hinges developing and therefore greater deflection before ultimate failure.

It is important to understand that although the static pushover analysis provides a useful comparison of the model behavior under different loading conditions, under design loading, none of the model-load scenarios reach the yield point. The closest any of the setups gets to the point of yield is the wind model under earthquake load. Even in that scenario, the earthquake load needs to be increased by a load factor of 1.263 for yield to occur. It is shown that due to the limit states chosen, both models are relatively overdesigned. Figure 23 shows the initial portion of the static pushover curve with markers indicating points of yield and points where load factors are equal to 1.0 in order to demonstrate the response at design loads relative to overall behavior. The locations of the markers for design loads are very clearly within the limit for elastic response, however, they are not necessarily within the bounds of the desired limit state conditions. The wind model under earthquake load in particular exceeds the limit state drift by more than 300 mm.

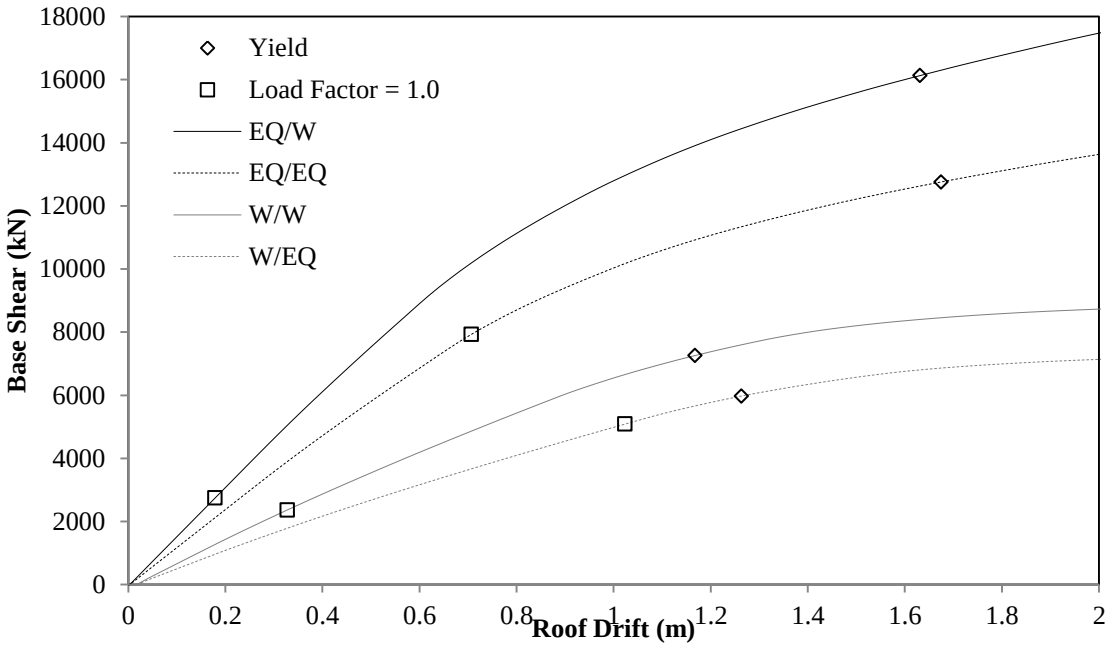

Figure 23. Static Pushover Curve displaying points of design load

To find the inherent wind resistance of earthquake designed buildings and inherent earthquake resistance of wind designed buildings, the static pushover curves can be used. For the earthquake model, the intrinsic wind resistance can be defined as the amount of

wind load it can resist without exceeding the roof drift limit state for wind of Δ_{lim} = 352.5 mm. From the EQ/W pushover curve, it is determined that for Δ = 355 mm, a load factor of 2.38 is required. The design wind load is then scaled to that value and the design necessary wind speed to generate that wind load distribution is subsequently calculated. The design wind speed is then found by back-solving using the wind design ASCE specifications. Once the design wind speed is established, the model response is verified with static load analysis. From this procedure, it is determined that for a 127 miles per hour wind speed, the earthquake model has a deflection of Δ = 351 mm which is within the limiting roof drift for wind design. Therefore, it can be concluded that for this situation, a structure designed for earthquake resistance can resist wind loads resulting from wind speeds up to 127 mph.

In a similar manner, the assessment of inherent earthquake resistance of wind designed buildings is performed. Using the W/EQ static pushover curve, it is ascertained that a load factor of 0.515 corresponds to the roof deflection of Δ = 711 mm which is closest to the partition damage limit state for earthquake design of Δ_{lim} = 705 mm. Although the approach in back-solving for the design spectral accelerations and PGAs is similar to the method for wind load, the relationship between design earthquake load and PGA is not as direct as the relationship between design wind load and wind speed. Since the back-solving is code based, there are some parameters that are defined by safety factors and not by physical characteristics of the load. This results in a substantial gap in the base shear coefficient, C_s, for peak ground accelerations between 0.35g and 0.4g. Table 8 displays the jump in base shear coefficient between the two PGAs and the resultant disparity in roof drift.

Table 8. Comparison of Base Shear Coefficient and Roof Drift

PGA (g)	Base Shear Coefficient, C_s	Roof Deflection, Δ (mm)
0.35	0.0107	244
0.40	0.0375	919

The lack of base shear coefficients between 0.0107 and 0.0375 is due to additional safety factors implemented for MCE 1-second spectral accelerations, S_1, greater than 0.6g. For a better estimation of the earthquake resistance of wind designed buildings, dynamic time history analysis is needed. Although the response of the structure to earthquakes in dynamic time history analysis is highly dependent on the particular characteristics of the ground motion, the use of an array of records chosen for the design scenario allows for the estimation of average response.

6.3 Dynamic Time History Analysis

One of the most effective methods in assessing the behavior of structures under earthquake loading is dynamic time history analysis. With this analysis process, earthquake loading is applied to the model in the same manner as the physical loading is applied to a real structure; instead of estimating earthquake lateral load based on an assumed load distribution, ground motion can be simulated with applied accelerations at the base of the structure. The application of ground motion in this fashion lets the structural system respond as it would in an actual earthquake, distributing the lateral loads according to the characteristics of the structure. Not only does dynamic time history analysis provide a more accurate assessment of earthquake loading due to its method of application, the availability of actual earthquake records allow for an approximation of the specific loading scenario of interest based on location and site conditions.

Using ZeusNL for dynamic time history analysis, a substantial amount of information about the structure response can be collected. The particular points of interest for comparison between the wind and earthquake models are maximum roof drift and maximum base shear for the assessment of global characteristics, maximum inter-story drift for intermediate characteristics, and plastic hinge development for local characteristics. Each of these parameters is evaluated by plotting the values against the spectral acceleration of the model for the given loading. This provides a more accurate comparison of behavior than plotting against PGA because it accounts for the different qualities of the ground motions.

6.3.1 Comparison of Static and Dynamic Analysis

Figure 24 displays the correlation between the base shear-roof drift curve from the static pushover analysis and the maximum base shear and roof drift points from the time history analysis for both models. Although the stiffness appears to be matched very well, the strength of both models is greater in the dynamic time history analysis than in the static pushover analysis. This is likely due to cyclic loading and the formation of plastic hinges that dissipate energy.

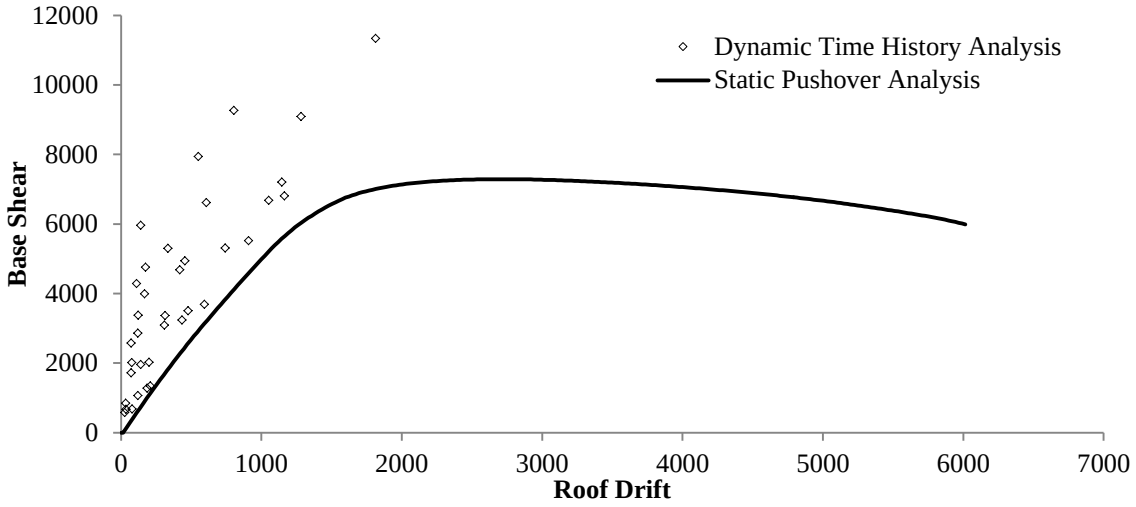

(a) Wind Model Response

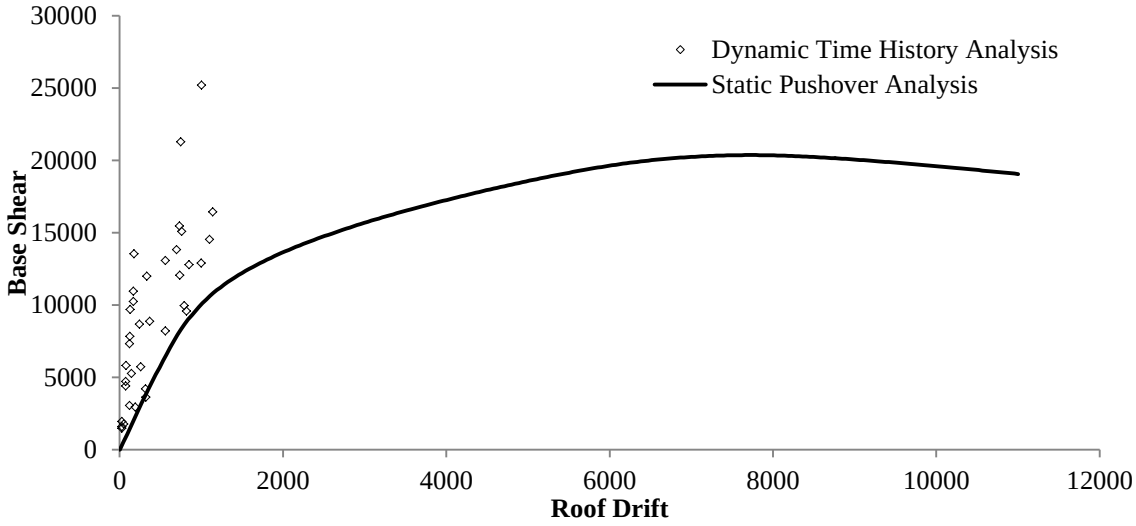

(b) Earthquake Model Response

Figure 24. Comparison of Base Shear vs. Roof Drift for Static Pushover and Time History Analyses

With regards to the global response of the two models under earthquake load, Figure 25 includes a comparison of the maximum roof drift and maximum base shear based on the model's maximum acceleration; the figures also display a linear regression line fitted to the data.

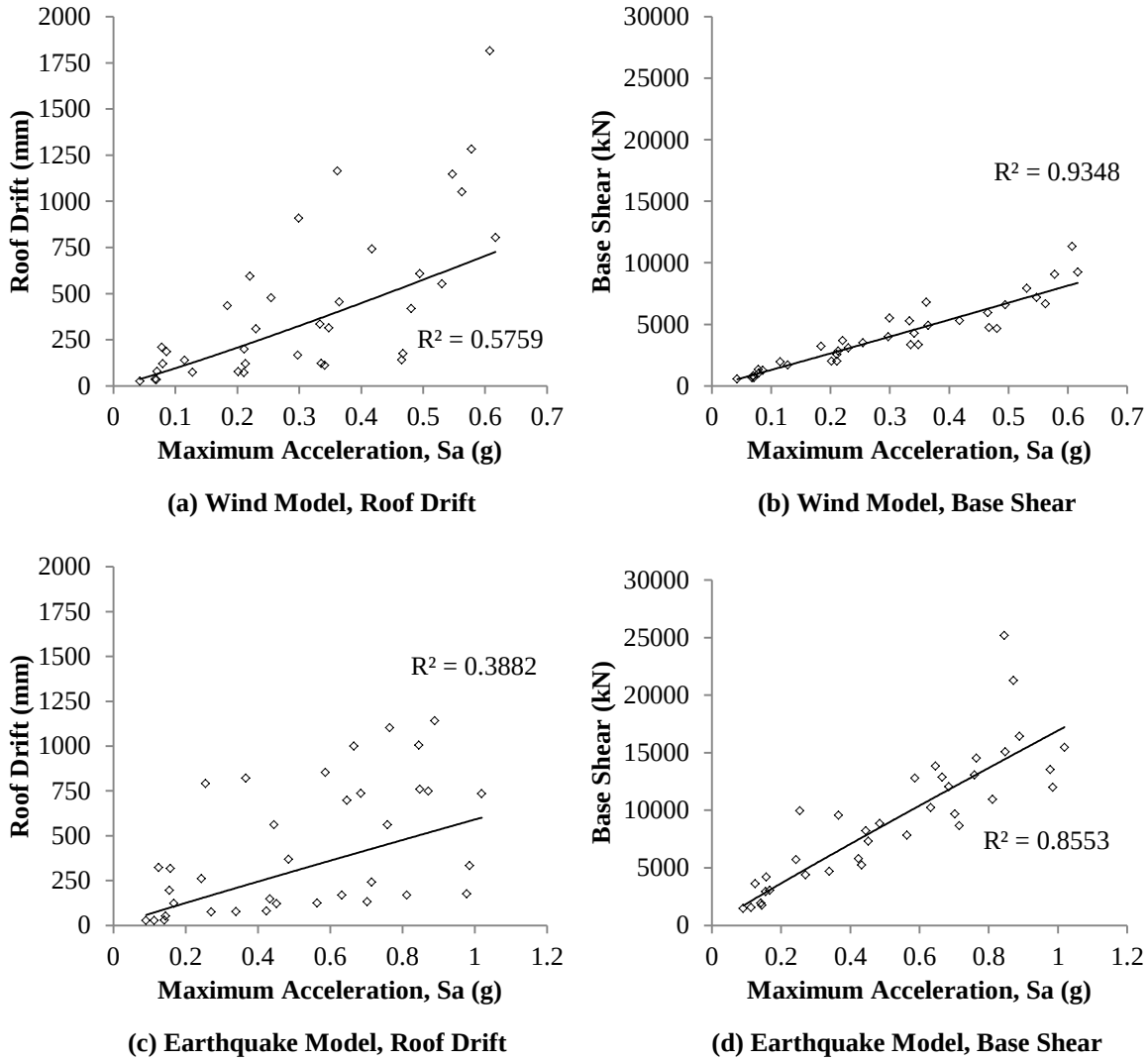

(a) Wind Model, Roof Drift

(b) Wind Model, Base Shear

(c) Earthquake Model, Roof Drift

(d) Earthquake Model, Base Shear

Figure 25. Global Characteristics against Maximum Acceleration with Power Regression

While the response does increase such that greater roof drift and base shear are associated with higher maximum accelerations, there is a significant amount of scatter in the data, particularly for maximum roof drift. Using the coefficient of determination, R^2, for the power regression, the relative scatter of the response of each model can be assessed. For both roof drift and base shear, the wind model has a better fit to the log-log regression

curve than the earthquake model. It is likely that the increased scatter for the earthquake model is due to its greater tendency for inelastic behavior. The larger inelasticity of the earthquake model will be further discussed when plastic hinge development is examined later in this section.

6.3.2 Assessment of Global Characteristics

While the plotting of points representing the global characteristics and performing power regression for the data is useful for assessing the scatter of the data, it is not a suitable method for the estimation of structural response. A method of presenting the data that is more effective in predicting response regarding the global characteristics of the wind and earthquake models is through incremental dynamic analysis (IDA). As a parametric analysis used to assess structural response to seismic loads, IDAs require the evaluation of the non-linear dynamic response of structures to multiple earthquake records with each record scaled to multiple values of intensity (Vamvatsikos and Cornell, 2002).

For a single record, the intensity measure (IM) is determined for several scale factors. In incremental dynamic analysis, the IM is typically defined as the PGA or spectral acceleration. Specifically, it can be defined as: (1) the peak ground acceleration, PGA, (2) the spectral acceleration for 5% damping for the natural period from the record spectra, $S_a(T_1,5\%)$ or (3) the maximum acceleration experienced by the structure, $S_a(a_{max})$. Although the records were scaled according to PGA, in the presentation of IDAs for this study, the third definition of intensity measure is used. This is to maintain a better comparison of response between records than PGA comparisons as previously stated, and also to judge the models based on the actual behavior as responding in a combination of modes and not just in the first mode. The damage measure (DM) is the parameter in IDAs that denotes the structural response characteristics. The flexibility of the DM definition allows for the study of behavior at multiple levels of structural characteristics using IDA (Vamvatsikos and Cornell, 2002).

With respect to the assessment of the wind and earthquake models for global characteristics, the DM is identified as peak roof drift and maximum base shear. For

intermediate characteristics, the DM is defined as maximum inter-story drift. Finally, the local characteristic DM is expressed with the number of floors with plastic hinges developing in the beams, and also the maximum stress experienced in the beams and columns. A presentation of the incremental dynamic analysis curves and discussion of the results are contained in the following figures and pages.

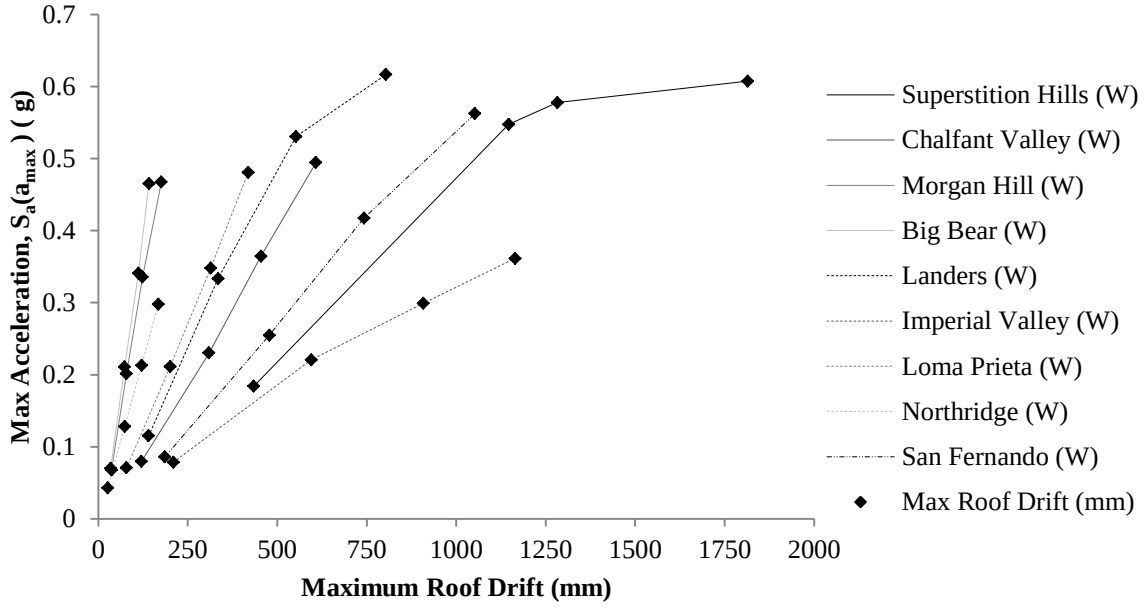

(a) Wind Model

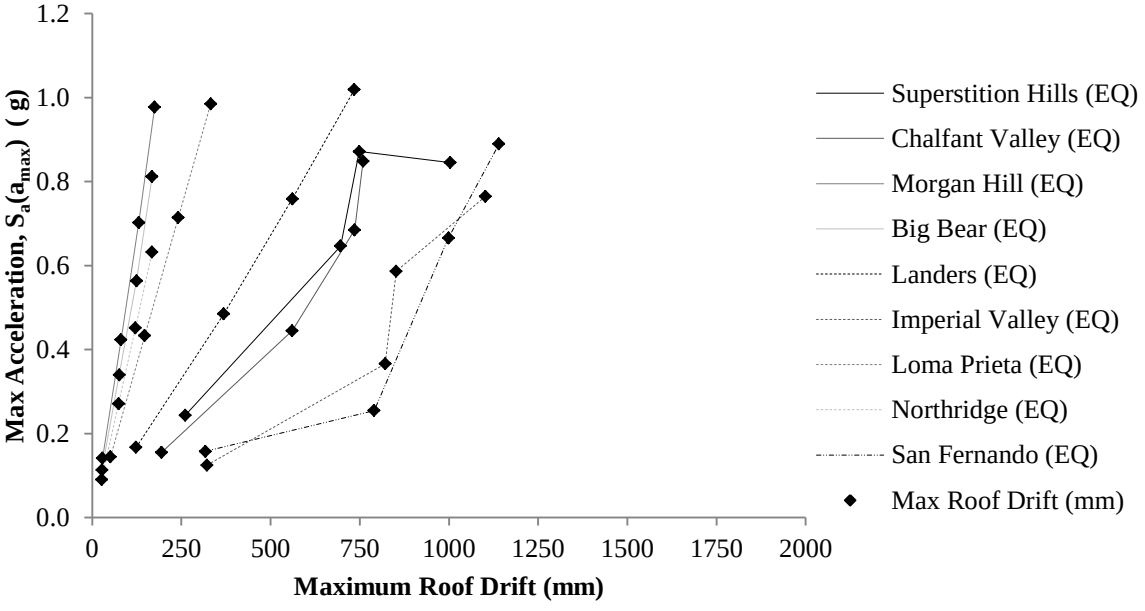

(b) Earthquake Model

Figure 26. IDA curves for both models where DM is max roof drift

Figure 26 shows that the earthquake model undergoes greater non-linear behavior than the wind model. The non-linear response of the wind model is limited to the higher max accelerations and also to the earthquake records that have more long period ground motion or longer durations. The IDA curve for Superstition Hills is the most non-linear among the curves for the wind model, and is also extremely non-linear for the earthquake model. As discussed in Chapter 5, this is expected since the record for Superstition Hills is an outlier for the set of records with an extended region of periods with high spectral acceleration. In addition to the greater distribution of the IDA curves for the earthquake model, the plots in Figure 26 also demonstrate that the earthquake model has significantly less roof drift for equivalent spectral accelerations. This upholds the conclusion that earthquake design for mid- to high-rise buildings results in buildings with greater stiffness than wind design.

To obtain an estimation of roof drift for a particular spectral acceleration, the average of the IDA curves must be derived. This is done by taking the average of the maximum roof drift values for the points within specific ranges of spectral acceleration. Figures 27 and 28 display the average IDA curves (DM = maximum roof drift) for the wind and earthquake model respectively.

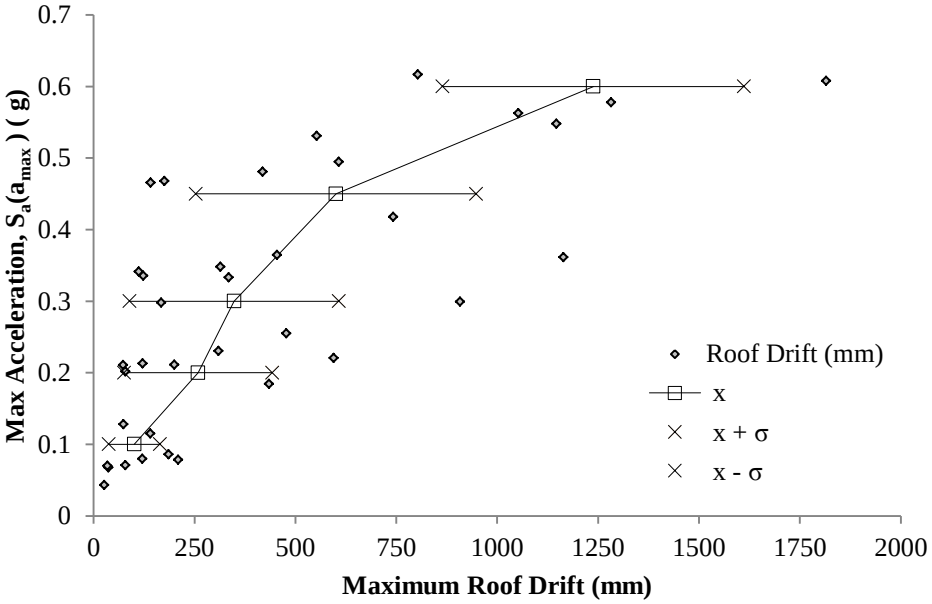

Figure 27. Average IDA curve for the wind model where DM is max roof drift

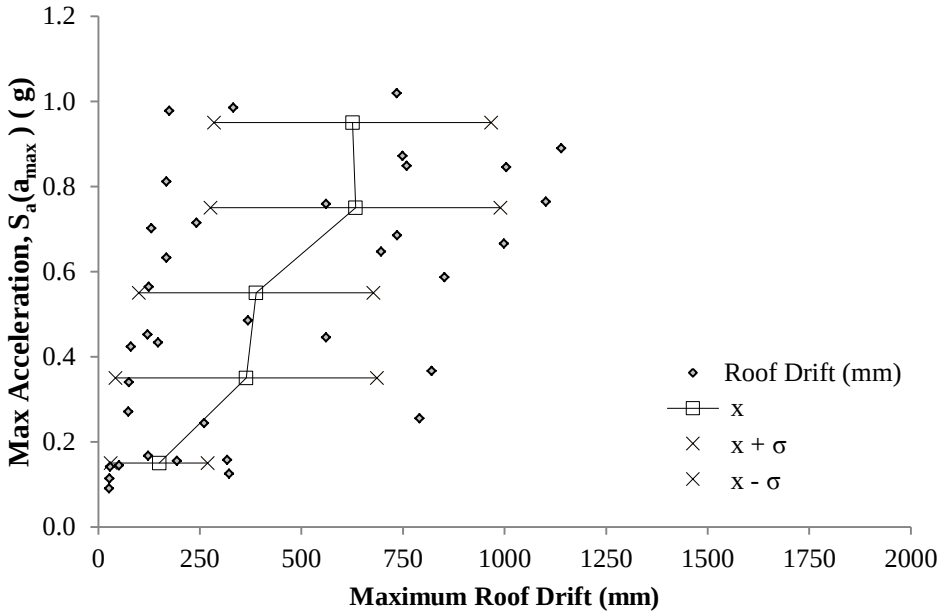

Figure 28. Average IDA curve for the earthquake model where DM is max roof drift

Plotting the averages against the median point of the spectral acceleration set for each range results in the average IDA for the model. The standard deviation range is also displayed. Note that although the average IDA curves provide an adequate estimation of roof drift and greater accuracy can be attained with more data points; if dynamic analysis was performed with each record scaled to more PGAs, the average IDA curves would provide a better approximation of structural response. Figures 29-30 contains the IDA and average IDA curves for both models where the DM is maximum base shear.

The average IDA curves for the max base shear damage measure for both models show that there is a greater correlation between maximum acceleration and base shear. This is reasonable since base shear is a force that is directly related to the acceleration of the building. As there is limited data supporting non-linear response, it is difficult to assess the strength of the structures; records scaled to higher PGAs would yield more information in that regard. Nevertheless, based on the average maximum base shear for the max acceleration range centered at 0.6g for wind and 0.95g for earthquake, the strength of the wind model is at least 9087.2 kN and the strength of the earthquake model is at least 15,730.7 kN. While the range of strength is similar, the wind model has greater strength from the dynamic analysis results than the static pushover analysis results, while the

earthquake model is just the opposite. The wind model has a greater strength capacity in response to seismic loading than indicated by the static pushover analysis. For the earthquake model, although the average IDA curve has an estimated strength that is more than 5,000 kN less than the predicted by static pushover analysis, the outlying data points representing Superstition Hills indicate that the base shear capacity of the earthquake model is greater than the 15,730.7 kN evaluated at a maximum acceleration of 0.95g. From observations of the base shear IDA curves, it is clear that the response of Superstition Hills is once again an outlier. It is likely that dynamic analysis for earthquake records scaled to higher PGAs will show that the strength of both models are greater than the strength from the static pushover analysis.

Once again, comparisons between the wind and earthquake models support the conclusions from the static pushover analysis that the earthquake model has greater strength than the wind model. However, it is important to understand that for the same ground motion, the earthquake model is subjected to greater base shears than the wind model; even though the base shear capacity of the earthquake model is significantly more than the capacity of the wind model, the applied load on earthquake models is also larger than the applied load on wind models. Other than the increased capacity, the disparity between the two models is not shown as drastically in the base shear IDA as in the roof drift IDA. In fact, there is only a 2,500 kN difference in base shear between the average IDA curves at 0.55g max acceleration. The relative closeness of the base shear IDA curves of the two models is explained very simply by Newton's second law: because base shear is a measure of force and forces are directly related to acceleration, similar accelerations yield similar base shears. Thus, the reason the earthquake model has higher base shears for comparable accelerations, is because it has a greater mass.

6.3.3 Assessment of Intermediate Characteristics

Since the global characteristics of the two models have been determined and compared, the next step is to assess the structural response of the models in terms of the intermediate characteristics. Using a damage measure of maximum inter-story drift (ISD), the model behavior at the intermediate level is displayed in the IDA curves in Figures 31 and 32.

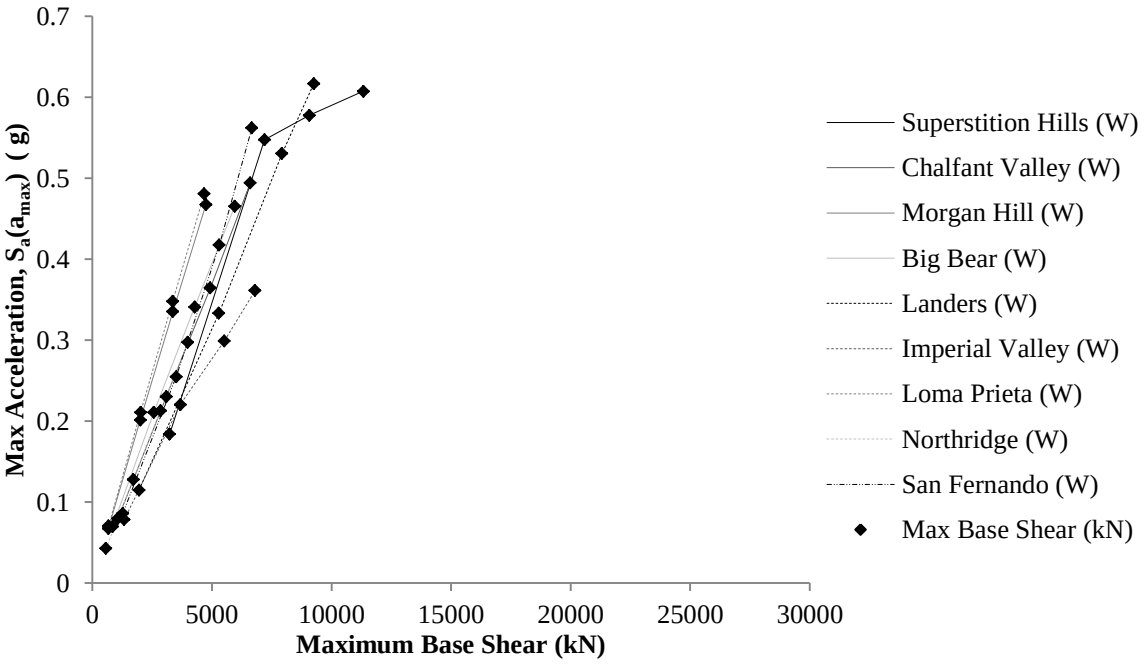

(a) Wind Model

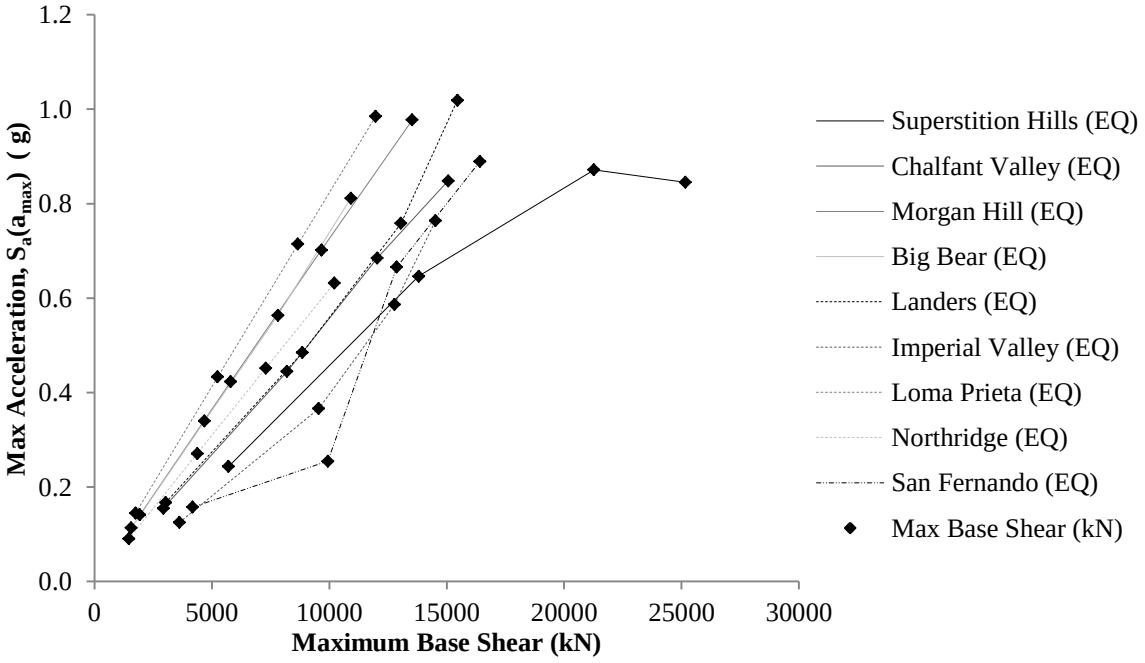

(b) Earthquake Model

Figure 29. IDA curves for both models where DM is max base shear

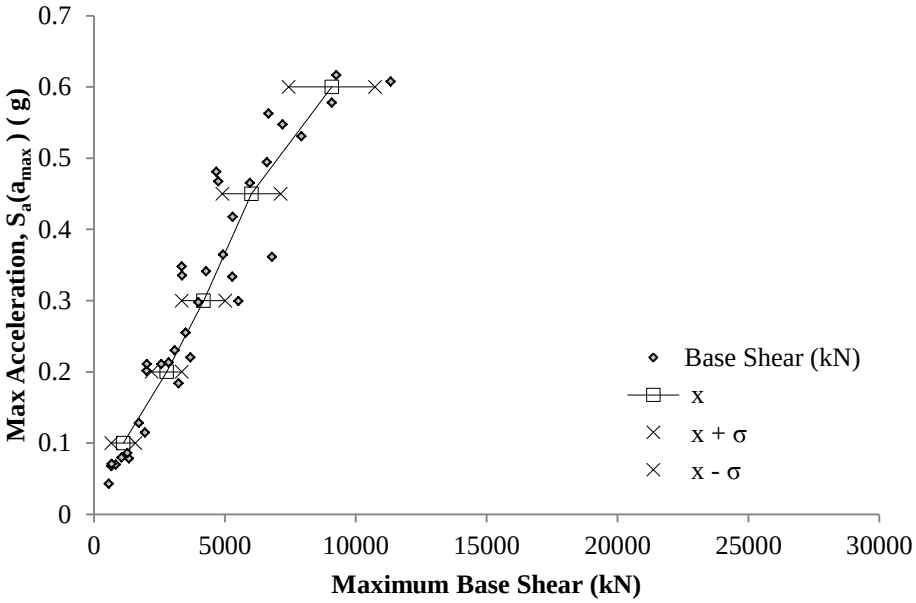

(a) Wind Model

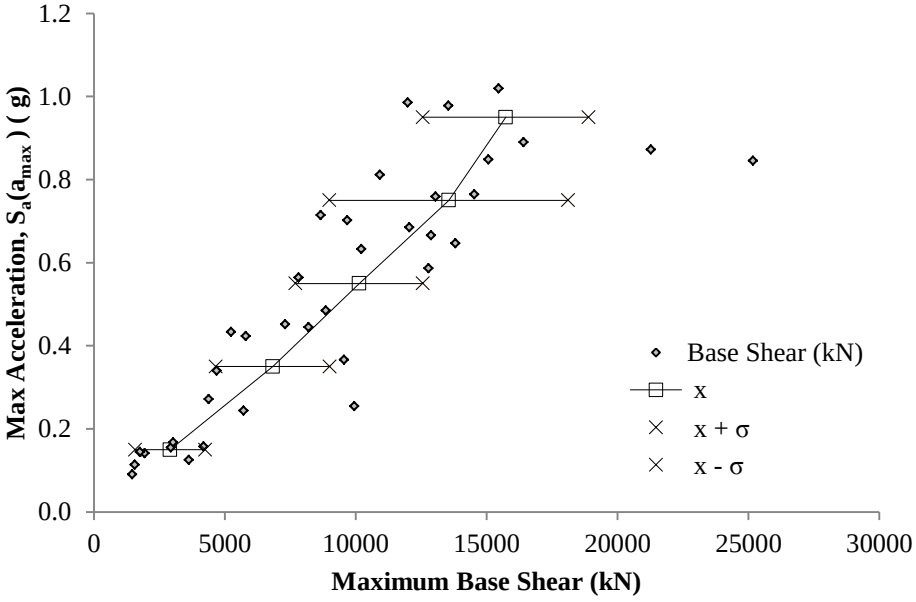

(b) Earthquake Model

Figure 30. Average IDA curves for both models where DM is max base shear

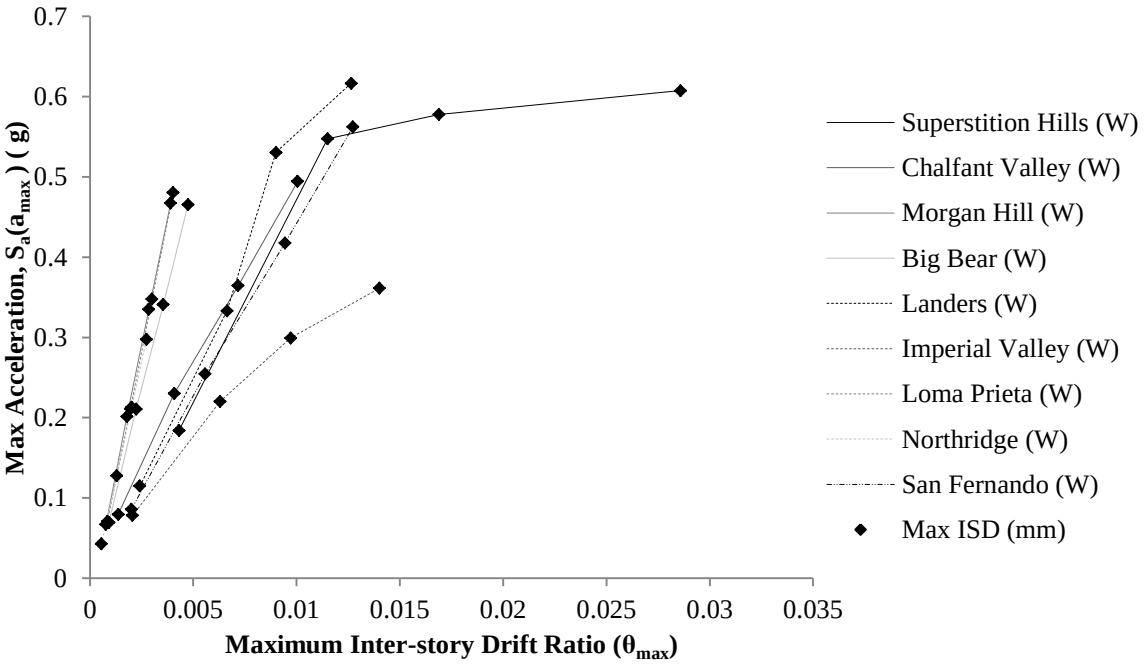

(a) Wind Model

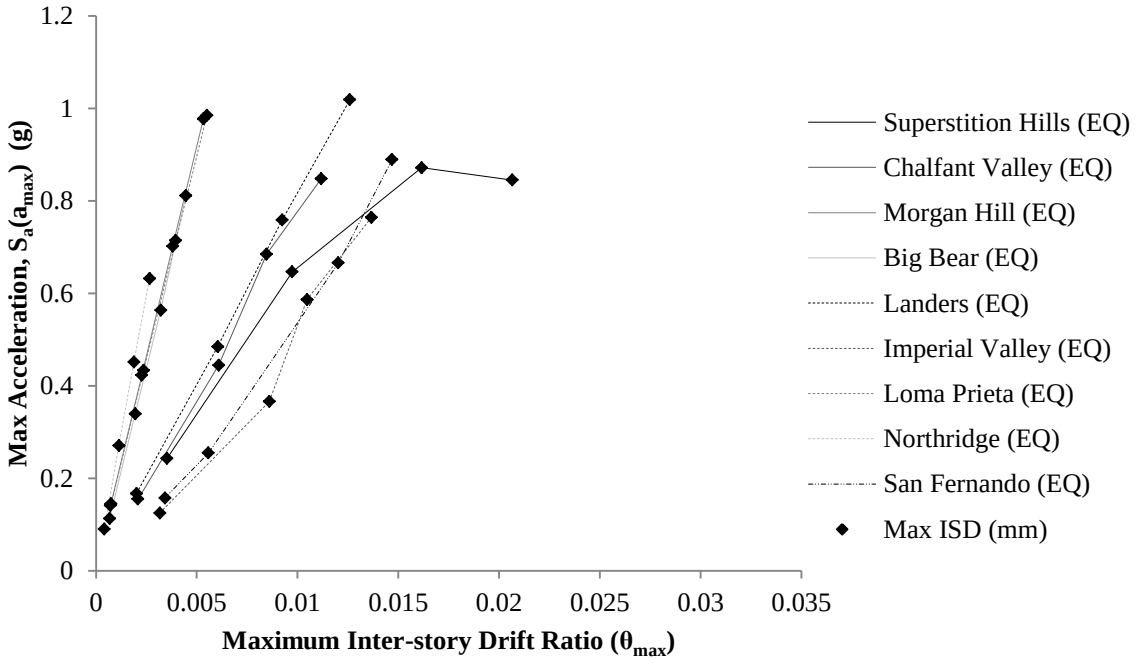

(b) Earthquake Model

Figure 31. IDA curves for both models where DM is max inter-story drift

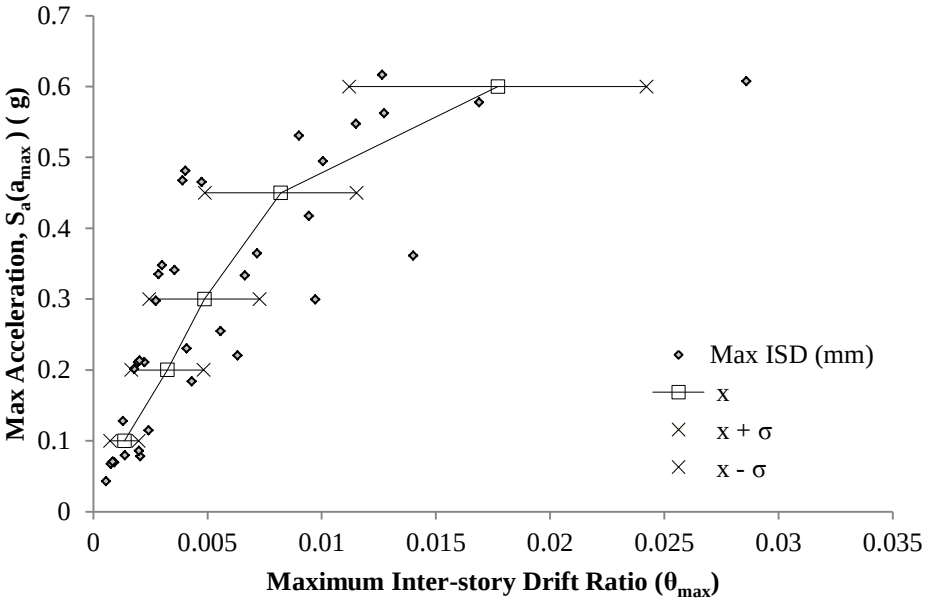

(a) Wind Model

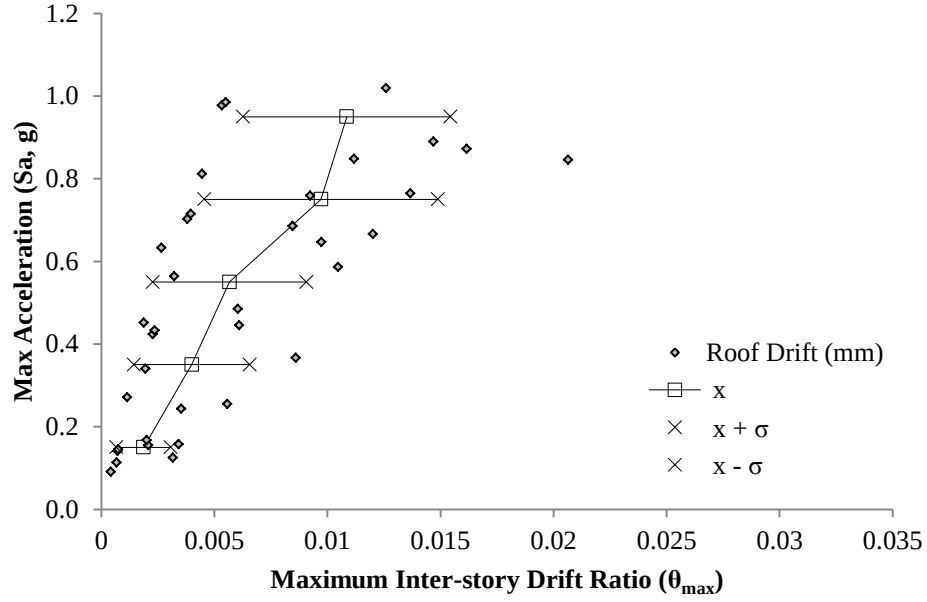

(b) Earthquake Model

Figure 32. Average IDA curves for both models where DM is max inter-story drift

When comparing the inter-story drift for the wind and earthquake models, the IDA curves and averages show that the wind designed building undergoes substantially greater levels of drift between floors than the earthquake designed building for the same load. This supports the global characteristic where total roof drift is larger for the wind than earthquake model. Also from the averaged IDA curves, using ISD as a damage measure provides a better picture of the disparities in response of the wind and earthquake models than the global characteristics. With a smaller standard deviation than roof drift as shown in Figures 27 and 28 and a smaller degree of linkage between the intensity and damage measures than base shear as exhibited in Figure 30, the inter-story drift average IDA curve displays a distinct contrasting structural response not observed from the other IDAs. While the average IDA curve remains predominately linear for the seismic design, there is a unmistakable non-linear response of the wind design after approximately 0.45g. From this IDA, it is demonstrated that non-linear behavior begins at lower loads for wind than earthquake designed buildings.

For a more detailed analysis of inter-story drift and how the characteristic differs between the two designs, the ISD concentration ratio, or ratios of maximum roof drift to roof drift if each floor is at maximum ISD is determined and compared for each record. Lower ratios indicate that the ISD is concentrated at only a few stories while higher ratios mean the inter-story drift is spread across a greater number of floors. To evaluate the variations between the wind and earthquake model, the difference between the ISD concentration ratios for the two for every scaled record is calculated and summed. It is found that the ISD concentration ratios are generally greater for the wind than earthquake model, meaning that in earthquake loading conditions, the inter-story drift is more evenly distributed among floors for wind designed buildings than seismically designed buildings.

6.3.4 Assessment of Local Characteristics

The final parameter assessed is the development of plastic hinges in order to obtain a closer examination of local behavior. With plastic hinges defined as the yielding of an extreme fiber of a section, the progression of plastic hinges for the two models subjected to all scaled records is assessed. To compare the creation of plastic hinges in beams compared

to columns, the stress in extreme fibers for the column base and corresponding beam of each floor along the fifth column line is measured. As neither model reached ultimate response under the selected records, it is expected that none of the columns will have plastic hinges. Instead, it is important to use the stress in columns relative to stress in the beams for comparison of the models.

Table 9 lists the number of floors with plastic hinges in the beams for each model along with the corresponding range of floors where plastic hinging occurs. Results from the Morgan Hill and Northridge earthquakes are not included in the table, as plastic hinging did not develop in either model for those records. Referring back to Figures 26, 29, and 31 that depict the IDA curves for roof drift, base shear and inter-story drift by earthquake, it can be seen that for Morgan Hill and Northridge, the IDA curves are linear in all cases. Other earthquakes, like Big Bear and Loma Prieta, are mostly linear with slight non-linearity for the records scaled to PGA = 0.7g and the minor non-linearity are supported by the small number of floors with plastic hinges for those records.

Table 9. Plastic Hinge Development

Earthquake Record	Wind Model		Earthquake Model	
	# Plastic Hinges	For Floors	# Plastic Hinges	For Floors
Superstition Hills				
0.1g	7	33 - 39	0	-
0.3g	38	7 - 46	22	23 - 44
0.5g	43	5 - 47	34	8 - 41
0.7g	44	4 - 47	39	6 - 44
Chalfant Valley				
0.1g	0	-	0	-
0.3g	0	-	0	-
0.5g	25	21 - 45	29	16 - 44
0.7g	39	8 - 46	34	13 - 46

Table 9. Plastic Hinge Development (cont.)

Earthquake Record	Wind Model		Earthquake Model	
	# Plastic Hinges	For Floors	# Plastic Hinges	For Floors
Big Bear				
0.1g	0	-	0	-
0.3g	0	-	0	-
0.5g	0	-	0	-
0.7g	4	43 - 46	0	-
Landers				
0.1g	0	-	0	-
0.3g	17	30 - 46	0	-
0.5g	43	4 - 46	15	30 - 44
0.7g	45	3 - 47	18	26 - 46
Imperial Valley				
0.1g	0	-	0	-
0.3g	24	22 - 45	5	35 - 39
0.5g	31	16 - 46	38	8 - 45
0.7g	34	13 - 47	40	6 - 45
Loma Prieta				
0.1g	0	-	0	-
0.3g	0	-	0	-
0.5g	0	-	0	-
0.7g	6	36 - 38, 43 - 45	0	-
San Fernando				
0.1g	0	-	0	-
0.3g	26	20 - 45	24	22 - 45
0.5g	37	10 - 46	35	11 - 45
0.7g	37	10 - 46	36	10 - 45

Once again, by comparing the amount of plastic hinging to the amount of non-linear response in the previous IDA curves, it is observed that there is a direct relationship between the number of plastic hinges and non-linear intermediate and global response. Superstition Hills, with the most distinct non-linearity has the greatest total number of floors with plastic hinges. Recalling to the previous examination of base shears, the higher number of floors with plastic hinges for Superstition Hills supports the earlier conclusion that more plastic hinges allow for higher strength. Although the plastic hinge results support the global behavior, the column and beam stresses are more useful for comparing the wind and earthquake models at a local level. Figures 33 to 35 present the IDA and average IDA curves for member stress.

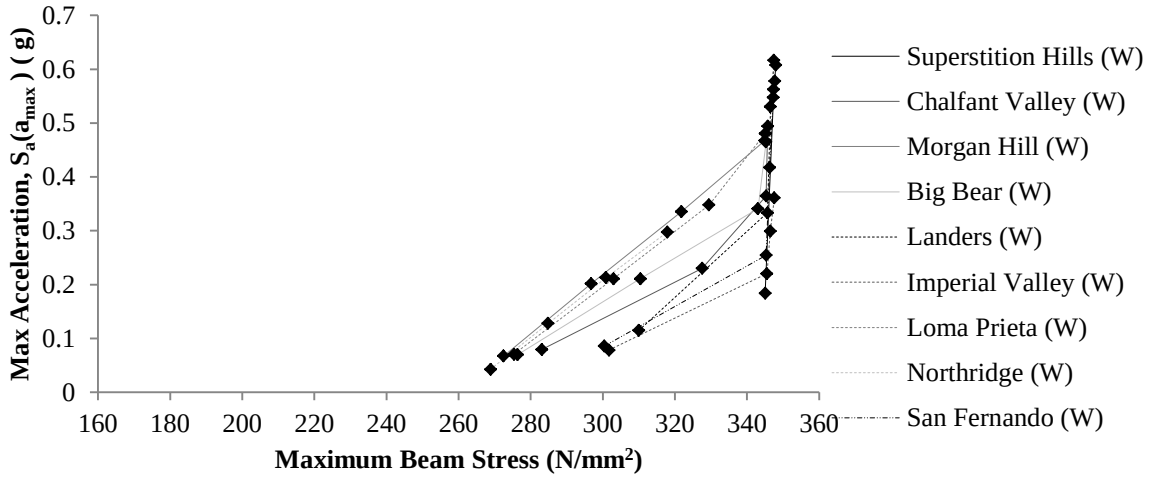

(a) Wind Model

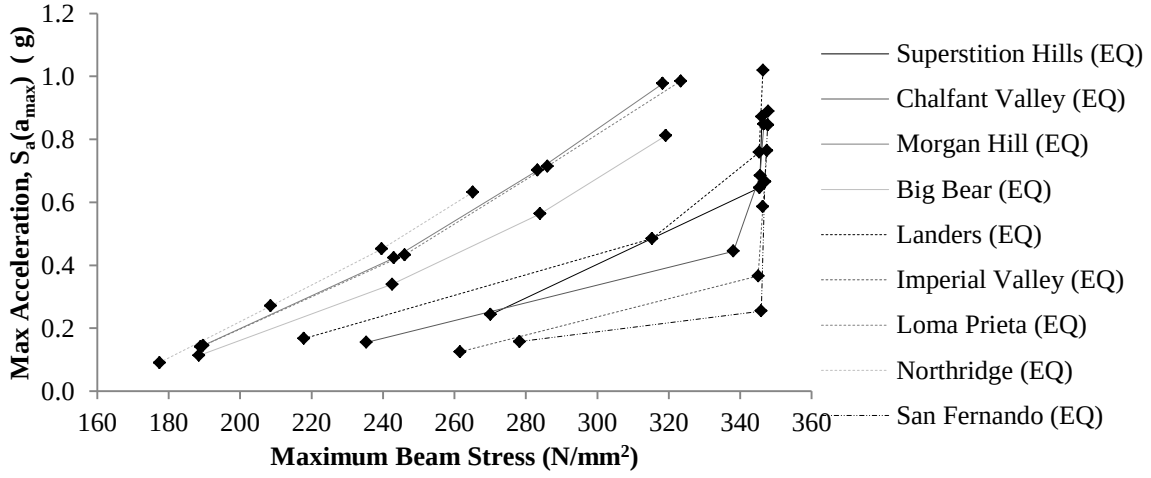

(b) Earthquake Model

Figure 33. IDA curves for both models where DM is max beam stress

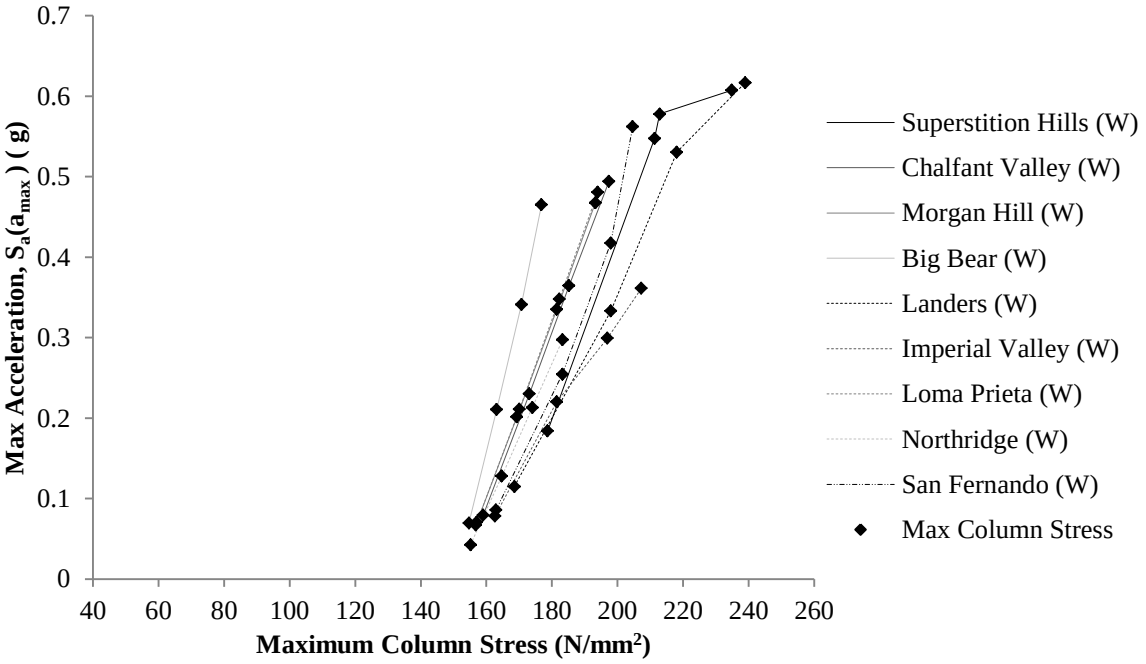

(a) Wind Model

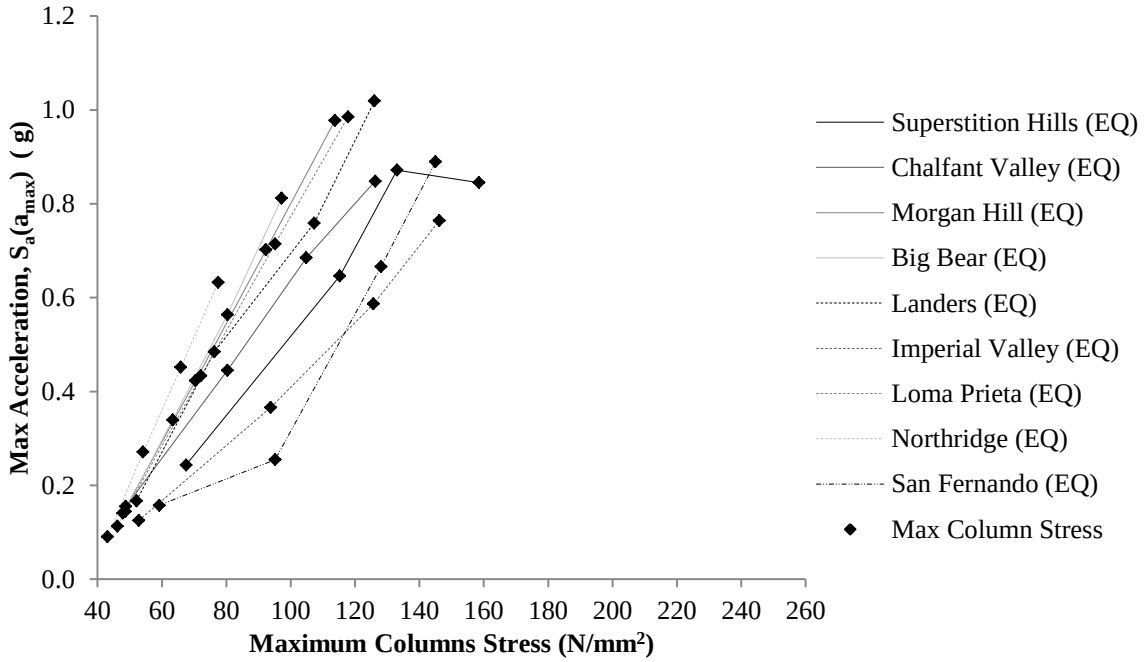

(b) Earthquake Model

Figure 34. IDA curves for both models where DM is max column stress

Solely from the comparison of the non-averaged IDA curves, it is obvious from Figure 33 that although the maximum stress in outer fibers for beams are similar for the two models, there is a considerable shift in levels of stress in the columns between the earthquake and wind models in Figure 34. The slopes of the linear portion of the IDA curves for max column stress are alike, but the column stresses for the wind model are shifted up so that the maximum stresses begins at around 150 N/mm2 instead of 40 N/mm2 as in the earthquake model. The non-linearity of the IDA curves in Figure 34 is not due to the members reaching yield stress and undergoing inelastic behavior, but rather is due to the plastic hinging in the beams which results in load transfer from the beams to columns. For a better comparison of the maximum column stress for the two models, the average IDA curves for wind and earthquake where the damage measure is max column stress are shown on the same plot in Figure 35 below.

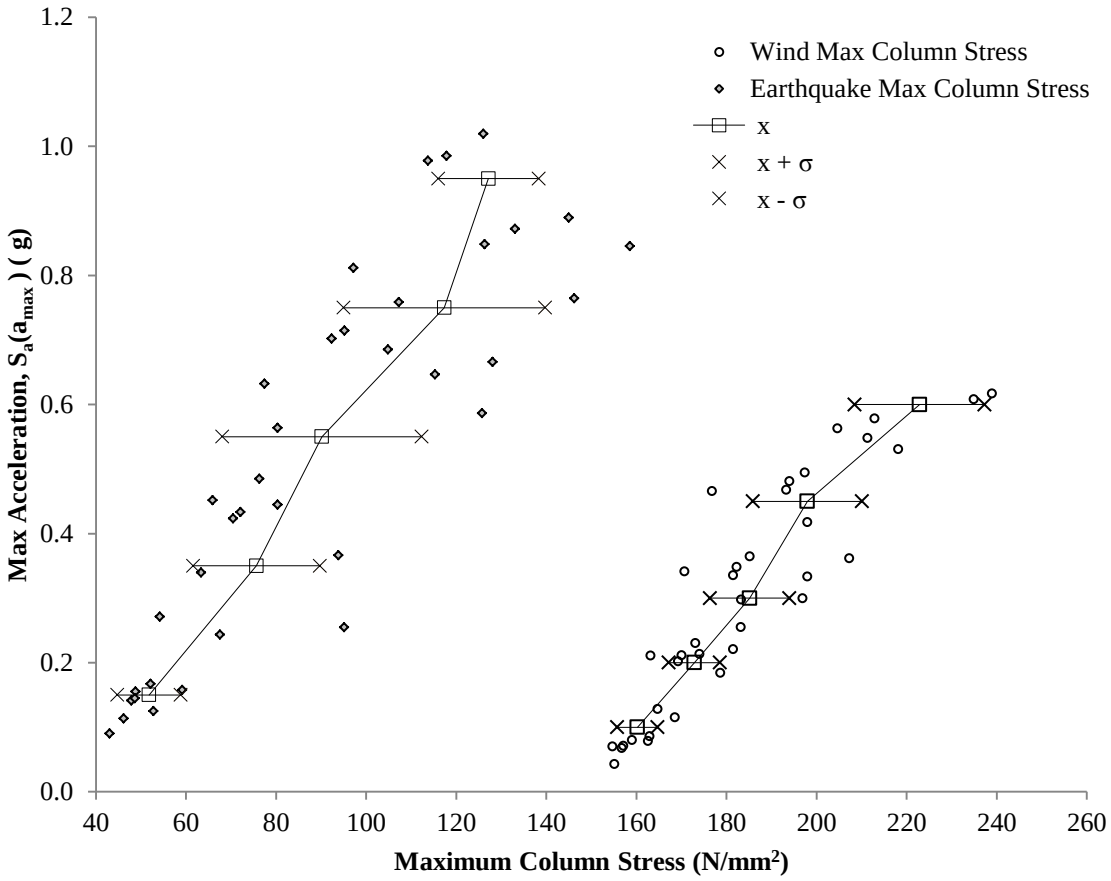

Figure 35. Average IDA curves for both models where DM is max column stress

These results indicate that although the number of plastic hinges for records up to PGA = 0.7g are similar for the wind and earthquake models, for greater loads, it is likely that the columns for the wind model will yield earlier than the earthquake designed columns. Since the column stresses are closer to yield for wind than earthquake, the wind model is expected to fail first. The lower max column stress for the earthquake model is due to the use of strong column-weak beam capacity design. Although the beams do yield before columns for the wind design as well, the greater load capacity before yield stress for the earthquake model ensures that the earthquake design will have greater ductility.

The development of plastic hinges does not provide significant insight into local behavior other than the determination of how local characteristics influence global response of structures. However, from the comparison of the stress levels for beams and columns at the members' exterior fibers, contrasts between the wind and earthquake model can be made. Due to the tendency of earthquake designed buildings to maintain ample residual stress capacity after beams yield, they respond with greater ductility than wind designed buildings under seismic loads.

6.3.5 Inherent Wind and Earthquake Resistance

The final application of dynamic time history analysis for the comparison of wind and earthquake designed mid- to high-rise structures is to return to the previous assessment of inherent wind resistance of earthquake design and inherent earthquake resistance of wind design. Previously, it was found that while it is suitable to determine wind resistance of earthquake design using static pushover analysis and code based wind loads, safety factors in the seismic design code limited the usefulness of the static analysis for the reverse case. To that end, the inherent earthquake resistance of wind designed structures can be determined using the average incremental dynamic analysis curve for the wind model where the damage measure is maximum roof drift. Using the IDA curve in Figure 36 on the following page, it can be determined that the wind designed building can resist earthquakes where the maximum acceleration, $S_a(a_{max}) = 0.471g$. This value is found using the mean value of the average IDA curve when the maximum roof drift is equal to the seismic drift limit of $\Delta_{lim} = 705$ mm. For a more conservative estimate, Figure 37 shows

the $S_a(a_{max})$ for the seismic drift limit based on the mean plus standard deviation. From Figure 37, the conservative estimate of seismic resistance of the wind designed structure is $S_a(a_{max}) = 0.34g$.

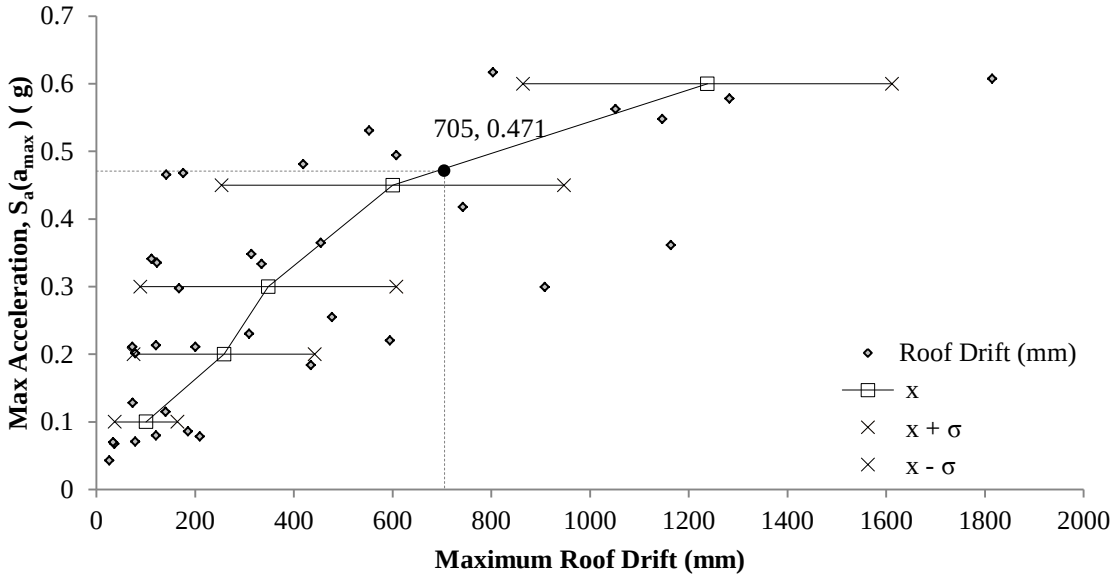

Figure 36. Estimation of earthquake resistance of wind model using wind mode IDA average curve where DM is max roof drift.

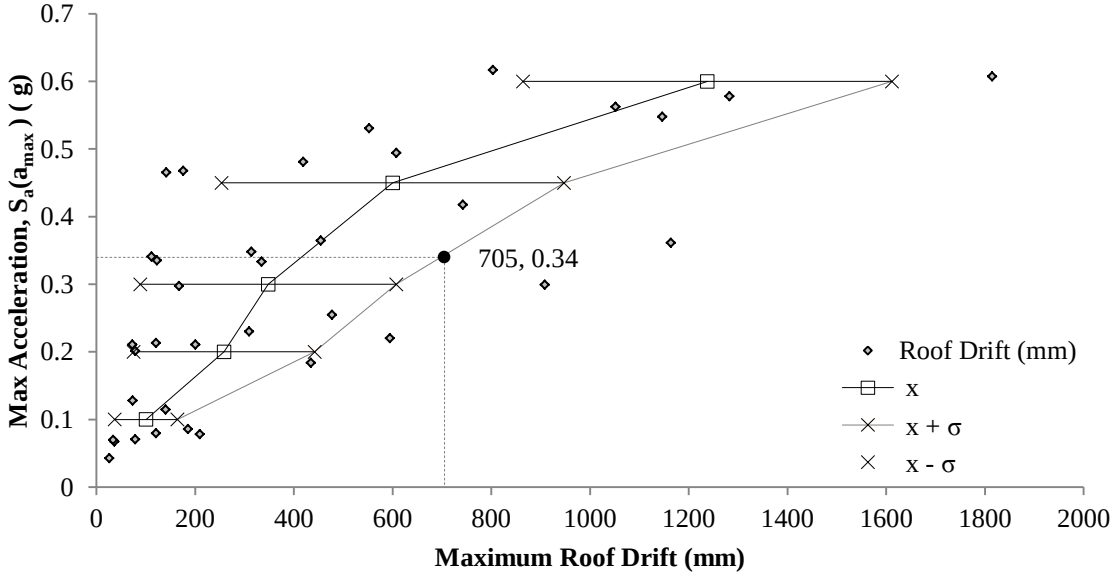

Figure 37. Estimation of earthquake resistance of wind model using wind mode IDA mean plus standard deviation curve where DM is max roof drift.

Dynamic time history analysis is an extremely useful method to assess structural response to seismic loading. By using natural records selected for the building's expected loading scenario, a realistic behavior of the structure can be determined. For this study, this method of structural analysis is particularly important for two reasons. First, the long first natural period results in the second and third modes having a greater influence on structural response. The tendency of long period structures to respond in a combination of modes mean that dynamic time history analysis provides a better estimation of behavior than static pushover analysis which assumes first mode response. Second, while static pushover analysis is adequate for global response, time history analysis is better for the evaluation of local and intermediate response by not assuming a specific distribution of lateral loads and allowing the system to distribute loads based on the structure. However, static pushover analysis remains useful in determining the effect of wind loads on structures. In general though, the combination of eigenvalue analysis, static pushover analysis, and dynamic time history analysis allows for a comprehensive assessment of the response of wind and earthquake designed mid- to high-rise buildings under wind and seismic loading.

CHAPTER 7: CONCLUSION

This thesis research explores the structural response of mid- to high-rise buildings subject to wind and earthquake hazards. The study first considers the advancements made by other researchers on the topic of multi-hazard structural design, and develops a thorough review of the characteristics of wind and seismic loads. Once a fundamental understanding of the hazards was established, analytical modeling allowed for realistic representation of buildings designed for wind and earthquake loads. Using various types of analysis including static pushover and dynamic time history analyses, the similarities and differences of the two structural designs were assessed. Close consideration of the contrasts in the structural response of the models at the global, intermediate, and local levels provides significant insight into the differences in wind and earthquake design. A better understanding of these disparities is beneficial for the design of mid- to high-rise buildings for multiple hazards. The findings of this research are summarized in the following paragraphs.

7.1 Summary

Mid-to-high rise buildings are often not governed by gravity loads, but from lateral loads from various natural hazards including high winds and earthquakes. Current design practices for tall buildings require the consideration of only the controlling load case for structural design. While effective for areas where there is only the risk of one hazard, this method underestimates the increased risk for multiple hazard regions and does not consider the differences in structural response to different load types. These variations in structural requirements necessitate the consideration of both loading cases during design.

In most multi-hazard areas, high wind events, such as hurricanes, are more common than earthquakes. Although the magnitude of lateral loads due to wind is generally less than loads from earthquakes, the limit state is in fact more stringent for wind design due to the relative frequency of high winds. Wind controlled structures are often designed to serviceability limit states where building displacements are restricted for occupant comfort and for immediate use after the hazardous event. Buildings controlled by earthquake

loading however, consider the diminished rate of recurrence of earthquakes and are designed for either life safety or repairable damage limit states to reduce the social and economic costs. These differences in limit states as well as design requirements from the different manners in which the lateral loads are applied to the structure result in variations in structural response to the two hazards.

The lateral load resisting systems of high-rise structures were modeled in two dimensions using the nonlinear analysis platform, ZeusNL. Eigenvalue, static pushover, and dynamic time history analyses, were used to study building behavior thereby providing the following conclusions:

- The natural periods for the first five modes of response are all longer for the wind design model than the earthquake model, which affects the earthquake loads.
- Although mass participation values show that the structures respond mostly in the first mode, the relatively low mass participation in the first mode – compared to low rise buildings – and low spectral accelerations associated with long periods indicate that the structures generally respond in a combination of modes.
- The substantially greater magnitude of global strength capacity that is required for earthquake design results in the earthquake design also having higher building stiffness.
- In dynamic time history analysis, for the same ground motion record, the earthquake model experiences greater accelerations due to its greater mass and stiffness. Higher accelerations translate to higher loads, so although the earthquake design has greater strength capacity, it is also subjected to greater loads.
- The use of capacity design with Strong Column-Weak Beam Theory for earthquake design provides the earthquake model with greater displacement ductility.
- Maximum inter-story drifts recorded for the dynamic time history analyses reflect the intermediate behavior of the frames; non-linear behavior begins at lower loads for the wind rather than the earthquake design.
- Under earthquake loading conditions, inter-story drift is more evenly distributed across floors for the wind model than the earthquake model.

- The greater relative stiffness of beams to columns at higher floors results in the beams in upper floors developing plastic hinges earlier than beams in lower floors.
- When subjected to the same seismic loads, the stress and resulting plastic hinging in beams are similar for the wind and earthquake design, however the stress in columns are significantly greater for the wind design than the earthquake design.
- For the specific structure analyzed in this study, an earthquake designed structure has an inherent wind resistance for wind speeds up to 127mph and a wind designed structure has an inherent seismic resistance for spectral accelerations up to 0.34g.

This thesis research delivers a solid background on the behavior of mid- to high-rise buildings under wind and earthquake loading. The establishment of this knowledge base advances the field of multi-hazard design by bridging the gap between the disciplines of wind and seismic structural design.

7.2 Future Work

While this study provides a greater understanding of how buildings designed for one hazard respond to additional hazards, further study can be done on methods to better combine wind and earthquake design aspects for multi-hazard design. Variations in building height for the model can also reveal how a structure's geometry affects its response to wind and earthquake loading; by varying structure height, recommendations for how to improve a wind controlled building for earthquake resistance can be applicable for a greater range of buildings. Another avenue for future work would be to study the response of reinforced concrete structures and the corresponding effects of stiffness degradation on multi-hazard design. With a complete comprehension of structural behavior across various building geometries and construction materials, the widespread use of multi-hazard design in mid-to high-rise buildings is possible.

REFERENCES

American Society of Civil Engineers (ASCE), (2006). "Minimum Design Loads for Buildings and Other Structures." ASCE Standard: ASCE/SEI 7-05, Reston, VA.

Associated Press (AP), (2009). "U.N.: 1,100 Dead in Indonesia Earthquake." October 1, 2009. Fox News <http://www.foxnews.com/story/0,2933,558283,00.html>.

Atkinson, G.M. and Boore, D.M. (1997). "Some Comparisons Between Recent Ground-Motion Relations" Seismological Research Letters, Vol. 68, No. 1, pp. 24-40, February 1997.

Beers, P.E. (2011). "Hurricane and Tornado Damage in Urban Areas – A Recent History." May 24, 2011. Pushing the Building Envelope <http://buildingenvelope.wordpress.com/2011/05/24/hurricane-and-tornado-damage-in-urban-areas-%E2%80%93-a-recent-history/>.

Bertuca, D.J. (2011). "Indian Ocean Tsunami Disaster- December 26, 2004 and Reconstruction." November 16, 2011. State University of New York at Buffalo <http://library.buffalo.edu/asl/guides/indian-ocean-disaster.html>.

Blake, E.S., Landsea, C.W., and Gibney, E.J. (2011). "The Deadliest, Costliest, and Most Intense United States Tropical Cyclones from 1851 to 2010 (And Other Frequently Requested Hurricane Facts)." NOAA Technical Memorandum NWS NHC-6, Miami, FL, August 2011.

Boggs, D. and Dragovich, J. (2008). "The Nature of Wind Loads and Dynamic Response." December 8, 2008. Cermak Peterka Petersen Inc. <http://www.cppwind.com/support/papers/papers/structural/240-2.pdf>.

Braile, L. (2003). "Earthquake Hazard Information- Photos of Earthquake Damage, Modes of Building Failure − Part 1." March 2003. Purdue University <http://web.ics.purdue.edu/~braile/edumod/eqphotos/eqphotos1.htm>.

Buresti, G. (2000). "Bluff-Body Aerodynamics- Lecture Notes" June 12, 2000. University of Pisa, Italy < http://www.mech.kth.se/courses/5C1211/BluffBodies.pdf >.

Crosti, C., Duthinh, D. and Simiu, E. (2011). "Risk Consistency and Synergy in Multihazard Design." Journal of Structural Engineering, ASCE, Vol. 137, No. 8, pp. 884-849, August 2011.

Duthinh, D. and Simiu, E. (2010). "Safety of Structures in Strong Winds and Earthquakes: Multihazard Considerations." Journal of Structural Engineering, ASCE, Vol. 136, No. 3, pp. 330-333, March 2010.

Elnashai, A.S. and Di Sarno, L. (2008). *Fundamentals of Earthquake Engineering.* Wiley Press. Chichester, United Kingdom.

Ettouney, M. and Alampalli, S. (2006). "Blast Hazard Considerations within a Multihazards Environment: An Application to the Theory of Multihazards." Proceedings of the 2006 Structures Congress, May 2006.

Ettouney, M., Alampalli, S. and Agrawal, A. (2005). "Theory of Multihazards for Bridge Applications." Journal of Bridge Structures: Assessment, Design and Construction, Taylor & Francis, Vol. 1, No. 3, pp. 281-291.

Ettouney, M. and Glover, N. (2002). "Engineering of Architectural Systems." Journal of Architectural Engineering, ASCE, Vol. 8, No. 1, pp. 7-9, March 2002.

Faison, H., Comartin, C., Elwood, K. (2004). "Housing Report: Reinforced Concrete Moment Frame Building without Seismic Details." September 2004. Earthquake Engineering Research Institute <http://www.world-housing.net/whereport1view.php?id=100108>.

Goltz, J.D. (1995). "Preliminary Reports from the Hyogo-ken Nambu Earthquake of January 17, 1995." National Center for Earthquake Engineering Research: Response, State University of New York at Buffalo.

Holmes, J.D. (2003). "Basic Bluff-Body Aerodynamics I." September 22, 2003. Louisiana State University <www.hurricaneengineering.lsu.edu%2FCourseMat%2F03Lect8BluffBodyAero.ppt&ei=N8MUT6_UOOKvsAKE6ZHVAw&usg=AFQjCNEvhdaOhJDuUdEabWQ7bzfM4k-bCA>.

Isaradharm, V. (1997). "Damage Due to Liquefaction." October 1997. University of California, Berkeley <http://nisee.berkeley.edu/bertero/html/damage_due_to_liquefaction.html>.

Jayachandran, P. (2009). "Design of Tall Buildings- Preliminary Design and Optimization." Keynote Lecture of the National Workshop on High-rise and Tall Buildings, University of Hyderabad, May 2009.

Joseph, L.M., Poon, D., and Shieh, S. (2006). "Ingredients of High-Rise Design: Taipei 101, the World's Tallest Building." Structure Magazine, pp. 40-45, June 2006.

Joyce, C. (2012). "How Fracking Wastewater is tied to Quakes." January 5, 2012. National Public Radio (NPR) < http://www.npr.org/2012/01/05/144694550/man-made-quakes-blame-fracking-and-drilling >.

Lorant, G. (2010). "Seismic Design Principles." June 2010. Whole Building Design Guide <http://www.wbdg.org/resources/seismic_design.php>.

Mays, T.W. (2005). "Illustrative Examples of Multi-Hazard Design in Coastal South Carolina." Solutions to Coastal Disasters, ASCE, May 2005.

Mid-America Earthquake (MAE) Center (2010). "The Maule (Chile) Earthquake of February 27, 2010: Consequence Assessment and Case Studies." MAE Center Report No. 10-04, April 2010.

Naeim, F. (2011). "CSMIP-3DV" March 1, 2011. NEEShub <https://nees.org/resources/2678>.

National Hurricane Center (NHC), (2010). "High Winds." February 2010. NHC Hurricane Preparedness < http://www.nhc.noaa.gov/HAW2/english/high_winds.shtml>.

National Oceanic & Atmospheric Administration (NOAA), (2007). "Hurricane Katrina-Most Destructive Hurricane Ever to Strike the U.S." February 12, 2007. NOAA Public Affairs <http://www.katrina.noaa.gov/>.

Powell, M.D. and Houston, S.H. (1996). "Hurricane Andrew's Landfall in South Florida. Part II: Surface Wind Fields and Potential Real-Time Applications" Weather and Forecasting, AMS, Vol. 11, No. 3, pp. 329-348, September 1996.

Rappaport, E. (1993). "Preliminary Report: Hurricane Andrew." December 10 1993. National Hurricane Center < http://www.nhc.noaa.gov/1992andrew.html>.

Schweizerischer Erdbebendienst (SED), (2001). "Earthquake Damage." April 2011. SED General Information <http://www.seismo.ethz.ch/eq/info/damage/index_EN>.

Singh, J.P. (1985). "Earthquake ground motions: Implications for designing structures and reconciling structural damage." Earthquake Spectra, Vol. 1, Issue 2, pp. 239-270.

Taher, R. (2010). "General Recommendations for Improved Building Practices in Earthquake and Hurricane Prone Areas." Architecture for Humanity <http://blog.lib.umn.edu/taff0015/myblog/AfH_Improved%20Building%20Practices%20for%20Hurricane%20and%20Earthquake%20Prone%20Areas.pdf>.

Taylor, A.W. (2011). "High Rise Buildings: 2011 Japan Earthquake – Lessons Learned for the Pacific Northwest." June 15, 2011. University of Washington <http://www.seaw.org/documents/JEQ6-HighRise.pdf>.

United States Department of State, (2011). "Background Note: Haiti". October 19, 2011. Bureau of Western Hemisphere Affairs <http://www.state.gov/r/pa/ei/bgn/1982.htm>.

Vamvatsikos, D. and Cornell, C.A. (2002). "Incremental dynamic analysis." Earthquake Engineering and Structural Dynamics, Vol. 31, Issue 3, pp. 491-514, March 2002.

World Bank, (2011). “The Recent Earthquake and Tsunami in Japan: Implications for East Asia”. East Asia and Pacific Economic Update. March 2011. Volume 1 <http://siteresources.worldbank.org/INTEAPHALFYEARLYUPDATE/Resources/550192-1300567391916/EAP_Update_March2011_japan.pdf>.

Yang, T. (2006). “Topic: Wind Loads.” September 5, 2006. University of California, Berkeley < http://peer.berkeley.edu/~yang/courses/ce248/CE248_LN_Wind_loads.pdf >.

APPENDIX A: MEMBER SIZES

Figure depicting section dimension definitions:

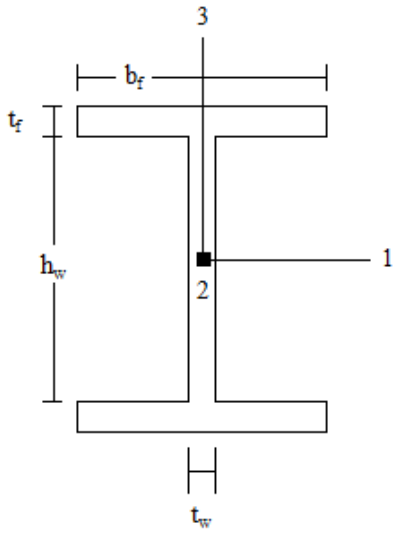

Figure depicting column line layout:

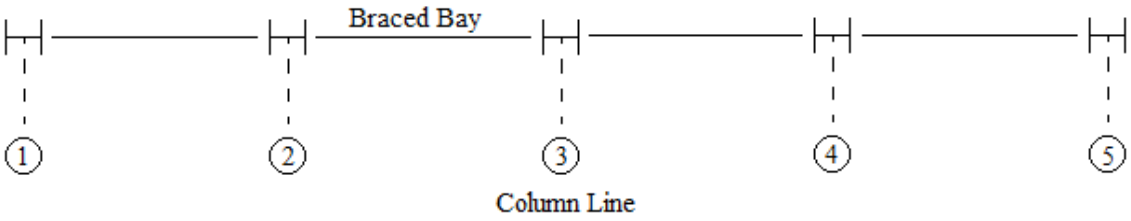

Wind Model Member Sizes:

Section Name	Location	Section Dimensions (mm, mm^2)				
		b_f	t_f	h_w	t_w	A
baseint	Columns for Floors 1 - 9	1000	75	1300	65	234500
tenint	Columns for Floors 10 - 19	850	65	1100	55	171000
twntyint	Columns for Floors 20 - 29	700	55	850	40	111000
thrtyint	Columns for Floors 30 - 39	550	45	700	20	63500
frtyint	Columns for Floors 40 - 47	400	25	550	10	25500
beam (W16X40)	Beams for All Floors	178	13	381	8	7676
brace	Braces for All Floors	150	20	200	10	8000

Wind Model Axial Load Capacity of Base Columns:

Column Line	Gravity Only		Static Load	
	P (kN)	Squash (%)	P (kN)	Squash (%)
1	17,539	21.68	14,860	18.37
2	29,295	36.21	19,417	24.00
3	29,965	37.04	39,832	49.23
4	28,934	35.76	29,867	36.92
5	17,672	21.84	19,429	24.02

Earthquake Model Member Sizes:

Section Name	Location	Section Dimensions (mm, mm^2)				
		b_f	t_f	h_w	t_w	A
baseint	Columns for Floors 1 - 9	1600	180	2000	100	776000
tenint	Columns for Floors 10 - 19	1450	160	1900	80	616000
twntyint	Columns for Floors 20 - 29	1200	105	1700	75	379500
thrtyint	Columns for Floors 30 - 39	900	65	1400	45	180000
frtyint	Columns for Floors 40 - 47	700	45	1100	25	90500
beam (W16X50)	Beams for All Floors	180	17	383	10	9950
brace	Braces for All Floors	150	20	200	10	8000

Earthquake Model Axial Load Capacity of Base Columns:

Column Line	Gravity Only		Static Load	
	P (kN)	Squash (%)	P (kN)	Squash (%)
1	19,741	7.37	12,844	4.80
2	33,047	12.34	-3,531	-1.32
3	33,514	12.52	70,209	26.22
4	32,781	12.24	34,237	12.79
5	19,795	7.39	25,119	9.38

NGA #	Event	Year	Station	Magnitude	Mechanism	R_{rup} (km)	V_{s30} (m/s)	Low Freq. (Hz)
68	San Fernando	1971	LA-Hollywood Stor FF	6.61	Reverse	22.8	316.5	0.25
176	Imperial Valley	1979	El Centro Array #13	6.53	Strike-Slip	22	249.9	0.25
447	Morgan Hill	1984	Agnews State Hospital	6.19	Strike-Slip	24.5	239.7	0.25
553	Chalfant Valley	1986	Long Valley Dam (Downst)	6.19	Strike-Slip	21.1	345.4	0.12
729	Superstition Hills	1987	Wildlife Liquef. Array	6.54	Strike-Slip	23.9	207.5	0.12
770	Loma Prieta	1989	Gilroy Array #7	6.93	Reverse-Oblique	24.8	333.9	0.25
901	Big Bear	1992	Big Bear Lake-Civic Center	6.46	Strike-Slip	9.4	338.5	0.12
850	Landers	1992	Desert Hot Springs	7.28	Strike-Slip	21.8	345.4	0.07
988	Northridge	1994	LA- Century City CC North	6.69	Reverse	23.4	278	0.14

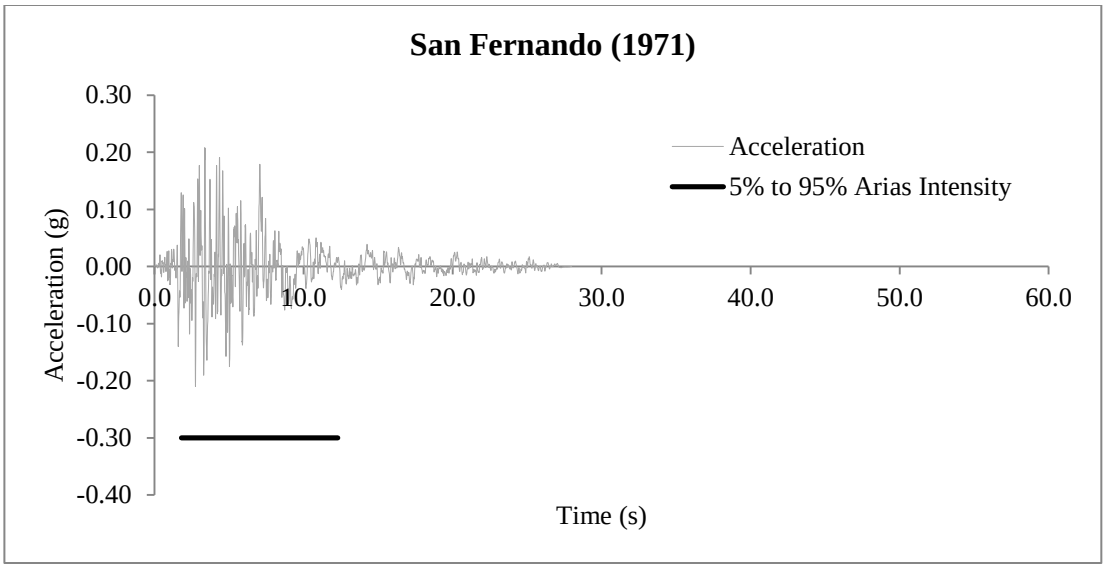
San Fernando (1971)
0.30
0.20
0.10
0.00
-0.10
-0.20
-0.30
-0.40
Acceleration (g)
0.0
10.0
20.0
30.0
40.0
50.0
60.0
Time (s)
Acceleration
5% to 95% Arias Intensity

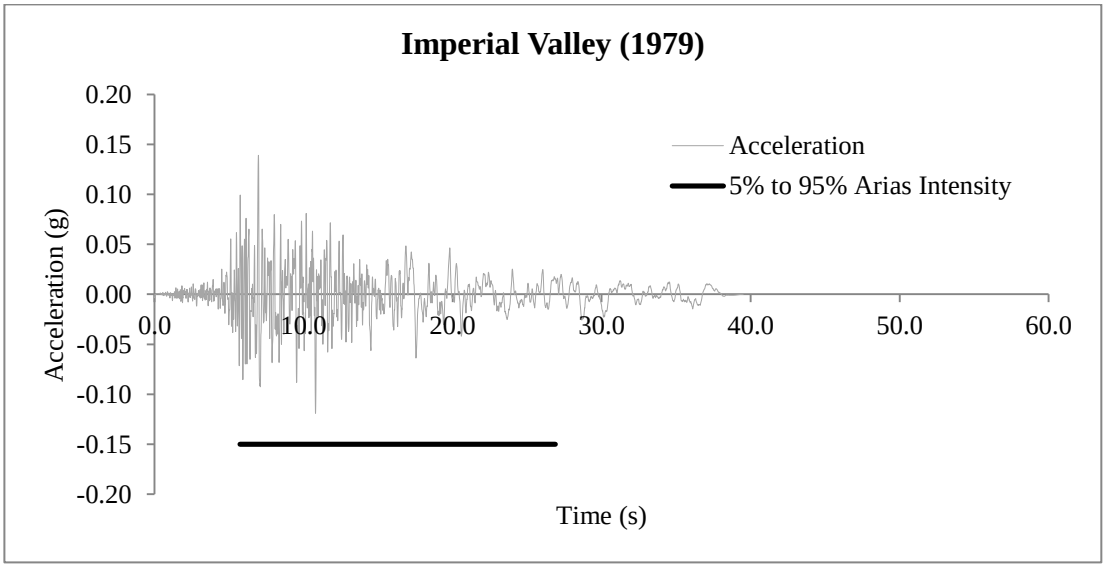
Imperial Valley (1979)
0.20
0.15
0.10
0.05
0.00
-0.05
-0.10
-0.15
-0.20
Acceleration (g)
0.0
10.0
20.0
30.0
40.0
50.0
60.0
Time (s)
Acceleration
5% to 95% Arias Intensity

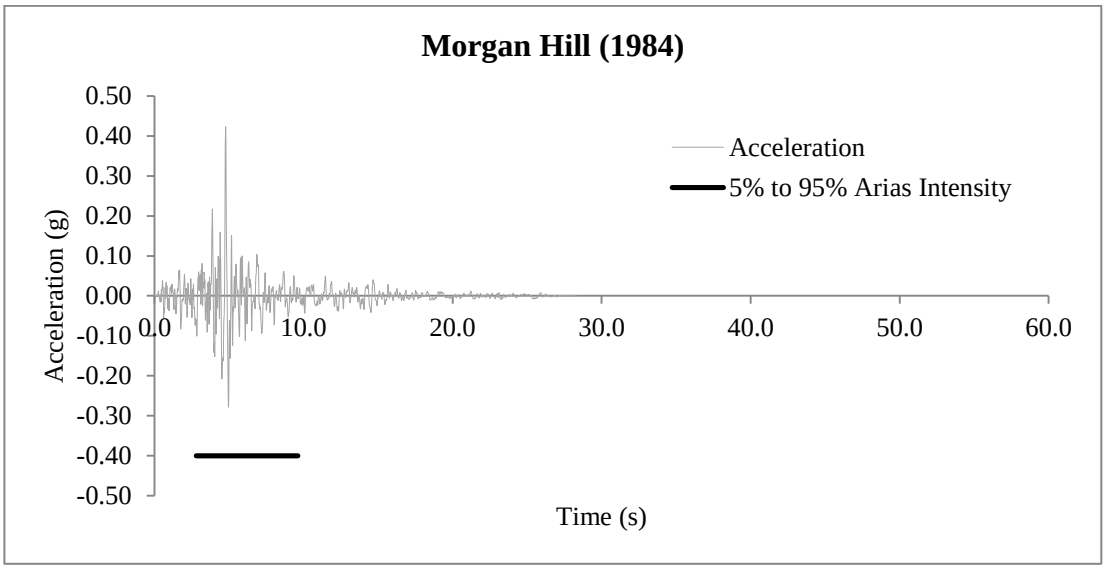
Morgan Hill (1984)
0.50
0.40
0.30
0.20
0.10
0.00
-0.10
-0.20
-0.30
-0.40
-0.50
Acceleration (g)
0.0
10.0
20.0
30.0
40.0
50.0
60.0
Time (s)
Acceleration
5% to 95% Arias Intensity

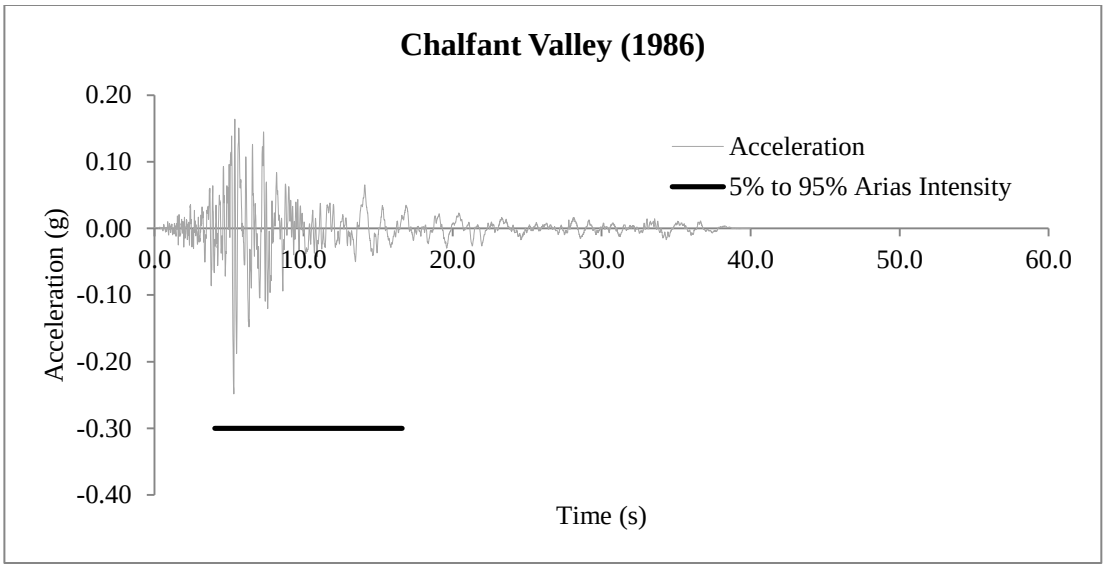
Chalfant Valley (1986)
0.20
0.10
0.00
-0.10
-0.20
-0.30
-0.40
Acceleration (g)
0.0
10.0
20.0
30.0
40.0
50.0
60.0
Time (s)
Acceleration
5% to 95% Arias Intensity

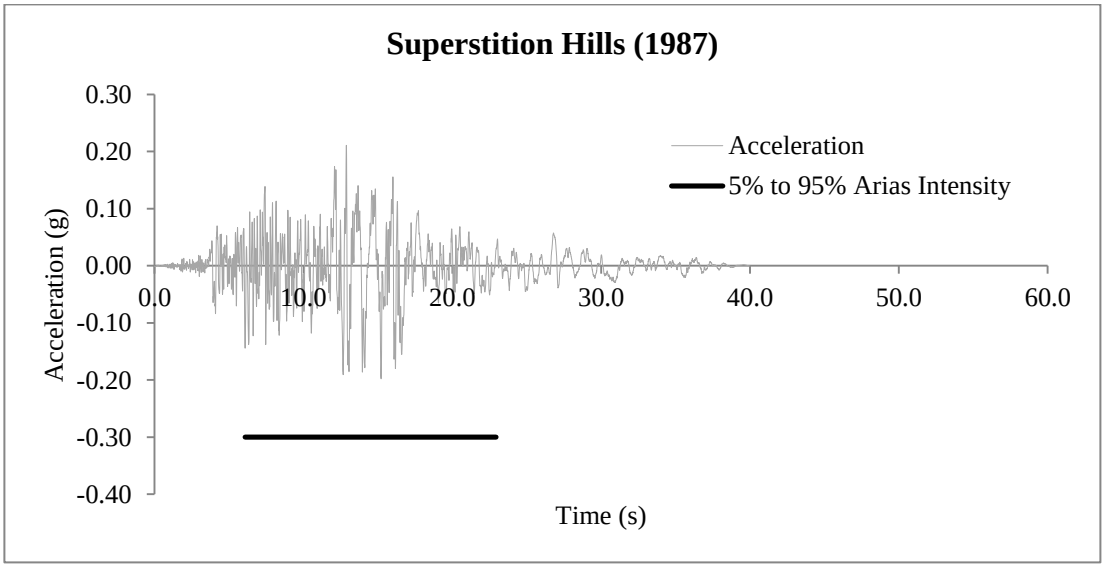
Superstition Hills (1987)
0.30
0.20
0.10
0.00
-0.10
-0.20
-0.30
-0.40
Acceleration (g)
0.0
10.0
20.0
30.0
40.0
50.0
60.0
Time (s)
Acceleration
5% to 95% Arias Intensity

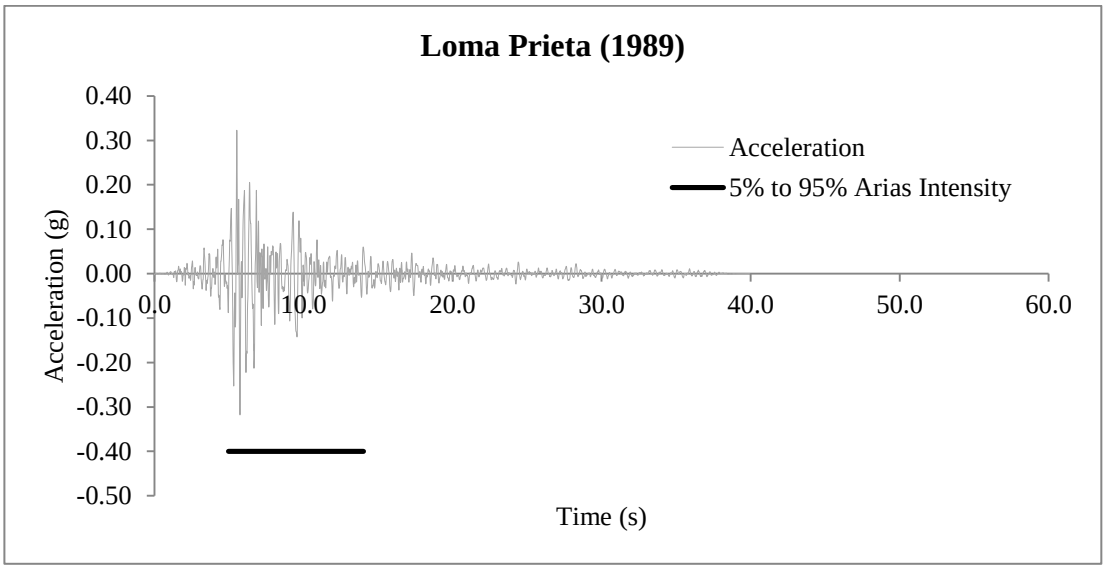
Loma Prieta (1989)
0.40
0.30
0.20
0.10
0.00
-0.10
-0.20
-0.30
-0.40
-0.50
Acceleration (g)
0.0
10.0
20.0
30.0
40.0
50.0
60.0
Time (s)
Acceleration
5% to 95% Arias Intensity

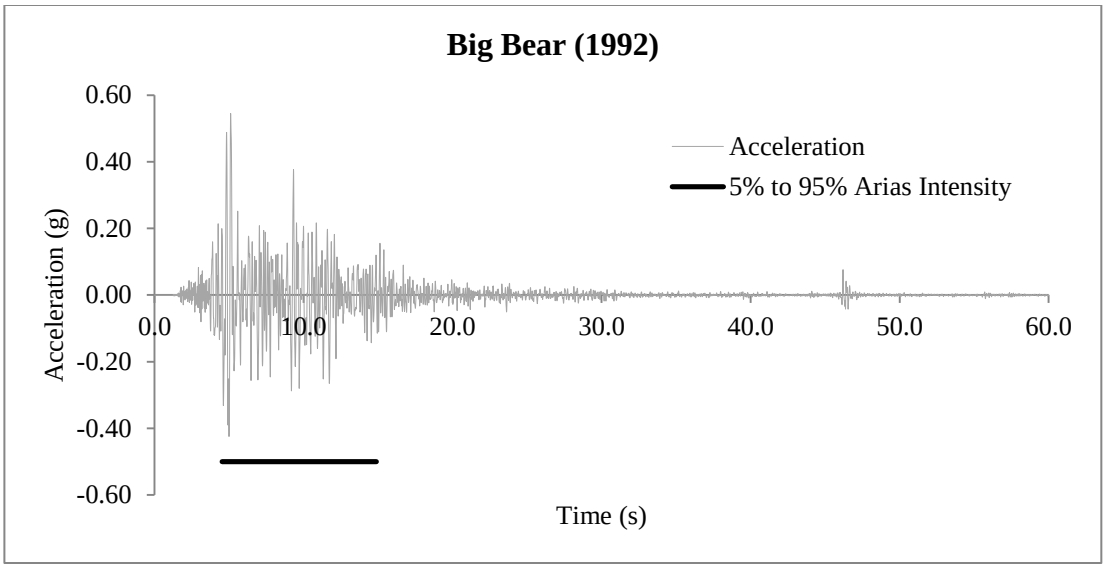
Big Bear (1992)
0.60
0.40
0.20
0.00
-0.20
-0.40
-0.60
Acceleration (g)
0.0
10.0
20.0
30.0
40.0
50.0
60.0
Time (s)
Acceleration
5% to 95% Arias Intensity

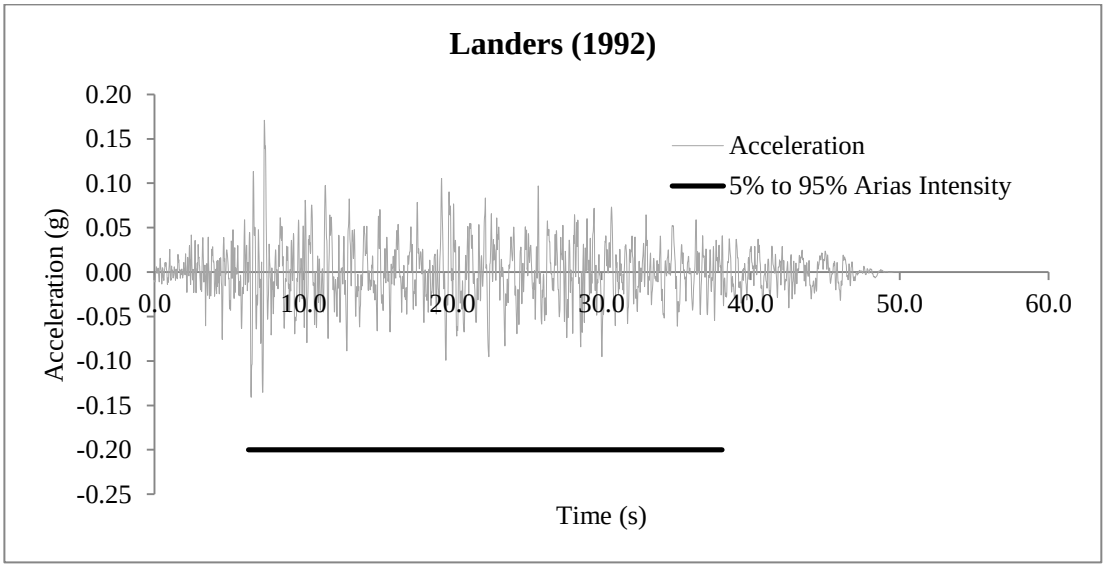
Landers (1992)
0.20
0.15
0.10
0.05
0.00
-0.05
-0.10
-0.15
-0.20
-0.25
Acceleration (g)
0.0
10.0
20.0
30.0
40.0
50.0
60.0
Time (s)
Acceleration
5% to 95% Arias Intensity

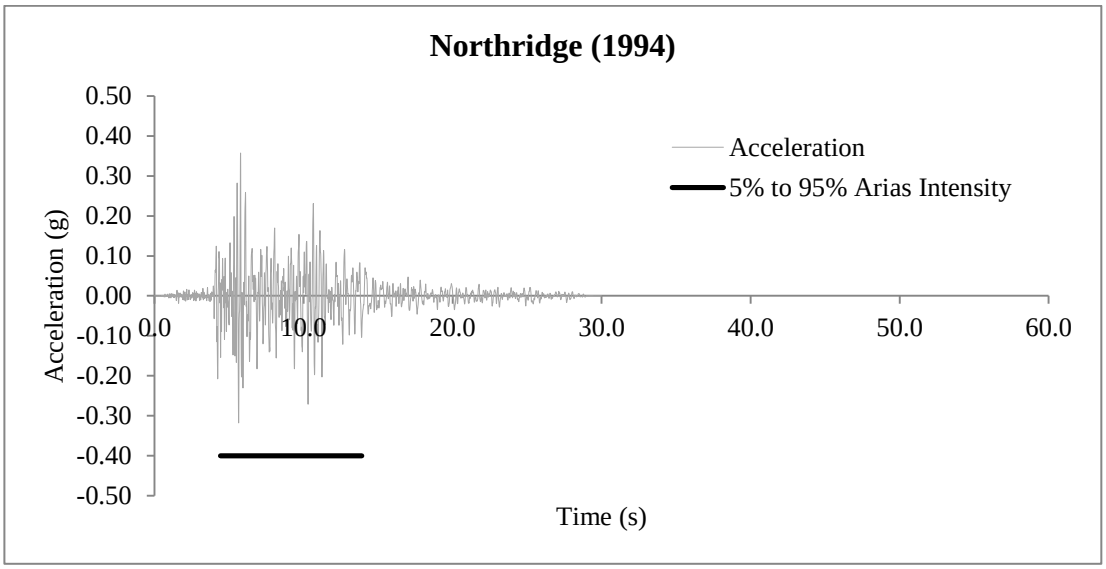
Northridge (1994)
0.50
0.40
0.30
0.20
0.10
0.00
-0.10
-0.20
-0.30
-0.40
-0.50
Acceleration (g)
0.0
10.0
20.0
30.0
40.0
50.0
60.0
Time (s)
Acceleration
5% to 95% Arias Intensity